NI

NASA TECHNICAL MEMORANDUM

NASA TM-82451

A QUANTITATIVE STUDY OF FACTORS INFLUENCING LAMELLAR EUTECTIC MORPHOLOGY DURING SOLIDIFICATION

By W. F. S. Kaukler
Space Sciences Laboratory

November 1981

NASA

George C. Marshall Space Flight Center
Marshall Space Flight Center, Alabama

MSFC - Form 3190 (Rev June 1971)

TECHNICAL REPORT STANDARD TITLE PAGE

1. REPORT NO.	2. GOVERNMENT ACCESSION NO.	3. RECIPIENT'S CATALOG NO.
NASA TM-82451		

4. TITLE AND SUBTITLE	5. REPORT DATE
A Quantitative Study of Factors Influencing Lamellar Eutectic Morphology During Solidification	November 1981
	6. PERFORMING ORGANIZATION CODE
7. AUTHOR(S)	8. PERFORMING ORGANIZATION REPORT #
W. F. S. Kaukler*	
9. PERFORMING ORGANIZATION NAME AND ADDRESS	10. WORK UNIT NO.
George C. Marshall Space Flight Center Marshall Space Flight Center, Alabama 35812	11. CONTRACT OR GRANT NO.
	13. TYPE OF REPORT & PERIOD COVERED
12. SPONSORING AGENCY NAME AND ADDRESS	Technical Memorandum
National Aeronautics and Space Administration Washington, D.C. 20546	14. SPONSORING AGENCY CODE

15. SUPPLEMENTARY NOTES

*Universities Space Research Association Visiting Scientist

16. ABSTRACT

The work was carried out to obtain a quantitative evaluation of the factors that influence the shape of the solid-liquid interface of a lamellar binary eutectic alloy. The experiments were performed using alloys of Carbon Tetrabromide and Hexachloroethane which serve as a transparent analogue of lamellar metallic eutectics. The experimental apparatus that was used was designed to permit direct observation of the solid-liquid interface under very closely controlled conditions. The observed interface shapes were analyzed by computer-aided methods.

The solid-liquid interfacial f . energies of each of the individual phases comprising the eutectic system were measured as a function of composition using a "grain boundary groove" technique. The solid-liquid interfacial free energy of the two phases could be evaluated directly from the eutectic interface. Various data were measured: the phase diagram for the system, the heat of fusion as a function of composition, and the density as a function of composition.

It was concluded that the shape of the eutectic interface is controlled mainly by the solid-liquid and solid-solid interfacial free energy relationships at the interface and by the temperature gradient present, rather than by inter-lamellar diffusion in the liquid at the interface, over the range of growth rates studied.

17. KEY WORDS	18. DISTRIBUTION STATEMENT
	Unclassified – Unlimited William F. Kaukler

19. SECURITY CLASSIF. (of this report)	20. SECURITY CLASSIF. (of this page)	21. NO. OF PAGES	22 PRICE
Unclassified	Unclassified	263	NTIS

ACKNOWLEDGMENTS

Sincere thanks are given to all who contributed, even in the slightest way, to the effort which culminated in the form of this document.

Special thanks are given to the professors, technical staff, and graduate students of the Department of Metallurgy and Materials Science in the University of Toronto, Toronto, Ontario, Canada. The author thanks Prof. John Rutter of the Department of Metallurgy and Materials Science, University of Toronto, for his total supervision of the work from its inception, and Dr. John Cahn of the National Bureau of Standards, Washington, D.C., Prof. W. Neumann of the Department of Mechanical Engineering, University of Toronto, and Prof. W. A. Miller of the Department of Metallurgy and Materials Science, University of Toronto, for their supervision and criticism for some of the work.

1. FOREWORD

This work was carried out by Dr. Kaukler at the University of Toronto prior to his assuming his present position as a Visiting Scientist at the NASA Marshall Space Flight Center in the Materials Processing in Space Program. The work, however, is of great interest to the Materials Processing in Space Program because it offers for the first time the possibility of obtaining quantitative information on the growth of eutectic systems that can provide critical tests of the various theories of eutectic growth and can be used to investigate some of the subtleties of gravitational influences on the growth process.

The latter is of particular interest in the light of some recent low-gravity experiments which have shown conclusively that significant changes occur in the thickness and spacing of the α and β phases. This unanticipated result is still not understood but probably results from gravitational modification of the concentration field in the melt just ahead of the growth interface.

Dr. Kaukler's work at the Marshall Space Flight Center is an extension of this effort in an attempt to refine the theory of eutectic growth and to account for these unexpected gravitational effects. Since the research reported forms the background for his present work and is of general interest to other workers in the NASA Materials Processing in Space Program, the work is being made more widely available by issuing it as a NASA document.

Robert J. Naumann

2. PREFACE

It has always been the author's interest to dissect the mechanisms for the development of eutectic morphologies.

In the past, the dissection was performed by physically removing one of the phases, either by selective deep acid etching, by selective sublimation or by chemical vapor dissolution. These techniques made it possible to separate the individual morphologies of the phases in a eutectic microstructure and to view them in three dimensions.

Many years were spent physically dissecting the various eutectic microstructures but only after solidification. Many observations were made, but the "creating mechanisms" were not revealed in the as-cast microstructures.

Transparent organic models for freezing metal made observation of the growing solid-liquid interfaces simple to perform. Phenomena assumed to occur in metals were actually seen in real time, in situ, using the transparent organics. Experience with the organics reinforced the idea of using them as a research tool to elegantly probe the solidification of eutectic growth.

There is no doubt in the author's mind that the controlling mechanisms for the development of eutectic morphology directly influence the advancing boundary between solid and liquid.

3. TABLE OF CONTENTS

10. Experimental Observations and Results (ccntinued)

4. LIST OF ILLUSTRATIONS

5. NOTATION AND UNITS

Symbol Table	Meaning	Units
CBr_4	Carbon Tetrabromide	
C_2Cl_6	Hexachloroethane	
γ	interfacial free energy	(ergs/cm^2) mJ/m^2
G	temperature gradient	°C/cm
R, V	velocity (of interface)	micrometers/sec.
T	temperature	degrees C or K
ΔT	undercooling	degrees C or K
ΔH_f	enthalpy of fusion	J/gm
L	latent heat (heat of fusion)	J/gm
ΔS_f	entropy of fusion	J/m^3 °K
A	slope of λ vs. $R^{-1/2}$ (Tiller's Formula)	
ε	constant used in Tiller's Formula	dimensionless
ρ	density	g/cm^3
κ	curvature	1/micrometer
r	radius of curvature	micrometer
K	$K^2 = \gamma_{SL}/G\ \Delta S_f$	
$m\alpha$, $m\beta$	slope of liquidus (α, β phases)	°C/(w/o)
$n\alpha$, $n\beta$	slope of solidus (α, β phases)	°C/(w/o)
$S\alpha$, $S\beta$	half-widths of lamellae	micrometers
a, $a\alpha$, $a\beta$	Gibbs-Thomson coefficient $a = \frac{\gamma}{\Delta S_f} = \frac{\gamma T_E}{\rho \Delta H_f}$	

Symbol Table	Meaning	Units
d	Glicksman and Nash parameter	micrometer
δ	Glicksman and Nash parameter	dimensionless
λ	lamellar spacing = $2(S\alpha + S\beta)$ or grain boundary groove spacing in Glicksman and Nash method	micrometers
θ	Glicksman and Nash parameter	
η	Jackson and Hunt term $\eta = (a\beta\ m\alpha)/(a\alpha\ m\beta)$	
C_p	heat capacity at constant pressure	
X_1, X_2	molar concentrations	
D	diffusion coefficient	$cm^2/sec.$
ΔH_{mix}	enthalpy of mixing	
C, C_E, $C\infty$	concentration or composition	w/o
Co, Cα, Cβ		
Co^{α}, Co^{β}		
Bo, Bn	Jackson and Hunt coefficients	
R	universal gas constant	

6. SUMMARY

A QUANTITATIVE STUDY OF FACTORS INFLUENCING LAMELLAR EUTECTIC MORPHOLOGY DURING SOLIDIFICATION

The work reported in this document was carried out to obtain a quantitative evaluation of the factors that influence the shape of the solid-liquid interface of a lamellar binary eutectic alloy. The experiments were performed using alloys of Carbon Tetrabromide and Hexachloroethane which serve as a transparent analogue of lamellar metallic eutectics. The experimental apparatus that was used was designed to permit direct observation of the solid-liquid interface under very closely controlled conditions. The observed interface shapes were analyzed by computer-aided methods.

The solid-liquid interfacial free energies of each of the individual phases comprising the eutectic system were measured as a function of composition using a "grain boundary groove" technique. These interfacial free energies were observed to be isotropic. It was also found that the solid-liquid interfacial free energy of the two phases could be evaluated directly from the eutectic interface. Observations of the eutectic interface shape permitted evaluation of the solid-solid interphase interfacial free energies for the eutectic. Various data, necessary for the quantitative evaluations, were also measured, including the phase diagram for the system, the heat of fusion as a function of composition and the density as a function of composition.

From the observations made, it was concluded that the shape of the eutectic interface is controlled mainly by the solid-liquid and solid-solid interfacial free energy relationships at the interface and by the temperature gradient present,

rather than by inter-lamellar diffusion in the liquid at the interface, over the range of growth rates studied. It was shown that a surface tension balance at the junction of the solid-solid interface with the solid-liquid interfaces of the eutectic requires the presence of a torque, which was evaluated for the system under study. Under some conditions, special solid-solid interfaces that had very low interfacial free energies were observed. Forced convection experiments showed that the eutectic interface shape was only slightly influenced by flow of the liquid adjacent to the interface. It was also observed that response to quenching of the liquid adjacent to the eutectic interface was the very rapid growth of single-phase dendrites of the major phase, rather than two-phase dendrites.

7. INTRODUCTION

The research presented in this document was performed in order to analyze quantitatively, the factors that influence the manner of solidification of a lamellar binary eutectic. Certain aspects of eutectic freezing have been rigorously studied in the past. Types of eutectic morphology, lamellar and rod spacings, effects of constitutional undercooling in causing interface breakdown, and the presence of structural faults are a few eutectic characteristics that have been examined. Growth rate, temperature gradient and composition are all factors that have been manipulated in an effort to alter and control eutectic characteristics in a systematic manner.

It became evident that the "cast" microstructure of a eutectic alloy is developed at the solid-liquid interface, during solidification. As models for eutectic solidification were developed, attention was directed to the interfacial tensions encountered at the growth front as important quantities in determining interface shape. The usefulness of the models was limited, however, by the scarcity of values for the solid-liquid interfacial free energies for metals. These values were mostly obtained from bulk undercooling experiments by the application of the Gibbs - Thomson equation to homogeneous nucleation theory. Until recently, these measurements have not

been corroborated by other techniques of measurement.

The application of the Gibbs - Thomson relation to the curvature of the solid-liquid interface at a grain boundary groove (GBG) in a temperature gradient (see section 8.1.2) has provided another method for the measurement of interfacial free energy. The method is most readily applied to transparent materials [10, 13, 16] but it has been applied to a metal as well [42].

The pioneering work of Jackson and Hunt (see section 8.1.1) with transparent organic materials brought two important facts to light. First, the easily observed solid-liquid interfaces in certain transparent organic materials were shown to be effective models of metal solidification fronts. This was the case for both single phase and polyphase alloys. Second, the ease of generating and observing grain boundary grooves at solid-liquid interfaces allowed the implementation of the new interfacial energy measurement technique. These ideas constitute the working principles for this work.

In the work reported here, the grain boundary groove analysis method is applied to a polyphase interface. In order to properly implement the technique on a eutectic interface, grain boundary groove analyses were performed on alloys instead of pure materials. Supplemental measurements were necessary to evaluate the Gibbs - Thomson equation. These include the construction of a phase diagram for the system chosen,

measurement of the enthalpy of fusion for the alloys, and the measurement of the alloy densities.

All of the work was performed with one organic eutectic alloy system. The alloy system, Carbon Tetrabromide - Hexachloroethane, was first found by Jackson and Hunt and used to support experimentally their interface shape theories. The eutectic composition was reported as 8.6 weight percent Hexachloroethane. Knowledge of the eutectic composition, the melting points of the components and the eutectic temperature was the only information that was used to apply their theory to the system. Photographs of eutectic interfaces were compared to predicted interface shapes calculated primarily from solutions to the diffusion equation at the interface. No one had studied this organic alloy in any detail since the work of Jackson and Hunt.

This is the only system known which could be grown with sufficiently large lamellar spacings to permit any reasonable interface analysis. This feature made the interfacial measurements reported in this document feasible. The organic system selected has several other features which made it a nearly ideal model for lamellar eutectic solidification.

Control of the growth conditions during observation of the interfaces was another prerequisite for the work. The Temperature Gradient Microscope (described in section 9.1) was

designed specifically to operate with the organic system and to provide a maximum of versatility. The ability to achieve high thermal stability, slow growth rates and shallow thermal gradients were the important design parameters around which the apparatus was constructed. A method of obtaining high optical resolution of the interface profile was also needed. The organic was sealed in thin glass cells to provide the optimum geometry for study.

Similar apparatus has been used in the past for research, and to demonstrate solidification phenomena with transparent organics to students. Familiarity with the behaviour of these organic alloys was obtained in this work, by repeating most of the basic solidification experiments, with many compositions of the model alloy system. New cell designs were developed to expand the types of experiments further. An important new form of cell was the forced convection cell. In situ observation of convective phenomena at a growing eutectic interface revealed many effects both old and new. Most of these effects have not been directly observed previously.

The use of organic materials, thin cells and the thermal gradient microscope were found very well suited to the grain boundary groove analysis technique. With the same apparatus used for controlled eutectic growth, stable grain boundary grooves at stationary single phase solid-liquid interfaces could be prepared. Quantitative analysis of the interfacial

free energies then became feasible. Eutectic interface characterization was then nearly completed in a quantitative manner. This was the case for both stationary and slowly growing eutectic or single-phase solid-liquid interfaces.

Throughout this document, the phrases: interfacial free energy, surface tension, and interfacial energy, are used. These phrases are used in a synonymous manner in this report and are intended to mean, more precisely, "specific interfacial free energy".

8. THEORETICAL BACKGROUND

8.1 Historical

8.1.1 Lamellar Eutectic Growth Theory

Solidification of eutectic alloys results in numerous and varied microstructures. Classification of these structures has been attempted several times [2, 17, 18]. According to Scheil [17], eutectics can be broadly classified into two groups, those with normal microstructures and those with abnormal microstructures. (The more commonly accepted terms for these eutectic types are now regular and anomalous, respectively.) Growth that produces a "normal" microstructure was thought to occur when both phases solidified side by side with equal velocity. [17] Examples of eutectics that solidify in this way are the common lamellar and fibrous types. Anomalous eutectic structures include all those which have less regularity than the regular eutectics. An example is the "Chinese Script" microstructure. [17, 40] Others are presently working on the problem of characterizing these complex morphologies in detail from metallographic sections. [30, 31]

Lamellar eutectics are the most interesting of the regular types as many metal eutectics have a lamellar morphology. The lamellar type of morphology is also simpler to analyze mathematically. The lamellar morphology is best

represented as an infinite plate structure. In metal lamellar eutectics, these plates are only a few micrometers or less thick. Due to the symmetry of this structure, the solid-liquid interface profile of a growing lamellar eutectic can then be represented conveniently in a two-dimensional Cartesian coordinate system. These traits make the study of lamellar eutectics more attractive to those who wish to study eutectic solidification.

In the past, the following workers have performed a two-dimensional mathematical analysis of lamellar eutectic growth: Hillert [19], Tiller [21], Jackson and Hunt [8], Glicksman and Nash [20, 84] and Nash [27]. They developed realistic solid-liquid interface profiles from "first principles" analysis of the conditions for eutectic growth. The descriptive analysis which follows is a modified version of the classic Jackson and Hunt theory. [8, 2, 7, 38]

Growth of a eutectic occurs by an "unmixing" action in which a liquid transforms to two solids ($L \rightarrow \alpha + \beta$) as shown in the hypothetical simple binary phase diagram, Fig. 8.1. Under equilibrium conditions, a liquid of eutectic composition, C_E, made up from components A and B will solidify at the invariant temperature T_E, to form a two-phase solid made up of the phases α and β with the respective compositions $C\alpha$ and $C\beta$.

The formation of lamellae from the liquid occurs

Fig. 8.1

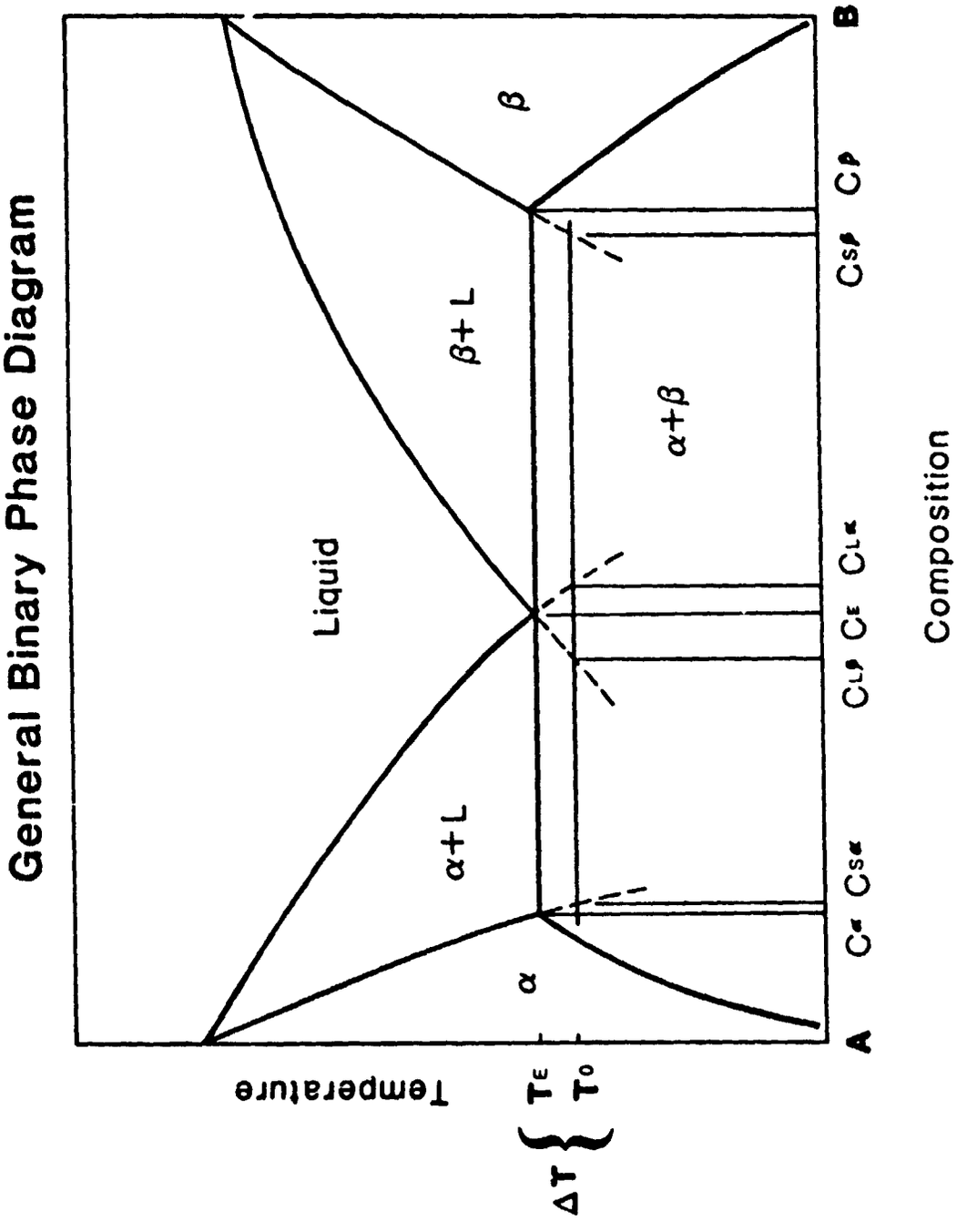
General Binary Phase Diagram
Liquid
β
β+ L
α+β
α+L
α
A
B
Cα Csα
CLβ CE CLα
Csβ Cβ
Composition
Temperature
TE
To
ΔT

by simultaneous edgewise growth of the two phases of the eutectic into the liquid, so that the solid-liquid interface is made up of alternating layers of the α and β phases in contact with the liquid. The initial simplification made by Jackson and Hunt, as well as other workers, was that the solid-liquid interface was planar and isothermal.

As the lamellae grow into the liquid, solute is rejected into the liquid from the solid-liquid interfaces of the two phases. The amount of rejected material could be calculated from the phase diagram in the same way it would be calculated for a single phase interface if there were no interlamellar diffusion. During steady state growth a layer of rejected solute would build up in the liquid adjacent to each of the interfaces. This buildup would cause each of the two phases to grow from liquid rich in solute and therefore from liquid greatly undercooled with respect to T_E. Growth can in fact proceed without substantial undercooling because the solute rejected by one phase is a major component of the adjacent phase. The concentration gradient of solute requires the rejected solute to be consumed by solidifying to form the neighbouring lamella rather than diffusing into the bulk liquid. Lateral diffusion is the response to the rejection of solute which permits freezing at temperatures much closer to T_E than would otherwise be possible. Only diffusion in the liquid is considered since diffusion in the solid is nearly always several orders of magnitude slower. There are three components

to the diffusion path: one component is directed into the liquid away from the interface along the growth direction or normal to the solid-liquid interface, and the other components project normal to this direction parallel to the solid-liquid interface. The diffusion path component parallel to the plane between the phases and parallel to the solid-liquid interface should not concern one in the analysis as this component does not contribute to the mass balance or, alternatively, there is no concentration gradient to drive diffusion in this direction. This concept conforms with the two-dimensional analysis which was already adopted.

The material rejected into the liquid from one lamella is the major constituent of the neighbouring lamellae. This fact increases the diffusive flux of the eutectic constituents by providing good sources and sinks for the constituents of the lamellar phases. The efficiency of cross-diffusion of solute is maximized by reducing the diffusion distance. A planar interface is therefore the most efficient morphology.

The interface is isothermal and undercooled by a temperature ΔT, to a temperature T_o. As the diffusion coefficient becomes smaller, or the growth rate larger, the undercooling increases (provided the lamellar spacing does not change as well).

Because of the physical separation between the phases, diffusion of solute from the liquid near the midsection of a

lamella to the neighbouring lamella is more difficult than the cross-diffusion of the solute from the region in the liquid near the phase boundaries. The result is variation of the liquid composition across the solid-liquid interface of a lamella, symmetrical about the middle (centre line) of the lamella. The point of maximum solute buildup at the interface occurs in the middle of each lamella and the deviation from eutectic composition approaches a minimum at or near the phase boundaries.

The consequence of this assertion is t .he composition of the solid which forms varies from point to point across the width of a lamella. The result of this conclusion is that the local interface temperature (the local undercooling) must also vary in accordance with the aforementioned variation in local composition. The finding is that there is an abrogation of the initial assumption of the isothermality of the solid-liquid interface.

Jackson and Hunt (as well as others) preserved interfacial isothermality by local compensation of the variations in solute induced undercooling. This was done by offsetting the local variation of undercooling along the solid-liquid interface with an equivalent, but opposing contribution of curvature of the interface. [8, 7, 2] The addition of curvature is consistent with the direct observa ion of eutectic interfaces, with the surface tension balance at the interphase boundaries and with the Gibbs - Thomson relationship

between undercooling and solid-liquid interfacial energy (see section 8.1.2). Jackson and Hunt asserted that the net curvature at all points on the interface is such as to keep the interface isothermal (i.e., uniformly undercooled).

The Jackson and Hunt analysis does not include thermal parameters such as thermal conductivities or gradients. This is justified by stating growth occurs under steady state conditions (the interface velocity is constant). They found a solution to the diffusion equation with the boundary conditions obtained from the planar geometry presented for a lamellar eutectic solid-liquid interface. This solution, reproduced below, gives the local liquid composition ahead of the interface [8]:

$$C = C_E + C^{\infty} + Bo \exp\left(-\frac{V}{D} z\right)$$

$$+ \sum_{n=1}^{\infty} B_n \cos\left(\frac{n \pi x}{S\alpha + S\beta}\right) \exp\left(-\frac{n \pi z}{S\alpha + S\beta}\right)$$

$$Bo = \frac{Co^{\alpha} S\alpha - Co^{\beta} S\beta}{S\alpha + S\beta}$$

$$B_n = \frac{2}{(n\pi)^2}\left(S\alpha + S\beta\right) \frac{V}{D} \; Co \sin\left(\frac{n\pi \, S\alpha}{S\alpha + S\beta}\right)$$

when:

C = composition in liquid (eg. w/o B in A in Fig. 8.1)

C_E = eutectic composition (Fig. 8.1)

$C^{\infty} = C - C_E$ @ $z = \infty$

V = velocity

D = diffusion coefficient in liquid

$S\alpha$, $S\beta$ = half width of lamellae

z = distance into liquid from the interface @ z = 0

x axis is normal to growth direction

x = o in middle of α phase

$Co = Co^{\alpha} + Co^{\beta}$

$Co^{\alpha} = C_E - C\alpha$ (Fig. 8.1)

$Co^{\beta} = C\beta - C_E$ (Fig. 8.1)

A similar but independently developed version of this equation was formed by Donoughey and Tiller. [32] Note that the composition variation is a function of the lamellar widths but the known dependence of lamellar spacing (twice($S\alpha + S\beta$))

on growth rate is not provided for.

From the slope of the liquidi the local undercooling at this interface is quantified. Jackson and Hunt then fitted the appropriate amount of curvature to the interface depending on the Gibbs - Thomson coefficients. In order to obtain a "calculated" interface shape, the Jackson and Hunt solution requires a pair of angles for the tangents of each solid-liquid interface with respect to the normal to the growth direction at the junction between the phases. Besides the half widths of the lamellae, the last critical factor in the calculations for the interface profile was a term, η, which contained the ratios of the Gibbs - Thomson coefficients and slopes of liquidi: $\eta = \frac{a\beta\ m\alpha}{a\alpha\ m\beta}$ where $a\beta$, $a\alpha$ are Gibbs - Thomson coefficients and $m\alpha$, $m\beta$ are the slopes of the liquidi, for each phase.

Jackson and Hunt discovered the organic eutectic system, Carbon Tetrabromide - Hexachloroethane, froze the alloy unidirectionally on a temperature gradient stage and photographed the interfaces. The micrographs were measured and the calculated slopes of the liquidi were applied to the equations they derived to calculate interface profiles. They assumed the Gibbs - Thomson coefficients for each phase were equal and also adjusted the value of η until the calculated shapes matched the micrographs. Many of the parameters in the equations were not available at that time, but are available now as a result of the research reported here. All the variables for the

Jackson and Hunt equations are now available, and the interface profiles can be drawn. The results, using the data from this report, are drawn in Fig. 8.2. This figure shows a perspective view of the "calculated" growing interface and superimposed on this is the local composition of Hexachloroethane component in the liquid. The interface velocity was selected as one micrometer per second and the diffusion coefficient was assumed to be 2×10^{-5} cm^2/sec. Another combination of the values for the parameters needed in the Jackson and Hunt analysis could lead to the formation (development) of negative curvature at the tips of the lamellae in Fig. 8.2. [8] The data supplied for Fig. 8.2 were from experimental measurements described later in this report. Negative curvature would be the morphological manifestation of the solute-induced undercooling. The solute buildup ahead of each lamella as shown in Fig. 8.2 could, under other circumstances cause the negative curvature described in [8]. An interface with negative curvature can be found in section 10.2.1. The lamellar spacing and growth rate, in turn limit the time allowed for diffusion to occur. If the perturbations of composition in the liquid ahead of the solid (example Fig. 8.2) are reduced by decreasing the growth rate, then the temperature of freezing will approach the equilibrium temperature, T_E, from below on the phase diagram.

In the Jackson and Hunt analysis, contributions to interface undercooling other than solute diffusivity and curvature

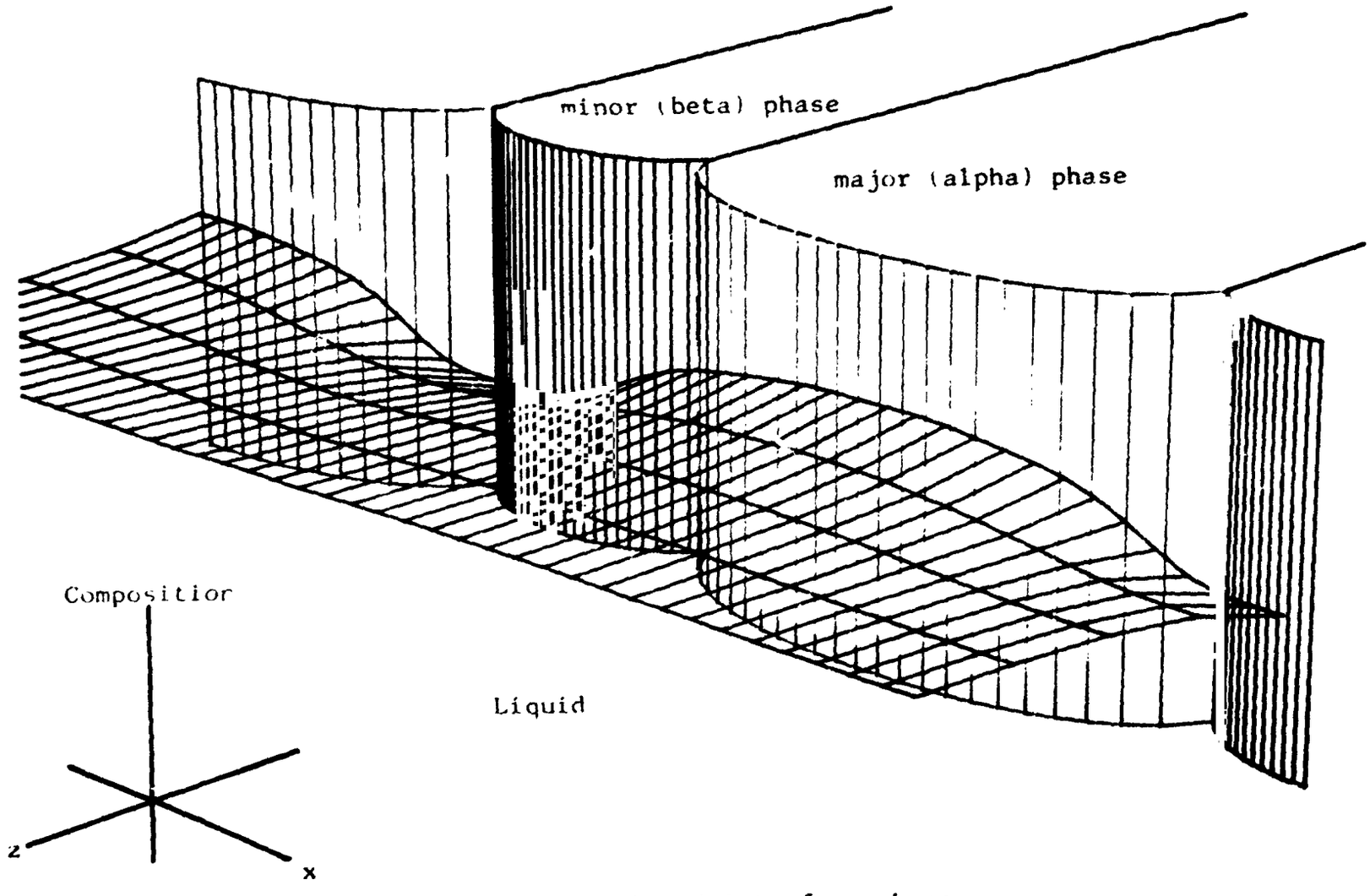

Fig. 8.2 Calculated interface shape and solute distribution.

were assumed to be nil. What follows is a compilation of the sources for undercooling in a growing eutectic solid-liquid interface.

From the phase diagram, the undercooling, ΔT_D, due to the composition variations resulting from diffusion in the liquid adjacent to the interface is given by: $\Delta T_D = m (C_E - C_L)$ where m is the slope of the liquidus, C_E the eutectic composition and C_L the composition of the liquid.

The second contribution to the undercooling comes from the curvature at the solid-liquid interface. Periodic curvature in the interface would allow equilibrium to be attained at all points on the (nearly) isothermal interface even though there are composition variations in the liquid in contact with the solid. Curvature, interfacial energy and undercooling are related through the Gibbs - Thomson equation. This relation is presented in section 8.1.2. A simplified version of the relationship between the radius of curvature and undercooling is given: $\Delta T_R = a/r$ where "a" is the Gibbs - Thomson coefficient, and "r" is the radius of curvature at a point on the interface. The two contributions to the undercooling used by Jackson and Hunt have been presented. The net resulting undercooling is: $\Delta T = \Delta T_D + \Delta T_R$

"When a solid forms below its melting point, the difference in free energy between the liquid and solid can be in part dissipated in irreversible processes or in part stored

in the solid as nonequilibrium structural components such as grain boundaries and substructures." [78] This statement implies that the formation of the solid-solid phase boundary during eutectic solidification is a contribution to the undercooling of the interface. The undercooling supplies energy for the formation of the phase boundary between the two solid phases. [21] The free energy difference per unit mass between the solid and liquid should correspond largely to the interfacial free energy of the α-β phase boundary (of the hypothetical alloy). Thus, the solid-liquid interface temperature depends in part on $\gamma_{\alpha\beta}$ (the interfacial free energy for the phase boundary between α and β). The relation between undercooling and interfacial energy was given by Tiller [21] as $\Delta T\gamma = 2\gamma_{\alpha\beta}/\lambda\Delta S_f$, where ΔS_f is the entropy of fusion per unit volume, and λ is the lamellar spacing.

Dendritic solidification of single phase alloys can exhibit one of two growth forms, faceted or nonfaceted. The faceted interface has an atomically smooth surface, while the nonfaceted surface is atomically rough. As a result, it is easier for an atom in the liquid to solidify onto the nonfaceted surface than on the faceted one, since there are fewer sites suitable for the atom to deposit on in the latter case. [4, 1, 3, 38] If the interface were stationary, its temperature would be the equilibrium temperature. The driving force for growth which causes liquid atoms to deposit on the solid is supplied

by an interfacial undercooling. This type of undercooling is the kinetic undercooling, ΔT_K. The rough, nonfaceted interface can grow more easily and faster than the faceted interface and with less undercooling. The growth characteristics of single phase interfaces are maintained by each phase of a eutectic. A eutectic interface grows with an undercooling which incorporates the kinetic undercooling from the solid-liquid interface of each phase. The typical lamellar eutectic is made up of two phases which grow in a nonfaceted manner. Therefore, the lamellar eutectic will grow with the lowest kinetic undercooling [2, 21, 35]. Frequently, during discussions of interfacial undercooling, the kinetic undercooling is neglected for lamellar eutectics because the magnitude, relative to the other contributions of undercooling, is negligible [7, 8, 21].

Together, the above contributions give the overall undercooling of the growing eutectic interface. The undercooling at each point on the interface is now given as:

$$\Delta T = \Delta T_D + \Delta T_R + \Delta T_\gamma + \Delta T_K$$

A relationship between interfacial undercooling (ΔT) and growth rate (R) was found by the workers in the early analysis of lamellar eutectic growth: Zener [22], Hillert [19], Tiller [21] and Jackson and Hunt [8]. The relationship is $\Delta T/R$ = constant. This predicts that as the growth rate increases, the interfacial undercooling increases. Experimentally, as well as theoretically, a relationship between lamellar spacing

($\lambda = 2 (S\alpha + S\beta)$) and growth rate was found. The form of this relation is $\lambda^2 R$ = constant. The relationship between λ and R was discovered by experiment on metal eutectics before the theories were conceived. [23, 76, 36, 28, 17, 35] The relationship between ΔT and R was verified only after the theories were refined and the experimental techniques developed. [24, 25] The experimental difficulty lay in the small temperature differences which these interfacial undercoolings represent (generally less than one degree Celsius).

In order to obtain the functional relationships from the theories discussed above, an assumption was made; the workers adopted a condition, an "extremum condition", which states that the solid-liquid interface will try to grow with the minimum possible undercooling, or alternatively, to grow with the greatest velocity for a given lamellar spacing. The experimental verification of the functional relationships does not, however, verify that the minimum undercooling condition is the controlling mechanism. For example, the condition is not based on a mechanism which allows the lamellar spacing to adjust itself under the influence of growth conditions. In addition, others [35] have found, through experiment, that growth does occur near but not necessarily at the extremum.

According to another altogether different analysis by Cline [26], stable lamellar growth could occur with spacings larger than that corresponding to a minimum uncercooling while

the interface is unstable with smaller spacings. Unfortunately, this analysis has only been performed on a mathematical model with an ideal, hypothetical eutectic.

The interface analysis by Colin, et al [33] tried to relate the diffusion problem in the liquid at the interface to the corrugated shape of the interface. Shape variations like leading distance of one phase over the other, and degree of convexity, appear to have significant effects upon the composition gradients in the liquid. The analysis uses the interface shape to define the conditions for solute diffusion.

R. W. Series et al [34] have, in a recent paper, improved the original Jackson and Hunt equations, and substantiate the results with measurements using electronic analogue techniques. This paper ties the phase diagram more closely to the composition equations and reduces the number of assumptions of the original Jackson and Hunt paper.

So far, planar, lamellar eutectic interfaces have been discussed. The inherent character of freezing eutectics can be altered by the presence of a suitable third component. The ternary component may be either deliberately added to change the properties of the material, or may be present as an impurity. In the past, changes in a eutectic microstructure have been induced by ternary additions or by altering the composition by using very pure components. Some of the changes include the removal of faceted features to produce smooth interfaces, grain size

changes, increased or decreased uniformity in the microstructure, the addition of new phases, etc. These changes have been called modifications [70, 72 - 76, 35, 7, 19, 36]. A lamellar to fibrous transition has also been observed when growth rates reached a critical value without changes in composition. Some believe this may, as well, be an impurity induced modification [7, 26].

From a survey of the literature, two forms of modification emerge. One form of modification is the result of constitutional undercooling of the interface in a way analogous to single phase planar interfaces [5, 7, 15, 26]. The ternary solute is rejected into the liquid and builds up at the interface. The result of constitutional undercooling of a planar eutectic interface is the breakdown of the interface to eutectic cells (colonies) or dendrites. After breakdown the solid-liquid interface extends from a thick layer of solid with liquid channels separating the regions of all solid from all liquid. This layer can be over two hundred micrometers thick. This behaviour is analogous to cell and dendrite formation in single phase materials [72, 73]. In addition, the local growth direction of the interface is at an angle and may even be normal to the heat flow direction. As a result, the final microstructure shows less uniformity than the structure from a unidirectionally grown planar eutectic interface. The second form of modification is believed to be [35, 17, 70, 71, 74, 77] the result the action the ternary component has on the

nature of the solid-liquid interfaces of the two phases or on the solid-solid interphase interface. It seems possible that the modification can occur with the interface maintaining its planar character (author's comment). An interesting aspect of this type of modification is the small concentration of ternary which can induce the changes. As well, a further increase of the concentration may not promote an additional change. Examples of the second type of modification are the addition of sodium to the Al-Si eutectic casting alloy or of magnesium, cerium or silicon to Fe-C eutectic [70, 75, 36, 7, 74].

During controlled solidification of eutectics, one could prevent constitutional undercooling effects by application of the proper temperature gradient and growth rate combinations without changing the composition. This is true even when the constitutional undercooling is caused by the rejection of solute (which is itself a component of the eutectic) which results from the use of off-eutectic compositions. The detailed mechanisms of how the solute may interact with the eutectic interface are, to date, not fully understood or substantiated. Comprehensive discussions of some of these mechanisms are found in the literature [5, 7, 15, 17, 19, 26, 35, 36, 40, 43, 70 - 77].

8.1.2 The Formation of Grain Boundary Grooves

When three phases are simultaneously in contact with one another, the interfaces bounding these phases must meet along a line. This line is here called a trijunction. An interface will exist between two crystals of the same structure and composition if there is sufficient difference between the two crystal orientations. This is a grain boundary. The remainder of this section will relate to the condition where two of the three phases at a trijunction are grains, the third phase is liquid, and one of the three interfaces is a grain boundary. For the remainder of this discussion, the trijunction is considered to be isolated from external influences. The system properties are assumed to be isotropic as well and, initially, the system is assumed to be isothermal; the effect of a temperature gradient will be considered subsequently. Of primary interest is the behaviour of the local geometry of the interfaces at the trijunction when the grains are in contact with their melt.

Each of the three interfaces will have an interfacial free energy associated with it. Every interface has a force exerted at each point in its surface proportional to the interfacial energy. This force is surface tension. These forces act at the trijunction simultaneously such that the tensions are directed outward; normal to the line of trijunction.

The forces at the trijunction are balanced when

equilibrium is attained [66, 63]. The angles formed between the interface planes must correspond to the magnitude of the forces. Looking along the line of the trijunction, these interfaces will form a shape similar to a capital "Y". The trijunction therefore has symmetry about the grain boundary. An alternate geometry which is convenient to use in order to study the interfaces is described next. Advantage will be taken of the symmetry of the interfaces and so the view of a section normal to the trijunction will be sufficient.

In order to apply the methods of interfacial free energy measurements used here, the trijunctions must have temperature gradients applied such that heat flows along the direction of the grain boundary. The experimentally derived shape of such a grain boundary groove is shown in Fig. 8.3. The feature of interest is the cusp or groove that is formed in the solid at the trijunction. As a consequence of the isotherm orientation, the solid-liquid interfaces curve from the base of the cusp at the trijunction and align themselves along the equilibrium temperature isotherm for the alloy, at $T_{equilibrium}$.

The required surface tension balance at the trijunction must still apply and it is assumed (as others have) that this is the case [2, 11, 12, 14, 21, 37, 79]. The force vectors which represent the interfacial free energies are shown in Fig. 3.3. The force vectors are tangent to the interfaces at the trijunction and indicate the angles described earlier. Because of the curvature of the solid-liquid interfaces, the only site where

the equilibrium angles are maintained is at the trijunction.

The isotherms are drawn in Fig. 8.3 for a solid-melt combination in which both phases have equal thermal conductivities. Clearly, the geometry shown in the figure describes a situation where the trijunction temperature is below the equilibrium melting temperature. In other words, the cusp contains undercooled liquid, with the coolest liquid, at the trijunction, having a temperature, $T_{undercooled}$ as shown in Fig. 8.3.

The cusp was formed because the grain boundary intersected the solid-liquid interface. The solid-liquid interface, regardless of temperature gradient, would still be a plane and rest at T_E if there were no grain boundary intersecting it. The force balance of the interfacial tensions is also required, and thus some depression of the solid-liquid interface was required. The transition of the solid-liquid interfaces from the T_E isotherm plane to the trijunction has a functional dependence on temperature. The degree of undercooling of the liquid in the cusp can be determined from knowledge of position on the interface and temperature gradient. The actual shape of the groove formed can be calculated. The interface curvature required to match the undercooling will follow the Gibbs - Thomson relation, given here for a two-dimensional curvature [7, 63, 14, 10].

$$\Delta T = \frac{\gamma_{SL}\, T_E}{\rho \Delta H_f r}$$

γ_{SL} = Interfacial free energy of solid-liquid boundary

T_E = Equilibrium temperature for infinate radius of curvature

ρ = density

ΔH_f = Enthalpy of fusion

r = radius of curvature

ΔT = undercooling

As a result, the local radius of curvature must go from infinity (curvature = 0) at the equilibrium isotherm (T_E) to a minimum at the root of the cusp. Bolling and Tiller [14] were the first to derive the exact expression for the grain boundary groove shape in two dimensions by solving the equations for curvature and the Gibbs - Thomson relation analytically. The assumptions they made were that the interfacial energies were isotropic, the temperature gradient was linear, the liquid and solid had equal thermal conductivities and that the groove is isolated. The magnitude of the grain boundary energy need not be known since the equilibrium dihedral angle (at the base of the groove) is assumed to be zero. The expression that they derived is [14]:

$$x = f(y) = \text{coordinate of interface}$$

$$= K \ln \left[\frac{2K + (4K^2 - y^2)^{1/2}}{y} \right] - (4K^2 - y^2)^{1/2}$$

$$+ K \left[\sqrt{2} - \ln (\sqrt{2} + 1) \right]$$

where:

$K^2 = \gamma_{SL}/G \, \Delta S_f$

C = temperature gradient

ΔS_f = Entropy of fusion per unit volume

The x axis lies on the T_E isotherm, and the y axis is on the grain boundary.

This expression can be used to draw one side of a grain boundary groove (the other side is a mirror image about the grain boundary).

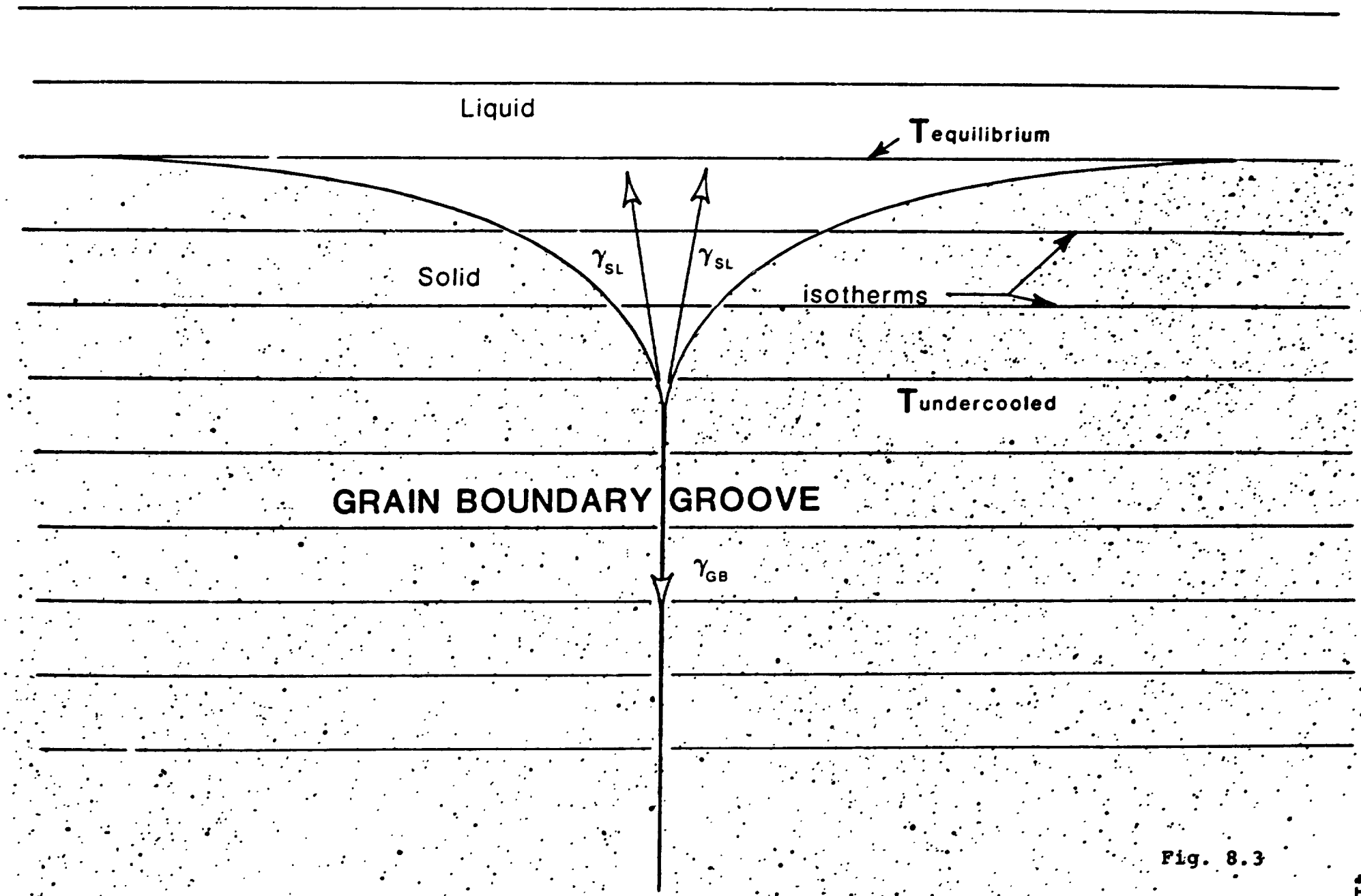
Liquid
T equilibrium
Solid
γ_{SL}
γ_{SL}
isotherms
T undercooled
GRAIN BOUNDARY GROOVE
γ_{GB}

Fig. 8.3

8.1.3 Methods for Measuring Solid-Liquid Interfacial Free Energy

There is no direct method for the measurement of a solid-melt interfacial free energy (γ_{SL}). This section lists several methods that have been used for indirect measurement of γ_{SL}. These methods are based either on the application of the Gibbs-Thomson equation or on contact angle measurement.

To this day, the most comprehensive source of measured solid-liquid interfacial free energies of metals is from the classic experiment by Turnbull and Cech [86, 79, 7]. The method has been applied to non-metals as well. In these experiments, homogeneous nucleation temperatures of undercooled melts were related to the solid-liquid interfacial free energy between the nucleus and melt. This method requires knowledge of the solidification event, and a measurement of temperature. In this method, it is assumed that homogeneous nucleation is achieved.

Another method which uses direct specimen thermometry in order to evaluate γ_{SL} is the melting point determination of small crystals. A small crystal (but still large enough to exhibit its bulk properties), when heated, will melt by forming a thin skin of liquid over its surface, at a temperature that depends on its radius and interfacial free energy through the Gibbs-Thomson relationship.

Ideally, the small crystal should be spherical so that the Gibbs-Thomson equation could be applied directly. The

method has been applied to certain pure metal crystals. A transmission electron microscope was used to both measure the particle radius, and to follow the melting process by electron diffraction pattern analysis [79]. Note that observation of the crystal as well as thermometry is needed to perform the measurement.

The relationship between dendrite tip velocity and the undercooling of its melt has been known for a long time. There is, as well, a relationship between the curvature of the tip and the tip velocity, involving the solid-melt interfacial free energy. A quantitative description of this process has been made elsewhere [79]. The method requires the measurement of the velocity of an unbranched dendrite tip growing from a pure melt. The melt temperature during dendrite formation is also required. This involved method has been applied only to a few materials [79]. Note that the interface is moving and is not an equilibrated or stationary interface.

The following method of measuring the interfacial free energy is difficult to implement experimentally. In view of the relative ease of experimental application of the other methods, this method may not be suitable for any other but ideal conditions. The method employs the measurement of the shape instability of the solid-liquid interface during solidification. The data is analyzed by employing the Mullins-Sekerka theory of interfacial instability. In this method, the velocity of a planar solid-liquid interface is increased

until the interface becomes morphologically unstable. The interface takes on a wavy (periodic) surface characteristic which increases the interfacial area. The resulting change in the system energy depends on the magnitude of the interfacial energy. The method cannot, as yet, be applied to faceting materials or probably to materials having a large solid-liquid interfacial anisotropy. The best application has been to transparent materials, and the significant documented experimental measurement was performed on the ice-water interface [79].

The previous section dealt with the formation of a grain boundary groove in a temperature gradient. A measured value of the solid-liquid interfacial free energy can be obtained through geometrical analysis of such grooves.

A few methods of analyzing these grooves can be employed. First, it is necessary to prepare a photomicrograph of a groove which may appear much like Fig. 8.3. Using the Bolling and Tiller equation in the previous section, a series of calculated curves can be drawn, to the same magnification as the photomicrograph, knowing the experimental temperature gradient and the entropy of fusion for the material, and using the interfacial free energy as a parameter from one curve to the next [10]. An estimate of the interfacial free energy can then be made by comparing the calculated curves to the photomicrograph. This method was first applied by Morris [42] for

a grain boundary groove in lead. In this experiment a small quantity of antimony was rejected at the interface, during freezing at a very slow rate; then the specimen was quenched and sectioned. A special etchant brought out the groove shape by preferential attack of the segregated layer of antimony. This appears to be the only application of any of the grain boundary groove methods to a metal [42].

The grain boundary groove technique has been applied to a system containing solute by Jones and Chadwick [13], who determined γ_{SL} for ice-water interfaces, with varying salt concentrations present, using the Bolling and Tiller analysis. Results from this work show that the grain boundary groove technique can be applied to impure materials.

Two additional methods were recently developed for determining the interfacial free energy from analysis of grain boundary groove shapes. The first, the Glicksman and Nash analysis, assumes that the solid-liquid interfacial free energy is isotropic, as Bolling and Tiller did, but the Glicksman and Nash analysis allows for the difference between solid and liquid thermal conductivities and for the influence on groove shape by the proximity of the neighbouring grain boundary grooves. This method of analysis was adopted for use in this report. The second method of analysis by Arbel and Cahn [37] utilizes "vector thermodynamics" and differs from the others since the interfacial anisotropy is quantified. This generalized analysis would also apply to solid-vapour, solid-solvent or

solid-solid interfaces with grain boundary grooves in a thermal or gravitational gradient. A simple modification for unequal thermal conductivities is included in this analysis.

The last three methods to be described are all based upon contact angle measurement.

In an early paper by Glicksman and Vold, the dihedral angle formed at the trijunction of a grain boundary groove was measured for pure bismuth in a transmission electron microscope [80, 63, 79]. The interface was formed in situ by partially melting a thin foil of the metal with the electron beam. Low angle, symmetrical grain boundaries were studied. The misorientation between the grains was measured using diffraction patterns and the Read and Shockley [80] dislocation model used to determine the grain boundary energy. The solid-liquid interfacial free energy was then derived from the dihedral angle measurement.

The dihedral angle at the trijunction of a grain boundary groove can also be used to determine the solid-liquid interfacial free energy when the grain boundary is a general high angle boundary. In order to perform the calculation, the energy of the grain boundary must be known from another method.

The ratio between the solid-liquid and the grain boundary interfacial energies are sometimes measured by metallurgists. An independent measurement of the grain boundary energy would then give the γ_{SL}. This ratio was measured using

dihedral angle measurements of the junction between the solid-liquid interface of alloy melts and a random, high-angle grain boundary (Miller and Chadwick [81]). The relative energies were plotted for various compositions of a system, and the γ_{SL} data extrapolated to the pure solvent value. The ratio ($\frac{\gamma_{SL}}{\gamma_{GB}}$) for pure metals appeared to be a constant having a value of approximately 0.45. This value differs from that predicted by the homogeneous nucleation theory [81].

The solid-liquid interfacial energy of an alkali halide and its melt has been measured using a sessile bubble technique. A bubble of argon was placed onto the submerged surface of a Czochralski crystal. Growth of the crystal continued in order to freeze the bubble in place. The contact angle was then measured from a cross section through the bubble and crystal. The angle that was measured represents the angle formed between the liquid-solid surface and the bubble-liquid surface at the point of contact prior to further freezing. This is a form of wetting angle measurement [82].

If the solid-vapour and liquid-vapour interfacial free energies are known or can be measured, one can derive the solid-liquid interfacial free energy through Young's equation:

$$\gamma_{SV} - \gamma_{SL} = \gamma_{LV} \cos \theta_e \qquad [83, 63]$$

where θ_e is the equilibrium contact angle at the three phase junction, and the remaining terms are as defined previously [83, 63].

The magnitude of γ_{LV} for most materials is the least difficult of the interfacial free energies to measure. The γ_{SV} is probably the most difficult to measure. The surface free energies of non-metal interfaces have been measured by others in many fields. The properties of the systems studied allow the evaluation of the various interfacial free energies using methods based on capillarity and contact angle measurement. For example, methods for the measurement of γ_{SV} of various materials have been developed in the past [45,83,85] and then the value combined with the measured value of γ_{LV}, for example, in Young's equation ot obtain γ_{SL}. Such a method for measuring γ_{SL} is that of Neumann [83]. Simply, a smooth solid substrate is produced onto which a variety of liquid compounds are placed in contact in such a way to measure the contact angle of the sessile drop. Specifically, Young's contact angle is assumed to have been measured [83]. The liquids are selected such that $\gamma_{SV}<\gamma_{LV}$. A correlation is made between the measured angles and the known values of the various values for the liquids' γ_{LV}. The details of how one calculates γ_{SV} (substrate) are left to the reader. Neumann maintains that only one contact angle/ liquid combination is needed to obtain γ_{SV}. Water and some of the organic materials used for solidification models are among the list of measured data. Interestingly, all γ_{SL} for these compounds have values less than 1 erg/cm^2. Unfortunately, this method for measuring γ_{SV} will probably not be applicable to metals (author's comment).

Another technique for measuring γ_{SL} has evolved from such work as referred to above. In this method, by Neumann et al. [85], small particles with known surface free energies, are observed either to be engulfed or pushed by a slowly advancing solid-melt interface. A particle is engulfed if it is energetically favourable to replace particle-melt interface by the particle-solid interface. For a particle to be engulfed, the free energy of adhesion, ΔFa , must also be negative. $\Delta Fa = \gamma_{PS} - \gamma_{PL} - \gamma_{SL}$

where γ_{PS} is the particle/matrix interfacial energy

γ_{PL} is the particle/melt interfacial energy

γ_{SL} is the solid-melt interfacial energy.

When the interfacial free energies other than the γ_{SL} are known, observations of the particles at solidification fronts will give a measure for the solid-melt interfacial free energy. Again, full details for the interested reader are found in [85]. Typical values for γ_{SL} for the materials tested in this way are less than 0.01 erg/cm^2, and coincide with measurements obtained using other methods within the field of surface chemistry.

8.2 Analytical Methods and Materials

8.2.1 Organic Analogues for Metal Solidification

The use of organic models for solidification has truly increased the understanding of the freezing behaviour of metals and alloys. The use of transparent materials which freeze as metals do was pioneered by Jackson and Hunt [1, 3, 2, 4, 7, 8]. There is a major reason some organics can be models for metal solidification. Jackson attributes this to the low entropy of fusion for these organics [3, 4, 1]. This is believed to be due to the fact that the molecular shapes of these organics are spherical or compact. The name coined by Timmermans was "globular molecules" [50].

The crystal structure is also metal-like since the molecular packing arrangement leads to a cubic or close packed structure [51, 1]. The cubic structure is frequently found only in the highest temperature (solid) phase. The low entropy of fusion is compensated for, at lower temperatures, by a solid state phase transformation in which the majority of the remaining entropy is recovered. The cubic crystal structure gives these materials another metallic property, that of plasticity [50, 51]. As a group, these materials are rare and unique among organic solids.

The organic model materials also have other advantageous characteristics. One is the low fluid viscosity of the melt. This also helps to make solidification behaviour more metal-like.

Transparency is an obvious advantage while the low melting points further reduce the difficulty in observing the desired behaviour.

There are two disadvantages to organic models. As they have no structural use, as metals have, these materials are not as well studied nor are their properties well documented. The second disadvantage, with regard to metallic models, is that organics have much lower thermal conductivities than metals. For a metal, the typical thermal to chemical diffusivity ratio is 1000, while for an organic it is only about 10 [5]. Certain solidification phenomena in metals are directly attributable to high heat flows and rapid freezing velocities. Glicksman [5] feels that, because of this, organics should be studied with relatively low interface speeds.

Jackson and Hunt combined some organics in an effort to study polyphase solidification. They found several interesting systems and observed their growth characteristics [2]. Their observations led to the classification of eutectics into three categories, based on freezing morphology:

1. The nonfaceted - nonfaceted type, in which both phases of the eutectic freeze without any faceting surfaces.

These generally form lamellar structures and both phases behave in a metallic fashion.

2. The nonfaceted - faceted type, in which one phase has a higher entropy of fusion and grows in a faceted manner. The faceting phase is believed to represent the freezing behaviour of semi metals like silicon or intermetallic compounds.

3. Both phases are faceted, and crystals of each phase grow independently into the liquid at the freezing front. Such systems do not show metallic behaviour.

It was during this survey of organic eutectics that Jackson and Hunt came upon the system used in the present study, the Carbon Tetrabromide - Hexachloroethane system. In an important paper, [8] this system was used to illustrate how a real lamellar eutectic interface appears. Micrographs of the solid-liquid interface were used to support the mathematical analysis put forth in the paper to explain the mechanism of lamellar and rod eutectic freezing. As a model for metallic eutectic freezing, this system was ideal. Of major importance was the large lamellar spacing which formed in this system. There are, to date, no other eutectics, either organic or metallic, which have such large lamellar spacings. In other systems, an electron microscope would be required to obtain as clear a view of the solidifying front as can be achieved here with an optical microscope.

The most frequently used method to observe transparent

organic solidification involves the preparation of a thin, almost two-dimensional cell. An interface is formed across the cell by developing a controlled temperature gradient along the cell using a temperature gradient stage. There are several designs of a temperature gradient stage [60, 61, 1, 5, 9, 10, 42]. Interface movement may be obtained by moving the cell relative to the stage, with a virtually stationary interface relative to the microscope optics, or by gradient freeze, where the gradient moves, and the interface follows. The interface can then be viewed optically, in transmitted light, as a nearly two-dimensional feature.

8.2.2 The Glicksman and Nash Technique for Measuring the Solid-Liquid Interfacial Free Energy From Grain Boundary Grooves

In section 8.1.3, the principles of a technique for the derivation of interfacial free energy from analysis of grain boundary grooves was outlined. In general, however, the condition of equal thermal conductivity of liquid and solid required by the Bolling and Tiller analysis, in 8.1.2 and 8.1.3, described earlier, is not met. More recently, Glicksman and Nash [12] have extended the analysis of grain boundary grooves to include the dependence of groove shape on differences in thermal conductivity between solid and liquid and also on the effect of another, nearby grain boundary. In order to account for these variables, they used a computer program to solve the new equations and boundary conditions. They also introduced a new, simple scheme to perform the geometrical measurements from grain boundary groove shapes to obtain γ_{SL}. Fig. 8.4 shows the construction used for the measurements. Detailed knowledge of the root of the grain boundary cusp is not necessary; the only additional variable required is the ratio, R, of solid to liquid thermal conductivities. In the Glicksman and Nash method, the distances, d, and λ , are measured (on a photograph of the boundary groove) and combined to give $\delta = d/\lambda$. The definitions of d and λ are given in Fig. 8.4. A unique value of θ^2 (defined below) is then selected from the computer generated curve of δ vs θ^2 for the appropriate R. The term θ^2 is a parameter used in the

Glicksman and Nash method, $\theta^2 = \gamma_{SL}(\lambda^2 \Delta S_f G_s)^{-1}$. (The term G_s, is the thermal gradient in the solid.) Three curves are presented in Fig. 8.5 for three values of R: 0.5, 1.0, 2.0. γ_{SL} is then obtained from the equation: $\gamma_{SL} = \theta^2 \Delta S_f G_s \lambda^2$.

To date, this technique has only been applied to pure materials and, most often, to transparent ones. [11, 12, 16, 37, 79] In the work reported here, the technique was adopted to quantify the interfacial energies in a eutectic system. The analysis of the eutectic requires the measurement of γ_{SL} for binary alloys in the composition range of the eutectic.

Details of how the Glicksman and Nash method was used in this work, are found in Procedures, Section 9.4.8.

Fig. 8.4

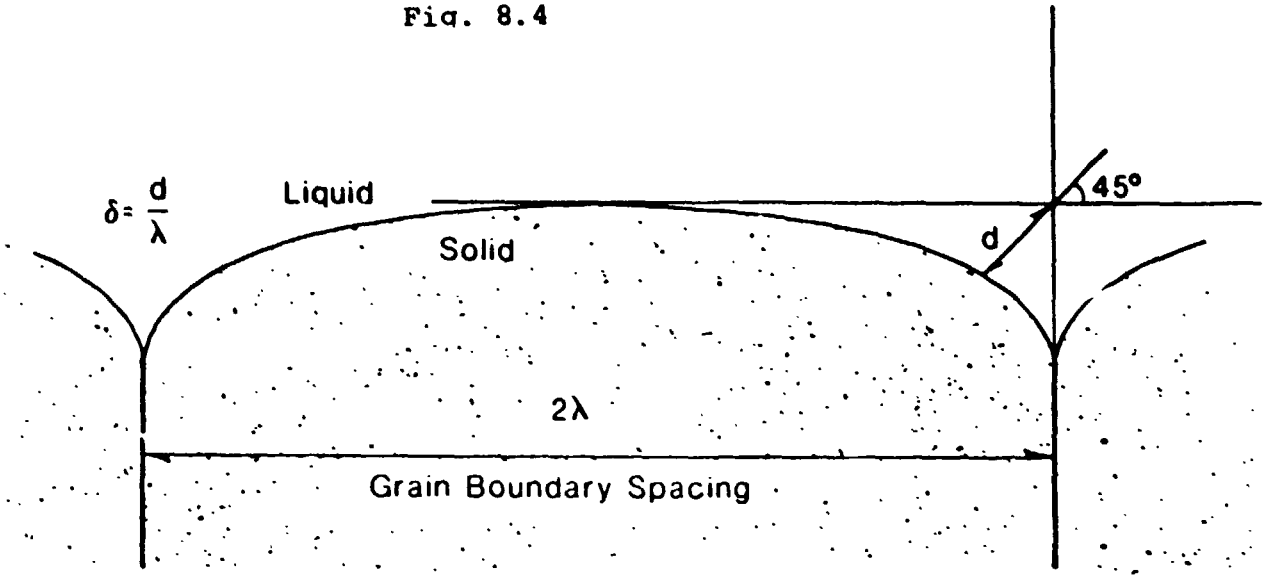

GLICKSMAN & NASH GROOVE MEASUREMENT GEOMETRY

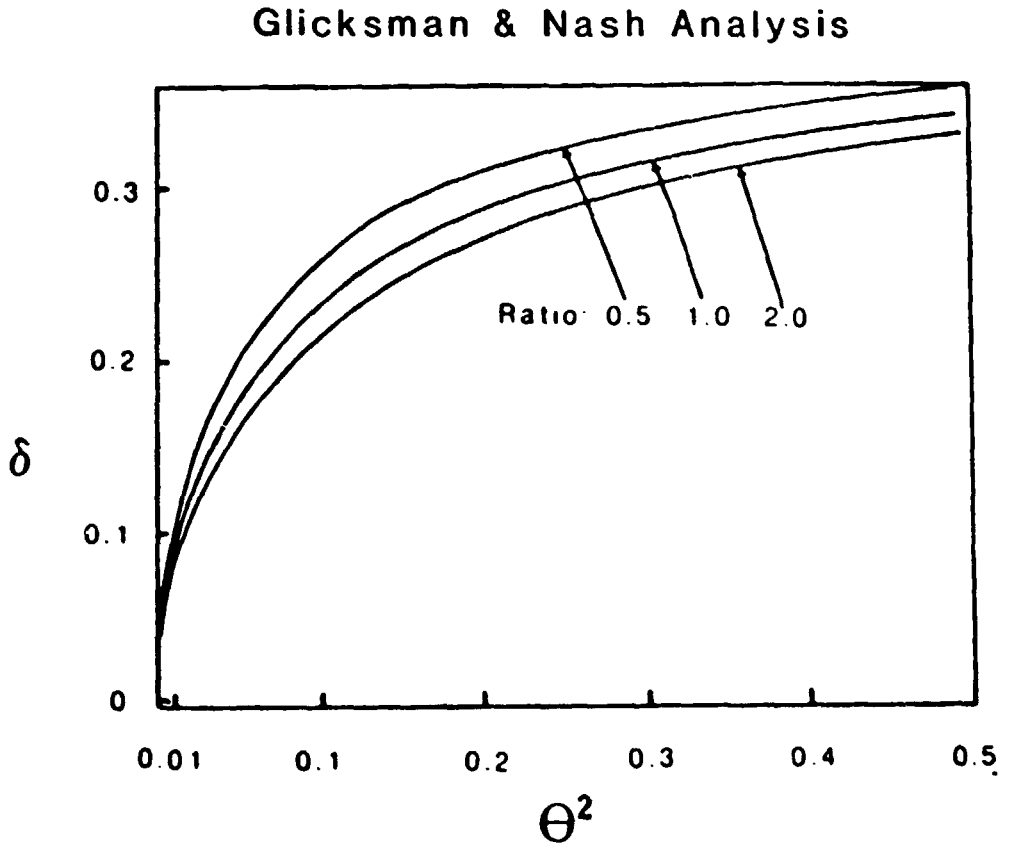

Fig. 8.5

8.2.3 Eutectic Interface Analysis (Shape)

A great deal of emphasis has been placed earlier in this report on the importance of measuring solid-liquid interfacial energies from grain boundary grooves. The ultimate purpose of performing the measurements was to apply the results quantitatively to the growth of a lamellar eutectic. In the past, quantitative measurements of eutectic alloys have only been performed on sectioned castings, or undirectionally grown samples. The ability to view, in situ, a growing eutectic interface (as done here) provides valuable information (both qualitatively and quantitatively) concerning the mechanism of the eutectic solidification process.

Effectively, the representation to the observer of the growing, lamellar eutectic interface generated with the apparatus described here, has only two dimensions. Photomicrographs of the interface were analyzed to obtain a variety of quantities which serve to characterize the interface. Graphic information from the micrographs was entered into a computer through a digitizer (see Section 9.4.9). In this way, shapes, angles and spacings were measured and the measurements further processed to obtain information about the curvature of the solid-liquid interfaces, angles of the phase boundaries at the trijunction, lamellar spacings, volume fractions, and the degree of undercooling present during freezing.

The quantities which were measured (see Section 9.4.5)

are summarized below:

(a) lamellar spacing vs. growth rate;

(b) volume fraction of the minor phase;

(c) volume fraction vs. growth rate (for one alloy);

(d) solid-solid interphase interfacial free energy, $\gamma_{\alpha\beta}$, and the torques found to act on this phase boundary;

(e) solid-liquid interfacial free energy of minor phase, $\gamma_{\beta L}$;

(f) solid-liquid interfacial free energy of major phase, $\gamma_{\alpha L}$;

(g) local curvature and undercooling everywhere on solid-liquid interface.

8.2.4 Literature Value for Properties of the Compounds Carbon Tetrabromide and Hexachloroethane

Selected properties of the two compounds used in this work are presented here in Tables 8.1 and 8.2. The data and source are given together.

Table 8.1 Carbon Tetrabromide (CBr_4)

Other name: Tetrabromomethane Molecular weight: 331.65 Melting temperature for α form: 90.1°C Boiling point: 189.5°C Monoclinic to octahedral transition temperature: 48.4°C Specific gravity: 3.42	Reference 64
Face centred cubic structure @ melting point $\Delta S_f / R = 0.79$	Reference 1
D_x (x-ray calculated density), cubic, 3.345	Reference 56
Transition temperatures (m - o) 46.85, 46.91, 46.9, 46.0°C ΔHt 4.282 cal. 15°/g ΔH melt 2.85 cal. 15°/g	Reference 53
Vapour pressure 298°K to the melting point: $\log p = \frac{-2650}{T} + 8.78$ mm Hg	
ΔH melt 3.957 kJ/mol @1 atm. 90°C ΔHt 5.95 kJ/mol @1 atm. 47°C ΔH evaporation 44.4 kJ/mol @1 atm. 190°C	Reference 57
ΔH melt @363.2°K 950 cal/mol of β Molecular weight: 331.68 for α	Reference 55
ΔSt 4.98 cal/mol deg ΔSm 2.60 cal/mol deg	Reference 46
Melt viscosity ≈1 poise	Reference 47
Vapour pressure of cubic CBr_4 Temperature range (47.89 - 55.76°C): $\log p = 8.567 - \frac{2578.9}{T}$ mm Hg ΔH sublimation 11,800 ± 300 cal/mol ΔS sub. @ 1 atm. 26.0 ± 0.8 cal. mol^{-1} deg^{-1}	Reference 48
ΔS_f 2.6 cal/deg mol.	Reference 49
γ_{LV} 49.6 ergs/cm^2	Reference 45

Table 8.2 Hexachloroethane (C_2Cl_6)

Other name: Perchloroethane Molecular weight: 236.74 Density: 2.09 gm/cm^3 Boiling point (triple point): 186.8°C ΔH sublime: 12.2 k cal/mol	Reference 52
Density: 2.091 gm/cm^3	Reference 64
There are three crystalline isomorphs. Rhomohedral melting point in a sealed tube. (186.8 - 187.4°C)	Reference 58
Cubic form: a = 7.51 Angstroms D_x = 1.856 gm/cm^3 or: a = 7.45 @ 80°C 7.32 @ 100°C	Reference 56
Transition temperatures: rhombic - triclinic 43.6°C triclinic - cubic 72 °C	Reference 53
melting point: 184.5°C boiling point: 186.8°C d_4^{20} 2.091 gm/cm^3 ΔH evaporation @ boiling point: 46.4 cal/g	Reference 54
lattice constant: 7.43 Angstroms	Reference 50

9. EXPERIMENTAL EQUIPMENT AND PROCEDURES

9.1 Temperature Gradient Microscope (TGM)

The primary experimental apparatus that was used in the present study will be described in this section. The apparatus has been named the "Temperature Gradient Microscope" (TGM). Its purpose was to permit the formation of solid-liquid interfaces under closely controlled conditions and to facilitate the observation of their characteristics. The instrument is itself made up of three principal subsystems; the optical, thermal and mechanical subsystems. The optical system consists of a microscope, light sources and cameras. The thermal system is the temperature gradient specimen stage, and the mechanical system is the motorized drive assembly used to push or pull a cell filled with the organic alloy.

Temperature gradient stages for similar applications have been described elsewhere [60, 61, 1, 5, 9, 10, 22, 42]. Most of these have followed the design first given by Jackson, Hunt and Brown [61]. The temperature gradient stage consisted of two temperature controlled blocks of metal (approximately 3 x 5 x 0.5 centimeters). A sandwich of alloy and thin glass plates sealed at the edges straddled the gap between the blocks. The block temperatures are adjusted to position the interface between the blocks. This design had potential difficulties which are overcome in the following design. The major

deficiency was the low resistance of the cell and temperature gradient stage to thermal transients. The design was not conducive to the production of high quality micrographs as well.

Good control of a slowly growing interface in a shallow temperature gradient was difficult because slight thermal fluctuations caused large interface movements. For example, the interfaces were not protected from environmental thermal transients, only thin glass plates contained the alloy, thus placing the thin organic layer and the interface in a thermally unstable environment. The temperature gradient was developed between metal blocks held at the required temperatures. Such blocks could not afford significant thermal mass to help resist thermal fluctuations caused by temperature controllers or atmospheric convection. The design readily permits the application of steep thermal gradients to the specimen. However, low thermal gradients were not easily obtained, certainly not with good thermal stability as well.

Usually small, slow speed motors were used to push the cells. Large adjustments of speed and direction reversals (for melting) were not commonly provided. The motor was frequently mounted to the stage and could introduce vibrations. This would pose a problem during the photography of the interfaces at high magnification.

The following design criteria were applied to the apparatus constructed for the present study:

1. Excellent thermal stability was required.
2. A precise, constant speed with a wide range of adjustment was required for moving the cells.
3. The highest possible optical magnifications and resolutions were needed, but without thermal interaction between the cold optics and the growing interface.
4. High mechanical stability was needed to minimize blurr in the micrographs.
5. High intensity illumination was desired, to shorten exposures and thus sharpen photographic images.
6. The temperature that the "liquid" end of the cell would be subjected to should be kept as low as possible to minimize the possibility of alloy degradation and to prevent leakage or explosion of the cells due to the relatively high volatility of the organic materials used.
7. Low thermal gradients were needed to exaggerate interface phenomena, such as grain boundary groove contours.

The apparatus shown in Fig. 9.1 satisfies these requirements.

The most significant design change from [61] is the new method of developing a temperature gradient in the sample. The organic filled cell rests inside a deep channel which has the temperature gradient developed along its length, in the surrounding walls of the channel. The cell is practically surrounded by the needed thermal environment. A high thermal

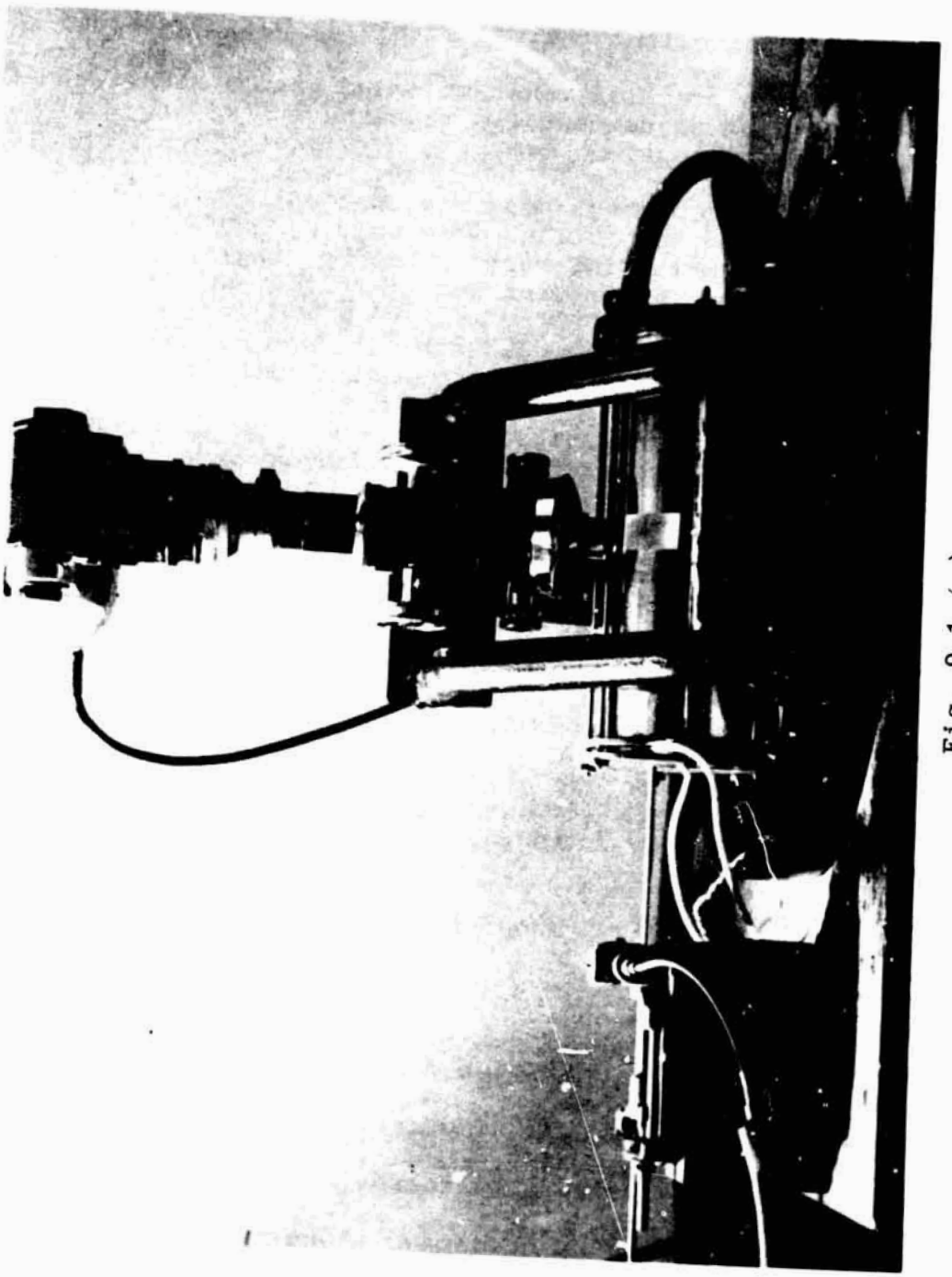

Fig. 9.1 (a)
The Temperature Gradient Microscope

Fig. 9.1 (b)
Cross Section Through TGM
1.1X Actual Size
Section taken through glass
insert and specimen

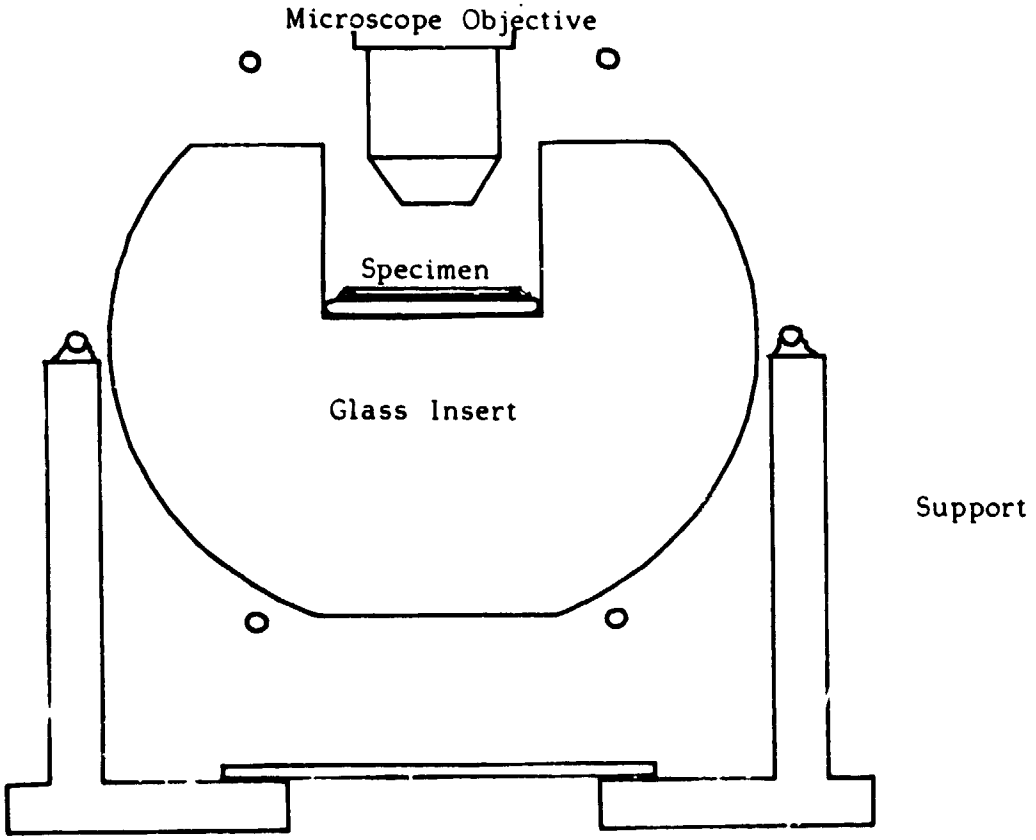

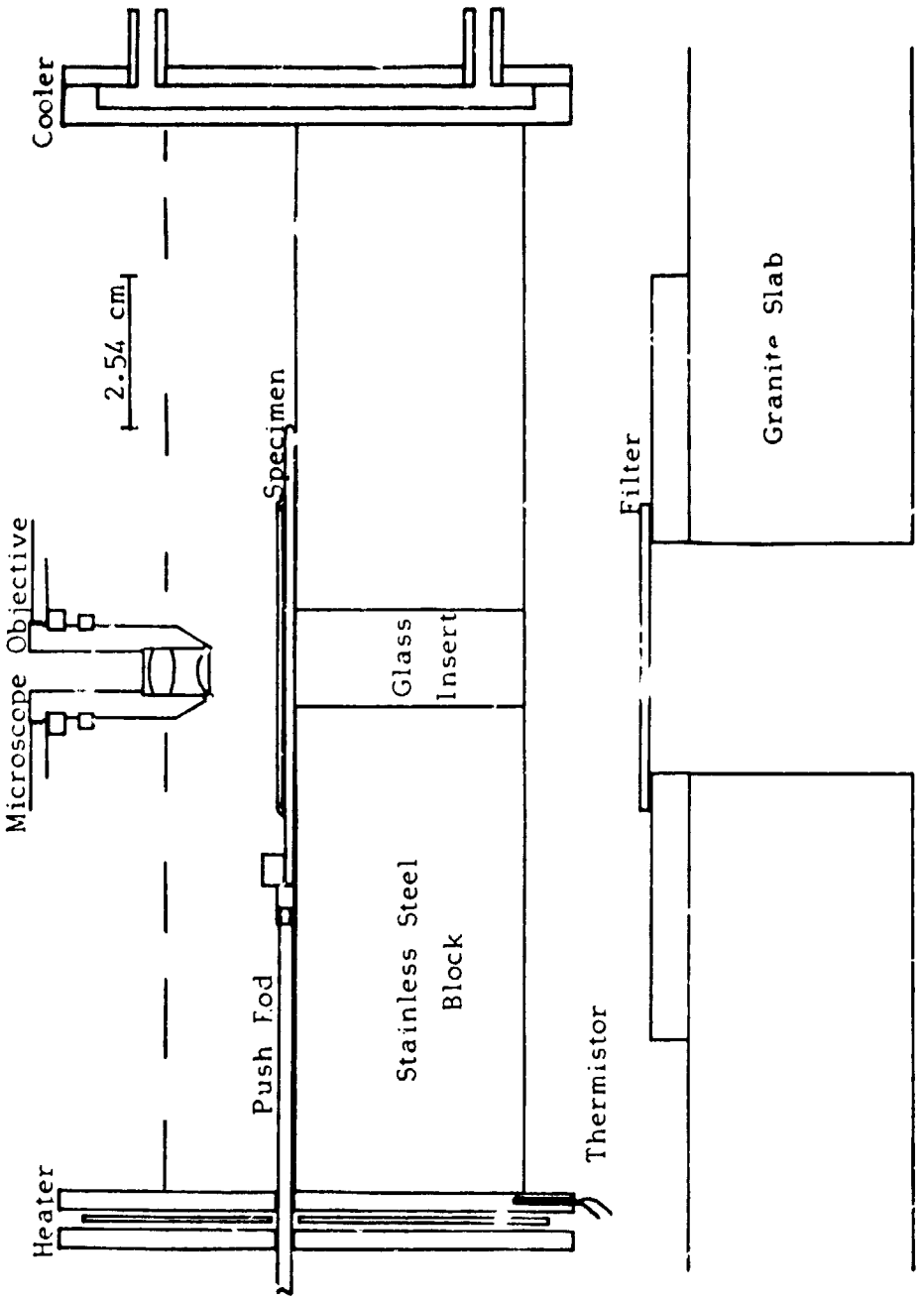

Fig. 9.1 (c)
Cross Section
of TGM
Longitudinal
Section

mass prevents thermal transients from influencing the interface shape or position.

Maximum interface position stability would result by completely surrounding the cell by the thermal environment. However, the deep channel was made to permit insertion of the sample, to guide the cell during growth, and to provide clearance for the microscope optics. A glass insert was placed between the stainless steel blocks to transmit light and to steepen the temperature gradient a slight amount. (See Fig. 9.1) The upper and lower surfaces of the glass insert were polished optically flat and parallel to one another. The metal blocks were machined from 310 stainless steel. This steel alloy had the lowest thermal conductivity of any metal and a large heat capacity. The high thermal resistance prevented thermal transients from reaching the interface during growth. The copper end plates served to distribute the heat uniformly over the whole face of the end of the stainless block. The heater consisted of a wire wound "pancake" resistance element sandwiched between the copper plates. The assembly was temperature controlled by a thermistor and custom designed proportional control circuit (see Appendix for circuit) that regulated temperatures to within 0.1 degrees at the hot end. The other copper end plate is best thought of as a "cooler". This end plate was hollow and had temperature controlled water passed through it. These copper assemblies were fixed to the stainless blocks by six threaded rods also

of stainless steel. (See Fig. 9.1) In addition, the area of contact (between copper and the stainless steel) was filled with lead-tin solder to ensure conductance of heat.

The microscope used was a standard metallurgical miscroscope. The tube and focussing gears were mounted on a sturdy steel frame (Fig. 9.1). Most of the micrographs were taken using a special, long working distance (1.1 cm), high power (32x) objective (Leitz UMK 50). A 35 mm reflex camera, or a television camera could be attached to the microscope by means of suitable couplings. The images were formed by projection from the microscope eyepiece, with no camera lens.

A dual light source was constructed. It consisted of an electronic flash tube and reflector assembly, mounted above a quartz-halogen low voltage incandescent lamp. Light from the incandescent source passed through a hole in the reflector of the flash tube assembly and through the glass flash tubes into the glass insert of the Temperature Gradient Microscope. The flash apparatus was also specially constructed and employed two flash tubes mounted side by side in order to obtain even illumination. The flash was synchronized with the camera. The light source was situated directly below the Temperature Gradient Microscope and aligned with the glass insert and microscope. All of the light was filtered with a blue dichroic filter mounted above the flash tubes. The heat generated by the incandescent lamp and flash tubes was

dissipated with a constant stream of pressurized air directed over their surfaces.

The Temperature Gradient Microscope sat on a large (60 cm x 45 cm x 5 cm thick) granite slab which, in turn, lay on a fully inflated automobile tire and rim. An opening was cut in the wheel to accommodate the light source. The substantial weight of the Temperature Gradient Microscope and granite slab when combined with the tire gives excellent pneumatic vibration isolation.

The last part of the apparatus is the mechanical drive used to move the cells. A seventy-two step stepping motor is the heart of this assembly. Each step of the rotation was controlled by a variable oscillator circuit. (See Appendix for circuit.) The motor could rotate clockwise or counterclockwise with a 300:1 speed range. Motor speed was very constant over long periods of time (maximum $\pm$ 0.015 percent) once set. Reproducibility of the speed setting was limited by the use of a dial ($\pm$ 3 percent in the slow speeds). Motor rotation was monitored digitally from the shaft when precise speeds were needed or accurate knowledge of the cell's position was needed. The linear pushing rate was 15.625 micrometers per revolution of the stepping motor. A flexible coupling transmitted the shaft rotation to the reduction gear and threaded rod linear translator which rested on the granite slab. This arrangement served to isolate the motor vibrations from the Temperature Gradient

Microscope. The moving part of the linear drive had attached to it a stainless steel push rod. This rod passed through the heater end of the Temperature Gradient Microscope to couple with the cell. At the end of the rod was fixed a permanent magnet. At the hot end of some cells, a mild steel block was attached. The rod would then be able to both push and pull the cell through this magnetic coupling. Direction changes were accomplished by switching the motor rotation electronically.

With the apparatus, temperature gradients from five to twenty eight degrees Celsius per centimeter and growth rate down to 0.13 micrometers per second could be attained.

9.2 Operation of the Temperature Gradient Microscope

To initiate an experiment, the temperature control systems were activated, causing the desired temperature distribution to form and reach steady state. A waiting period of over one hour was required to achieve steady state due to the large thermal mass of the stainless steel blocks. The selected microscope objective was positioned near its working location so that it also could come to thermal equilibrium with the rest of the apparatus. Most experiments were performed with the cold copper end plate at zero to ten degrees Celsius, and with the hot copper end plate at a temperature as high as but usually less than one hundred and sixty degrees Celsius. The end temperatures could be adjusted to give any desired temperature gradient across the glass insert, from five to twenty-seven degrees Celsius per centimeter.

A cell, made as described in section 9.3, was then placed in the Temperature Gradient Microscope channel, and the push rod connected to the cell using the magnetic coupling. Through the microscope, the equilibrating interface was observed, using the incandescent light source. Draught shields were usually laid across the top of the channel to exclude air currents. It was found that the interface usually

reached an equilibrium position and remained stationary within five minutes of placing the cell in the Temperature Gradient Microscope.

A suitable motor speed and direction were then chosen and the power applied to move the cell. The relationship between motor RPM and cell velocity is given as an equation in the Appendix. Observations of the interface could be made visually via the microscope eyepiece or through the reflex camera, or on a television monitor. The flash, synchronized with the camera, was used when an exposure was made. It was necessary to move the microscope assembly in order to scan the morphology of the interface across the width of the cell.

A stationary eutectic interface could be obtained with this apparatus using the CBr_4 - C_2Cl_6 organic system. This was accomplished by first establishing eutectic growth with a planar interface at a velocity from two to eight micrometers per second. Then, over a period of fifteen to thirty minutes, the growth rate was gradually reduced by hand to a speed of one or two micrometers per second. Sample motion was then stopped and, to ensure that the interface was at zero velocity, a waiting period of up to ten minutes was allowed. Under certain circumstances, such interfaces could be maintained for up to twenty minutes.

The optics for photomicrography were standardized and the resulting magnifications onto the camera film plane

were measured with a stage micrometer, giving the results shown in Table 9.1.

Magnification on 35 mm Film

Table 9.1

5x	UMK50 objective	41.03x
8P eyepiece	" "	85.1x
10P eyepiece	" "	107.2x

All magnifications have ±0.2 percent accuracy.

The negatives could be enlarged ten to fifteen times or projected onto the digitizing tablet at twenty times. The television camera/monitor combination was also calibrated. The Sony 20-inch monitor, with the UMK50 objective and 8P eyepiece yielded a magnification of 984 times on the screen.

Photographs were taken using a special, high contrast, high resolution, medium speed black and white 35 mm film. The best film was found to be SO-115 and an alternate choice was High Contrast Copy Film, both manufactured by Eastman Kodak Co. The film was handled in the manner recommended by the manufacturer. When photographs of the interface were taken, a record of the motor RPM, selection of objective, eyepiece, filter, lighting, time of day and film frame number was made to accompany the photographic record.

Reliability of the Temperature Gradient Microscope short-term thermal stability was verified by using a dummy cell with a thermocouple embedded in epoxy. This cell was used to measure the magnitude and linearity of the temperature gradient by slowly pushing the cell along the surface of the glass insert

of the Temperature Gradient Microscope so that the thermocouple bead traversed the insert to measure its temperature. This procedure was repeated at widely different speeds (1, 10, 100 motor RPM). Over the speed range used in the solidification studies, ie., 0.13 to 20 micrometers per second, there was no measurable thermal lag between the thermocouple and the apparatus. Only at the highest velocities did the measured gradient differ from that taken at a very slow scan. This verifies that the interface temperature follows the local apparatus temperature over the large growth rate range (usually 0.13 to 10 micrometers per second). The thermal lag observed at high cell velocities was probably caused by the low thermal conductivity of the thick bottom of the cell.

The thermocouple/chart recorder combination was not adequately sensitive to test the long-term stability of the temperature profile on the glass insert. However, it is estimated that temperature fluctuations were less than 0.01 degrees Celsius over a ten-minute period, at any given location, based on the behaviour of solid-liquid interfaces held at zero velocity.

9.3 Organic Alloy Cell Designs

9.3.1 The Basic Cell

The basic cell used in this work is shown in Fig. 9.2. It consists of a standard microscope slide to which is glued a coverglass, forming a thin cavity to contain the organic material under study. Cells produced in this way varied in thickness from thirty to one hundred and fifty micrometers. The glue used was an epoxy type. Both an opaque, industrial epoxy with mineral filler, and the clear "Mastercraft" brand five-minute epoxy were found satisfactory. Certain other epoxy glues were not satisfactory.

Cells were filled with the organic material in either of two ways:

1. Small pieces of organic alloy were placed on a microscope slide and covered by a coverglass. Gentle heating melted the organic material so that it spread under the coverglass, producing an even, thin, void-free layer. After cooling, the cell edges were sealed on all four sides with epoxy.

2. A coverglass was preglued along three edges onto a microscope slide, leaving one long side open. (The glue acted as a separator between the glasses.) The empty cell was then filled by immersion into the melted alloy held at one hundred degrees Celsius in a container, immersed in a water

bath. The organic filled the cell by capillarity. The cell was sealed after the fourth edge was cleaned. If the space between the glass slides was too large, the melt was not retained when the cell would be removed from the immersion apparatus. This resulted in a limitation on the cell thickness that could be filled using this method.

Final steps of cell preparation consisted of cementing a second coverglass over the first, leaving an air space, and of the attachment of the small steel block at one end to form the magnetic coupling to the push rod of the Temperature Gradient Microscope. The second coverglass rested on the raised edge of the glue and acted to shield the specimen from draughts and from the "heat sinking" effect of the microscope objective.

Fig. 9.2

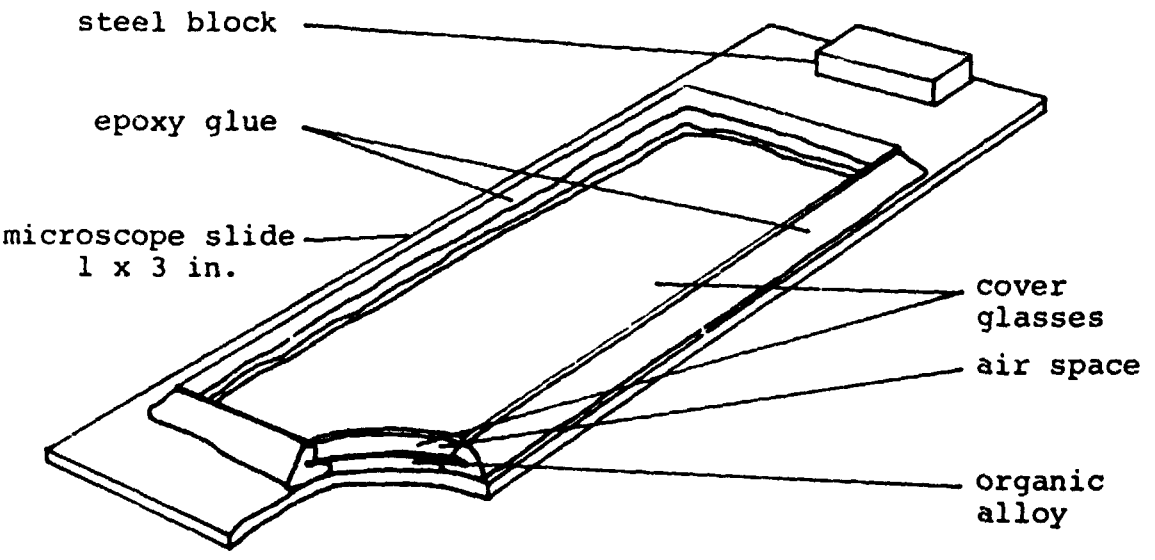

The Basic Cell

9.3.2 The Forced Convection Cell

In order to see the effect of altering the solute distribution in the liquid ahead of the solid interface, a series of convection cells were developed. Three basic types were utilized:

1. Simple Convection
2. Isothermal Convection
3. Pure - Impure Alloy Convection

First, the working principle of the convection cell will be described. Inside a basic cell (section 9.3.1), strategically placed solid barriers were fitted. Outside the cell, on the coverglass, a convection lever was fastened, using epoxy cement as shown in Fig. 9.3. Convection was induced within the cell by flexing the coverglass with the attached lever. This forces the melt under the coverglass to flow around the barriers in the cell. The cells were filled in the same way as basic cells, by submersion. The third side of the cell was not sealed prior to filling.

In practice, the cell was placed in the Temperature Gradient Microscope channel and stabilized with lead weights at each end of the cell. The solid-liquid interface was grown, as usual, in the cell but not allowed to solidify up to the barrier. Convection was initiated by displacing the end of the lever laterally for various distances and at various rates. As shown in Fig. 9.3, the base of the lever pivots on the barrier built into the cell, so that lever movement caused

liquid on one side of the barrier to be compressed, while that on the other side became expanded. Thus, the convecting liquid was forced to flow around the barrier and swept across the solid at the interface. In this way, precise manual control of the rate and direction of convective flow was obtained.

Due to the kinetic nature of such studies, visual analysis was performed utilizing video recording equipment and sequences of the experiment repeatedly studied. Quantitative measurements were not performed.

When tested, the simple convection cell worked admirably, but it was evident that the liquid being convected was hotter than that which it replaced. To perform a convection experiment in which the convected liquid temperature was the same as the liquid being replaced, the isothermal convection cell was designed. (See Fig. 9.3) In this cell, the barrier extends laterally within the cell to run parallel to the solid-liquid interface. The fluid in the channel between the interface and the barrier flows parallel to the isotherms and in a manner known as "plug" flow. The convection displacement was reduced as that liquid from the warmer part of the cell would not enter the field of view, often located in the centreline of the cell.

The third cell design (not illustrated) was similar to the convection cells described above, but contained two alloy compositions. The cell was filled in a slightly different way. The portion of the cell without the barriers was submerged in the higher melting point alloy up to the barrier position. The

cell was withdrawn from the melt, allowing the alloy to solidify, and then the other portion of the cell was filled by submerging into a melt of lower melting temperature alloy (e.g. an impure alloy) up to the solidified alloy level. The cell was then sealed and used as any other convection cell. The exception in the operation of the cell was that convection was used to quickly replace "pure" liquid at the solid-liquid interface with "impure" liquid, perhaps at the same temperature. Use of a coloured impurity showed that there was no significant liquid diffusion which would have mixed the impure and pure alloys prematurely.

Fig. 9.3(a)

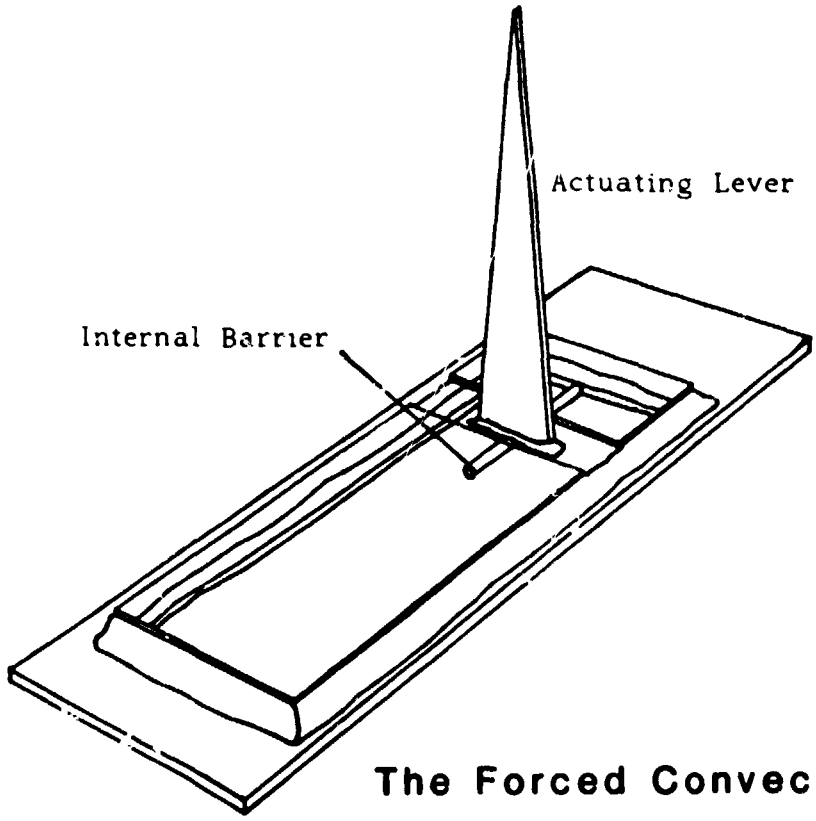

The Forced Convection Cell

Fig. 9.3 (b) Top View of Isothermal Convection Cell

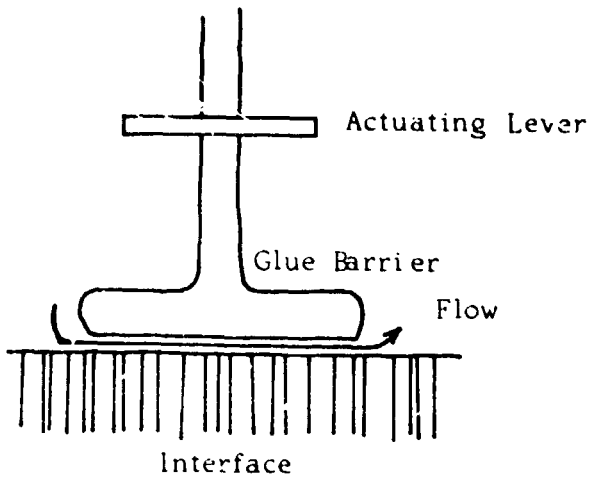

The Isothermal Convection Cell

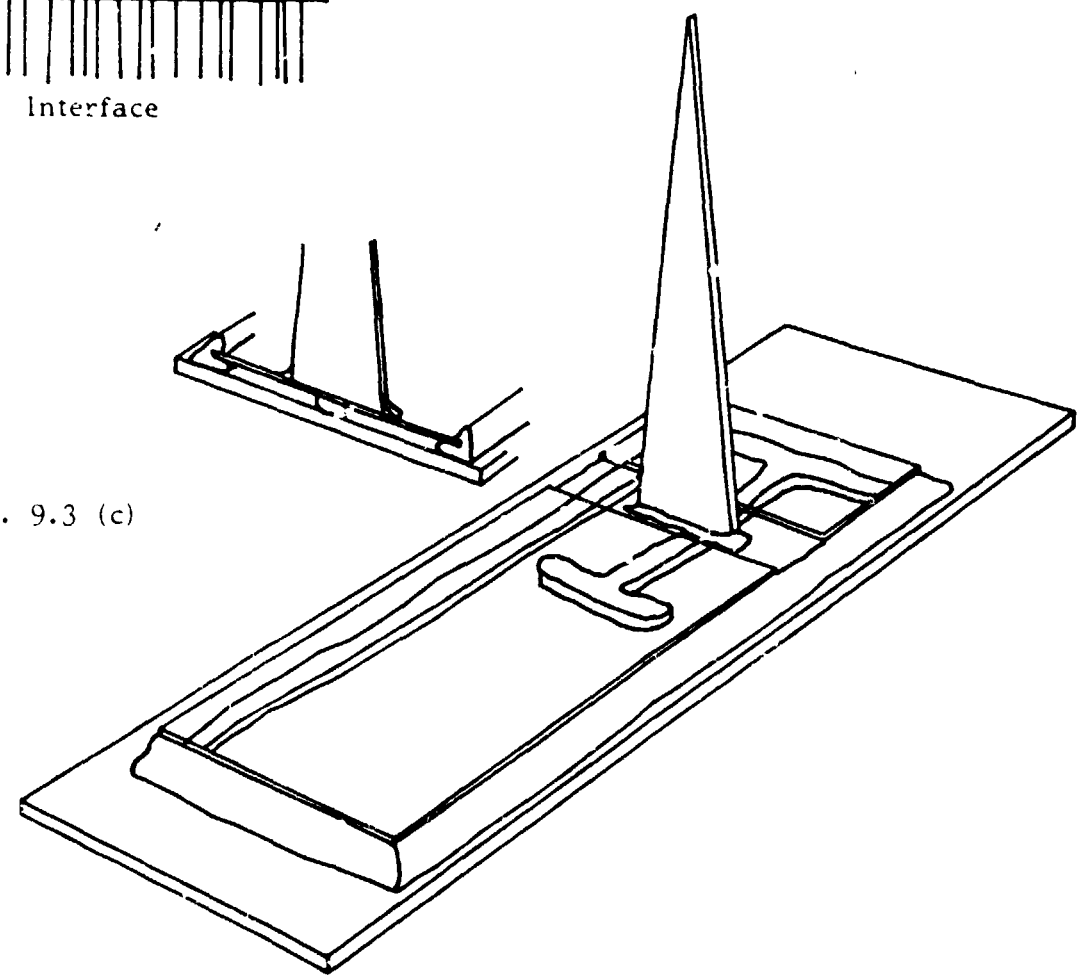

Fig. 9.3 (c)

9.3.3 The Nucleation Cell

Controlled, isolated undercooling of a eutectic melt and the observation of nucleation was made possible with this cell. Nucleation was observed by causing the event to occur in the field of view of the microscope. This was made possible by manufacturing a special cell with the edges of the cell at one end coming together to form a "V" shape, as shown in Fig. 9.4. Undercooling would be initiated by melting all the solid in the cell and then slowly cooling by moving the cell along the temperature gradient. The end with the "V" is the coldest part of the cell. Nucleation should first occur in the vicinity of the base of the "V". The event could be observed because this area of the cell constitutes the field of view in the microscope.

Fig. 9.4

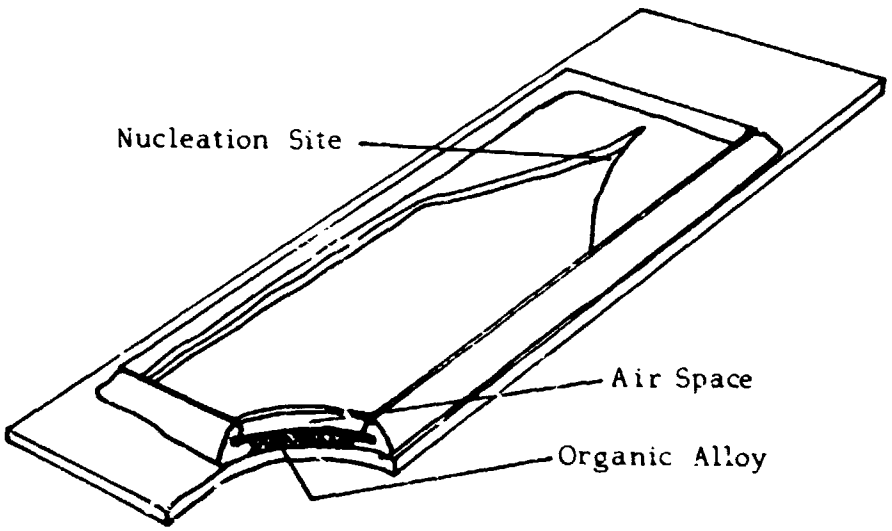

The Nucleation Cell

9.3.4 The Double Alloy Cells

These cells were constructed to permit the observation of the growth of an interface from pure liquid into impure liquid continuously. Growth was initiated by melting back into the region of the cell containing pure alloy. Unidirectional growth was established in the "pure" region of the cell and then continued into the "impure" alloy region of the cell. The transition was assumed to be a sharp one because liquid diffusion over large distances could not occur and it was assumed there was no convection in the liquid. Observations of the morphological changes were made as the compositional transition occurred.

Basic cells, sealed on three sides (both ends and one edge) were prepared. Half of the cell was filled with the control (pure) alloy by submerging only that portion of the cell. The other portion of the cell was filled with the second (less pure) alloy such that the void was filled without melting the previously solidified part of the specimen. This procedure requires that the second alloy have the lower melting point Generally, if the first alloy was pure, then the second alloy was doped with the impurity to lower its melting point and to subsequently study the effects of the impurity on the growth morphology.

9.3.5 The Thermocouple Cells

Two cell designs were used incorporating thermocouples. These cells are illustrated in Fig. 9.5.

Figure 9.5 (a) shows cells in which a single thermocouple was used, while

Figure 9.5 (b) illustrates a cell in which a second junction was embedded in the glue used to seal the cell.

The freezing temperature of the interface could be monitored with the single thermocouple cell. The double thermocouple cell was constructed so that only differences in the temperature between the interface and the surroundings would be observed. In this way, greater amplification of the signal and a sharper response would be obtained.

The thermocouples used in these cells were made of chromel and alumel wire only 0.0005 inch in diameter (approximately twelve micrometers). The thermal mass of these thermocouples is nearly negligible and conduction of heat along the leads is insignificant. The response time of these thermocouples is also exceptionally fast. For example, for wire twice the diameter (0.001 inch), the time to come to 63.2 percent of final temperature when taken from two hundred to one hundred degrees Celsius in still water is 0.002 second (data from Omega Engineering). The recorders used were Leeds-Northrup Speedomax with Azar scaling. Visible deflections of

Fig. 9.5

The Thermocouple Cells

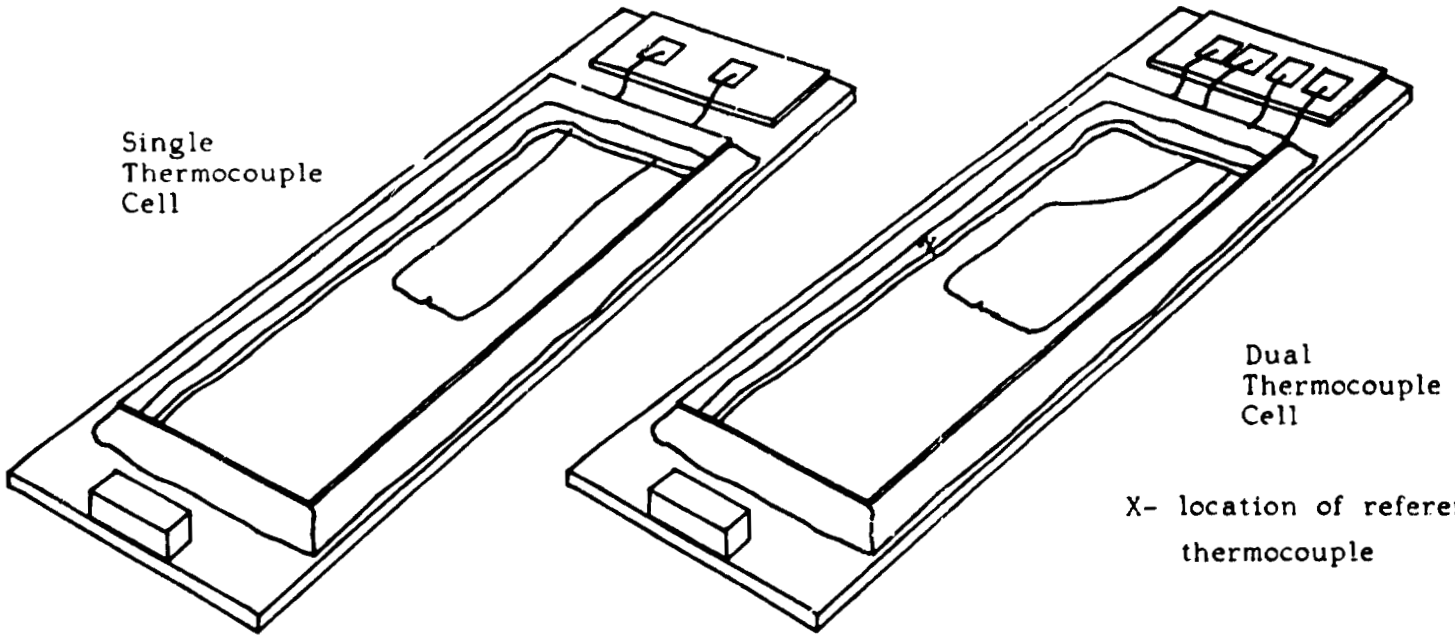

the recorder pen would result from 0.05 degree Celsius changes from a single couple and 0.02 degree Celsius from the differential arrangement. It is understood that better amplifiers and an oscillograph instrument would allow maximum advantage of the thermocouples to be obtained.

9.3.6 The Quenched Interface Technique

A thermal transient was applied to an otherwise normally growing interface. The transient was applied to the cell by directing a jet of cool, compressed gas onto the exposed surface of the cell. This sudden cooling effectively quenches the liquid adjacent to the slowly growing interface and causes dendritic breakdown.

Quenching of the interface was possible with any of the cell designs used, but best results were obtained when the draught protection was removed. The gas jet was obtained from a compressed gas cylinder with a lever operated valve. The most rapid cooling resulted from directing the gas jet onto the liquid just ahead of the solid.

The strength and duration of the blast of gas could be regulated to influence the type of quench applied. A gentle puff of gas would cause the interface to jump forward and then melt back. A long blast of gas could temporarily solidify the liquid ahead of the interface, for a second or two.

9.4 Organic Alloy System Analysis Equipment and Application

9.4.1 Purification of Carbon Tetrabromide

Purification of the as received carbon tetrabromide was performed by sublimation. The apparatus used is illustrated in Fig.9.6. Normal distillation was excluded from consideration because of inevitable degradation of the CBr_4 at the high temperatures necessary for that process. Zone refining was attempted but without success. Either the glass tubes containing the CBr_4 broke during the second pass, or the alloy degraded in situ from thermal effects. Fractional crystallization was also tried, but did not produce the desired purification.

Carbon tetrabromide has a high vapour pressure in the solid state. Therefore, it was decided to try to use sublimation as a purification method, in order to avoid subjecting the material to high temperatures. The dependence of vapour pressure on temperature is given in the list of properties, Table 8.1. Calculations showed that all of the CBr_4 vapour would condense at dry ice temperatures at pressures attained by a vacuum roughing pump. The degree of purification achieved was found to depend on the quality of the vacuum. (The partial pressure of the impure CBr_4 appeared to be very much lower

Fig. 9.6 Carbon Tetrabromide Purification Apparatus

1. Liquid Nitrogen Trap 2. Temperature controlled water bath 3. Dry Ice box 4. Impure CBr_4 5. Valve to mechanical vacuum pump

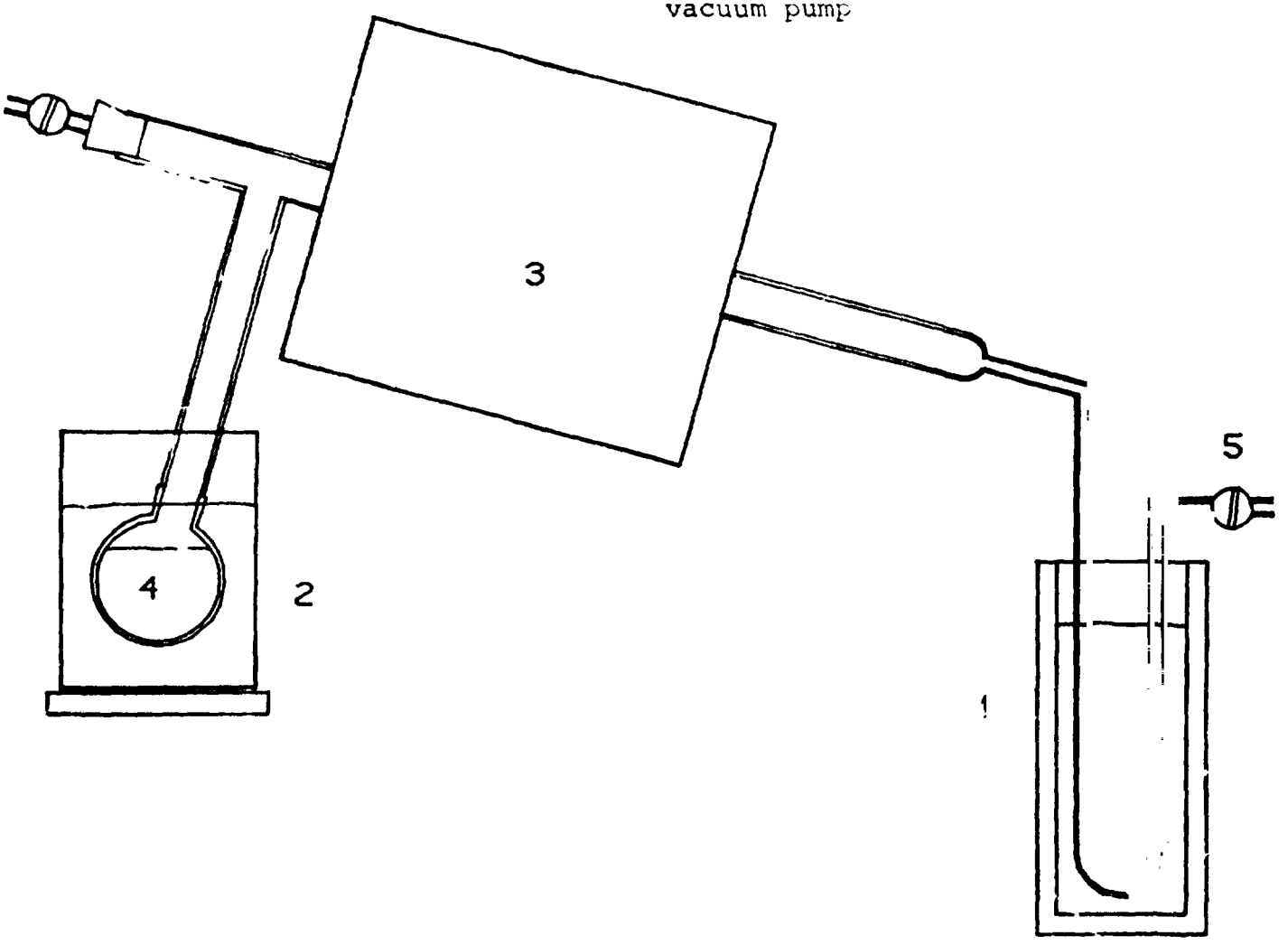

than that of purer CBr_4.)

Before loading the impure material in the apparatus, all surfaces which could contact the material were cleaned with reagent grade chloroform and then rinsed with analysis grade chloroform. Contact with metal was minimized as it was found that metals catalyse the breakdown of CBr_4. The system was sealed, with all parts at room temperature. The vacuum pump was turned on, a minute later the liquid nitrogen trap was activated, and then the dry ice placed in the box. The impure solid was heated to a controlled fifty to sixty degrees Celsius with an oil bath.

No more than two-thirds of the starting material was allowed to sublime. The residue was obviously dark brown and had black particles in it, while the condensate was a pure, translucent white and very crystalline. The purified material was removed from the tube, and later sublimed a second time to achieve even greater purification. The purified material was stored in a brown bottle.

A sample of purified material, when made into a cell, would be solidified at a growth rate of 7.7 micrometers per second in a temperature gradient of 25 degrees Celsius per centimeter, and maintain a planar interface (for a few minutes). Dendritic breakdown could not be induced even with a growth rate of 40 micrometers per second.

9.4.2 Density Measurements of Alloys

Two water displacement techniques were used to measure alloy density: the Archimedian method and Pycnomometry.

The Archimedian technique was implemented in the usual way. For this purpose, single lumps of the alloys were made by casting 0.8 to 31 gram specimens. A single forty gauge copper wire was cast into the lump and used for suspension. Surface roughness was removed by quickly melting and refreezing the outer surface. The single lump of alloy, prepared as described above, was suspended from a balance and submerged under water. The weight of water displaced is therefore measured. The standard calculations, including water density variation with temperature, were made to obtain the density of the specimen. As usual, bubbles were eliminated and repeated immersions performed until the sample was well wetted. This alloy system was well suited for the water displacement technique because there is no solubility of the alloys in the water as proven by zero weight loss while submerged at constant temperature.

It was found that sample weight continuously decreased while the specimen was in air at room temperature. This sample loss is the result of sublimation. Once a weight loss rate in air was established, the extrapolated weight at immersion could be found. Upon immersion, weight loss ceased, then continued when the sample was withdrawn. This protection of the sample by the water permitted density measurements to be made as a

function of temperature. The water was heated to eighty degrees, removed from the heat, and stirred frequently during the subsequent cooling. The water temperature and the immersed sample weight were monitored during cooling. With compensation for water density change with temperature [64], the rate of change of alloy density with temperature was determined. The result was sufficiently sensitive to detect the solid state phase transformation (at forty-five degrees Celsius) for the sixteen weight percent Hexachloroethane alloy.

A 50 ml pycnometer was used in some measurements with similar results to the Archimedian method. More consistent results were obtained by the latter method. Pycnomometry would be superior if large, void-free lumps of sample were not available. Tiny samples gave poorer results, but only because of the relative error introduced by sublimation losses.

9.4.3 Preparation of Organic Alloys

The specimens in this investigation were alloys of Carbon Tetrabromide and Hexachloroethane; most had compositions in the range from zero to twenty weight percent Hexachloroethane. The alloy components comprising each batch of material were weighed to at least the nearest milligram, then sealed together in a small glass bottle which was immersed in boiling water to melt and homogenize the alloy. The batches prepared ranged in weight from five to thirty grams, with twenty grams most usual. After filling a number of cells, the remaining alloy was stored in the sealed glass bottle, at room temperature in a dark cabinet. Contact with metals and prolonged heating were avoided, since both were found to accelerate decomposition of the organic alloys. During alloy preparation and filling of the cells, the alloys were molten no longer than ten to fifteen minutes. Selected impurities added to some samples included azobenzene, benzil, camphene, succinonitrile and cyclohexanol. All of the alloys prepared are listed in the Appendix, as well as a compilation of the basic properties of the impurities used.

9.4.4 Thermal Analysis

The thermal analysis described in this section was performed to help obtain phase diagram information. Generation of cooling curves was a preliminary step in the thermal analysis of the organic alloys. Melting curves were attempted as well. The simple apparatus used to determine cooling and melting curves for the organic alloys, is shown in Fig. 9.7.

The thermocouple and organic alloy were contained in a small tube which in turn was sealed in a larger tube with an air space between the tube walls. The assembly was immersed in an oil bath heated by a hot plate (Fig. 9.7), temperature was controlled manually. Smooth temperature excursions resulted from the thermal mass of the oil bath.

The thermocouple was in direct contact with a small volume of organic alloy. The whole system was transparent so that phase changes could be observed in situ.

Due to the low thermal conductivity of the organic material, melting curves were not useful. From cooling curves only liquidus temperatures were well defined and no solidus points could be found. The cooling curves were made at cooling rates always slower than one degree per minute. Some of the results were combined with the Differential Scanning Calorimetry data.

Fig. 9.7 Thermal Analysis Apparatus

1. Oil bath and hot plate 2. Thermometer 3. Thermocouple 4. Double-wall sample container tubes, with air space

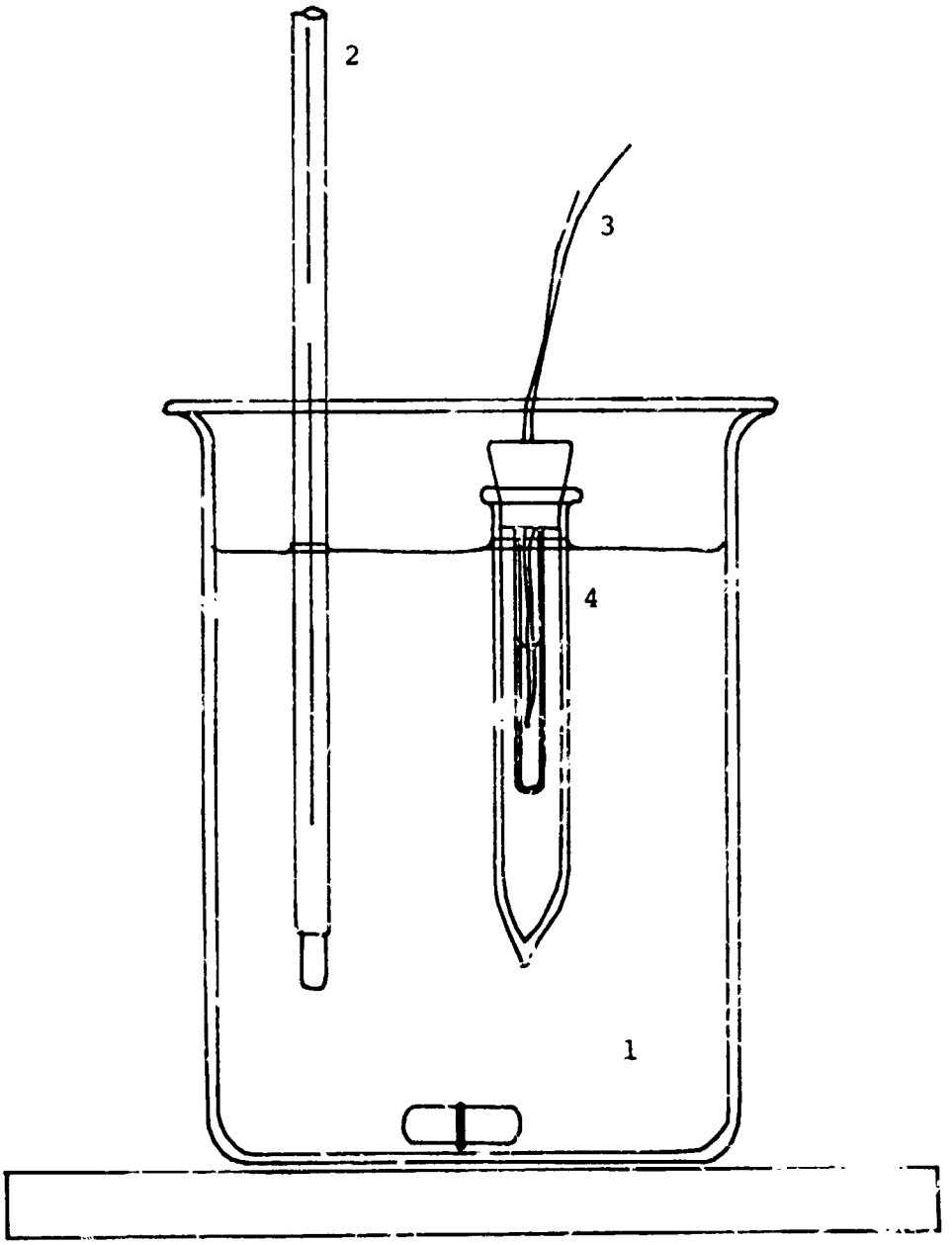

9.4.5 Operation of the Digitizing Tablet, Computer and Plotter

The "system" as described here refers to the graphics and computation facility in the Department of Metallurgy and Materials Science. The parts of the system were obtained from Tektronix, Canada, and consist of four interconnected components. Refer to Fig. 9.8. At the centre of the system is the Tektronix 4051 graphics microcomputer. Connected to the computer is the 4956 graphics tablet as well as the 4662 interactive digital plotter. There is as well a 4631 hard copy unit tied to the 4051.

While these three components are part of the Tektronix system, their individual functions can be summarized separately: the 4051 graphics computer was used to accept digitized data from the tablet, for record keeping, data manipulation and to perform polynomial regressions and other calculations; the graphics tablet (digitizer) was used extensively to help perform the various two-dimensional geometric analyses from photomicrographs of the interfaces and other diagrams or photographs by converting image data to digital coordinates; the plotter was used to display data, plot the data regressions and draw diagrams. Using suitable programs in the computer (the algorithms are described elsewhere), the system was used to measure the grain boundary grooves (see section 9.4.8), eutectic interface profiles (see section 9.4.9), capillary rise (see section 9.4.7), areas under the Differential Scanning

Calorimetry plots (see section 9.4.6) to obtain enthalpies of fusion, and to measure the eutectic lamellar spacings (section 9.4.9) and volume fractions (section 9.4.9).

The 4051 computer was programmed to accept digitized data and to process the data in a suitable fashion depending on the measurement being performed at the time. Both graphical and numerical data had polynomial regressions performed with them in the computer. The algorithm for the programme in the computer for regressions was developed in reference 65. The polynomial regression is a linear least squares type where the choice of order is made by the operator.

The primary input device was the digitizing tablet. The operator selects points on an image on the tablet surface and on command, these points are accurately converted electronically to X-Y coordinates which are transmitted to the computer for programmed manipulation. The tablet surface is five hundred by five hundred millimeters and has a point resolution of 1.27×10^{-4} meters and an accuracy of $\pm 100 \times 10^{-4}$ meters. Using the tablet is analogous to drawing a Cartesian Coordinate grid onto the images and reading the coordinates of the points electronically. Thirty-five millimeter film negatives (or slides) from the microscope could be projected directly onto the digitizer or, alternatively, enlarged onto photographic paper and the enlargement measured. Magnifications of up to twenty-five were possible with the projector.

The plotter is a flatbed digital plotter capable of a point to point plotting resolution, reproducibility and accuracy similar to the digitizer. The graphs in this report were all made (at least in part) on the plotter. One use other than plotting graphs, however, was the drawing to scale of the solid-liquid interface shapes. The theoretical Jackson and Hunt eutectic interfaces can be drawn, as well as Bolling and Tiller type grain boundary grooves.

Although not experimental apparatus, the system described was a valuable computational, graphical and image analysis tool which made this work feasible.

Fig. 9.8

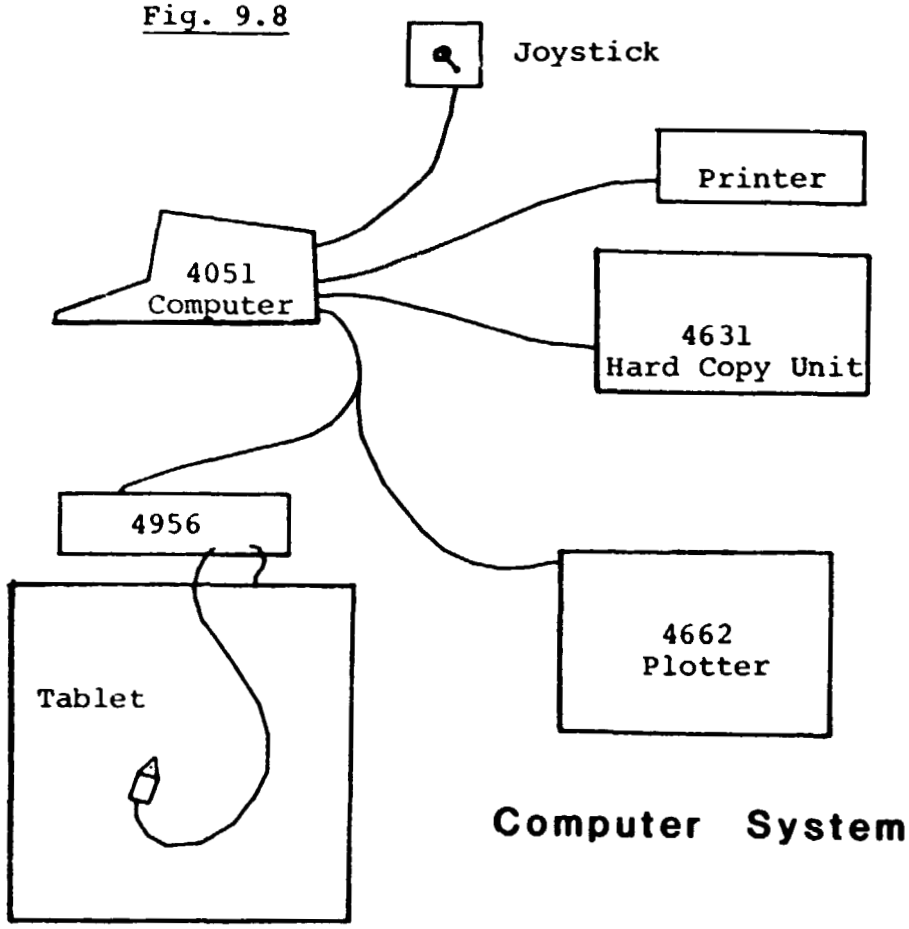

Computer System

9.4.6 Differential Scanning Calorimetry

The purpose of this section is to describe the operation and use of the Perkin - Elmer model DSC-2 differential scanning calorimeter. This device was used to obtain the transformation temperatures of melting and crystallization, and also to measure the enthalpy of fusion and crystallization of the alloys in the Carbon Tetrabromde - Hexachloroethane system. The instrument was used in the recommended manner as described in the instrument manual [62].

The method of scanning calorimetry is similar to the more common method of differential thermal analysis. The difference being the quantity being monitored is energy and not temperature. The difference in the amount of energy required to heat or cool the sample (and its container) in order to keep its temperature identical to a reference (an empty pan or a pan with a neutral specimen) is continuously plotted. The amount of energy is plotted against time and, concurrently, temperature since the sample and reference are both being heated or cooled at a predetermined, linear rate. The response of the sample to thermal change includes phase transformations, changes in heat capacity, and glass transitions or other reactions. Other than for such changes, the energy required to heat or cool the sample will not be registered. The resulting plot would be perfectly horizontal.

The device consists of two thermally regulated pads on which the reference and the sample rest. As the temperature

of both specimen/pad combinations is linearly raised or lowered, the difference in electrical energy needed to keep the sample at the temperature of the reference is graphed. The resulting graph has as abscissa, the programmed temperature, as the ordinate, the heat flow rate in calories per second. A simplified graph is shown in Fig. 9.9.

Often, materials have a change of heat capacity upon transforming from liquid to solid or vice versa. If this is the case, one needs to perform a baseline correction when making a measurement of heat of transformation. An integration of the area under the curve yields the energy supplied or removed to bring the sample to that temperature. A solid-liquid transformation is presented as a peak much like Fig. 9.9. The area under the peak represents the heat of fusion. If the heat capacity of solid and liquid differs, the baseline on either side of the peak would not be colinear. A baseline correction would be applied in order to separate the heat capacity change from the heat of fusion. For the alloys used in this study, the baselines were sufficiently colinear that a baseline correction was not required.

The area under the peak (Fig. 9.9) was measured with the help of the digitizer. The enthalpy calculation is based on a relative measure of the unknown peak area to the area from a standard peak from indium. The DSC-2 was calibrated using the indium standard prior to use and in order to obtain familiarity with the method.

The transition temperatures were also obtained from the plots by the extrapolation to the baseline of the slopes of the peaks as shown in Fig. 9.9. The extrapolation is used to separate the thermal resistance of the apparatus from the response curve of the specimen.

A small chip of the alloy (typically five milligrams and less than ten milligrams) was weighed, then sealed in the special aluminum pan. An empty pan serves as the reference. A chart speed, scale attenuation, heating or cooling rate and start and stop temperatures were then selected. The best combination of these parameters is found by trial and error.

When the DSC data were used for the phase diagram, the majority of the points were from melting data. There was uncertainty in the liquidus determination on freezing because of the unpredictable effect of undercooling. The data from the first melting cycle were the most reliable because the sample would redistribute itself within the container. The beginning and ending temperature of the melting reaction were used for the solidus and liquidus temperatures respectively. Although the instrument is sensitive, the solvus temperatures could neither be measured nor detected.

Fig. 9.9

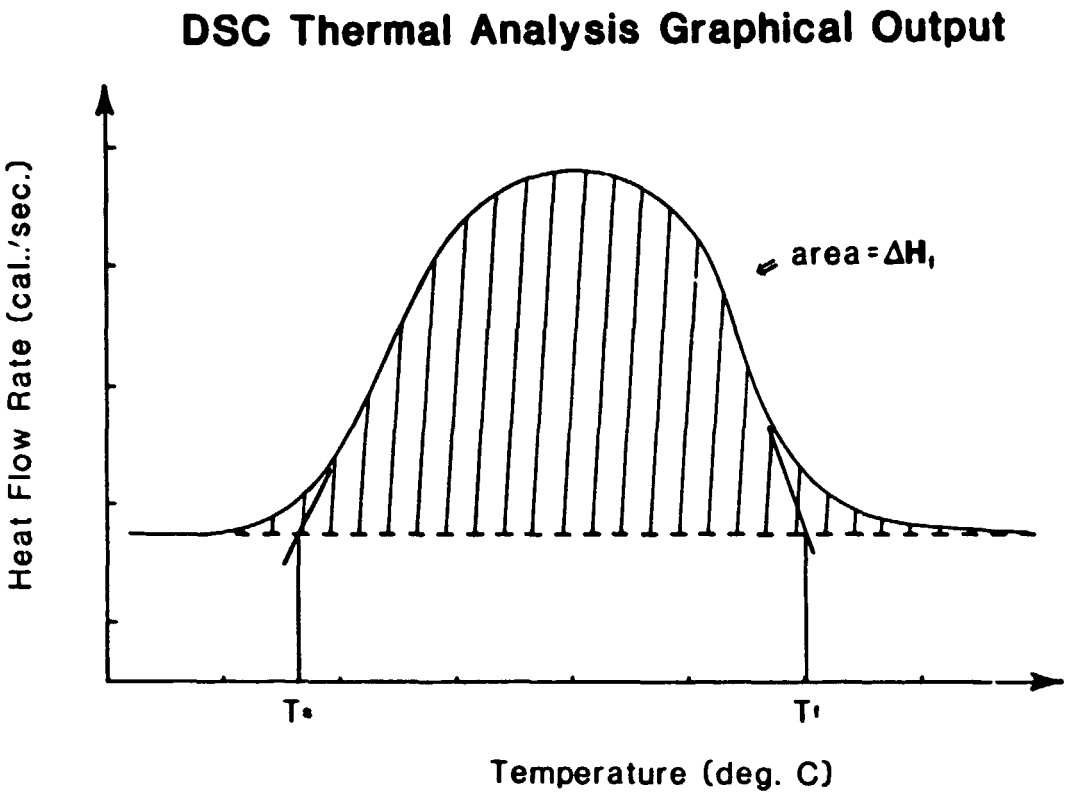
DSC Thermal Analysis Graphical Output
Heat Flow Rate (cal./sec.)
area = ΔH,
Ts
Tf
Temperature (deg. C)

9.4.7 Grain Boundary Groove Analysis

Basic cells were made and filled with alloys suitable for single phase grain boundary groove analysis. These cells were placed into the Temperature Gradient Microscope or onto an auxiliary apparatus in order to impress the temperature gradient onto the cell. The auxiliary gradient stage was similar to the type used by Jackson and Hunt, L. Morris and Rutter et al. [61, 42, 60]. There were two temperature controlled copper blocks with a fixed spacing between them in this stage design. This stage was used in order to obtain higher temperature gradients and interface temperatures than could be applied by the Temperature Gradient Microscope described in section 9.1. These higher temperature conditions were required when trying to obtain grain boundary grooves with high Hexachloroethane concentrations.

In a short time, (approximately fifteen minutes or less) after the cell was placed on the gradient stage, a stationary, planar solid-liquid interface was formed. During this waiting period, the temperatures stabilized and the grain boundaries at the interface migrated and reached their equilibrium conditions. Grain boundaries reach equilibrium when they cease to migrate and settle into a position nearly perpendicular to the isotherm. Equilibrium at the interface was considered to be achieved at this time. It was found experimentally that equilibrium was attained more rapidly when the temperature gradient was more steep. Longer equilibration times were needed as the solute

concentration increased from that of a pure component.

Steeper gradients cause rapid equilibration but create small grooves. Larger grooves allow better precision when micrographically analyzed. Optical photomicrographs were taken of the grooves and the Glicksman/Nash grain boundary groove technique applied.

The digitizer and computer were used to perform the measurements from the photomicrographs, to obtain the Glicksman/Nash parameters, and to calculate γ_{SL} using the stored polynomials.

The measurement sequence was as follows: (See also Fig. 9.10)

1. Six points on the interface isotherm were digitized and a straight line fitted to them.

2. A point at the base of the cusp in line with the grain boundary was digitized and a perpendicular from the isotherm was automatically calculated to go through this point.

3. The solid-liquid interface profile on one side of the groove was digitized with ten to fifteen points and a fourth order polynomial was fitted to these data.

4. A forty-five degree line to the isotherm was calculated to make the measurement for d. The distance d was then calculated from these lines.

5. The distance between the grain boundary being measured and the neighbouring one was then digitized.

6. The composition of the alloy, the gradient and the magnification of the micrograph were entered into the computer. The final interfacial energy was then calculated and presented along with the incidental parameters characteristic of the groove.

7. Steps three to six were repeated for the other side of the groove.

The quality of the analysis was checked by plotting the construction lines and digitized points. A check was made in the computer programme for over or undersize values of λ (the boundary spacing), and a warning given if the value was inadequate. The upper and lower limits found for inadequacy were chosen after careful analysis of the Glicksman/Nash technique. The limitations of the method are explained later in sections 10.3.1 and 10.3.4 and in the Appendix. Further manipulation was needed to correlate the data properly.

The selection of a fourth order polynomial to fit to the groove wall is not the best choice. A nonlinear regression to the data would be superior. Unfortunately, the required computer program is outside the means of this study, and its implementation would not be sufficiently justified.

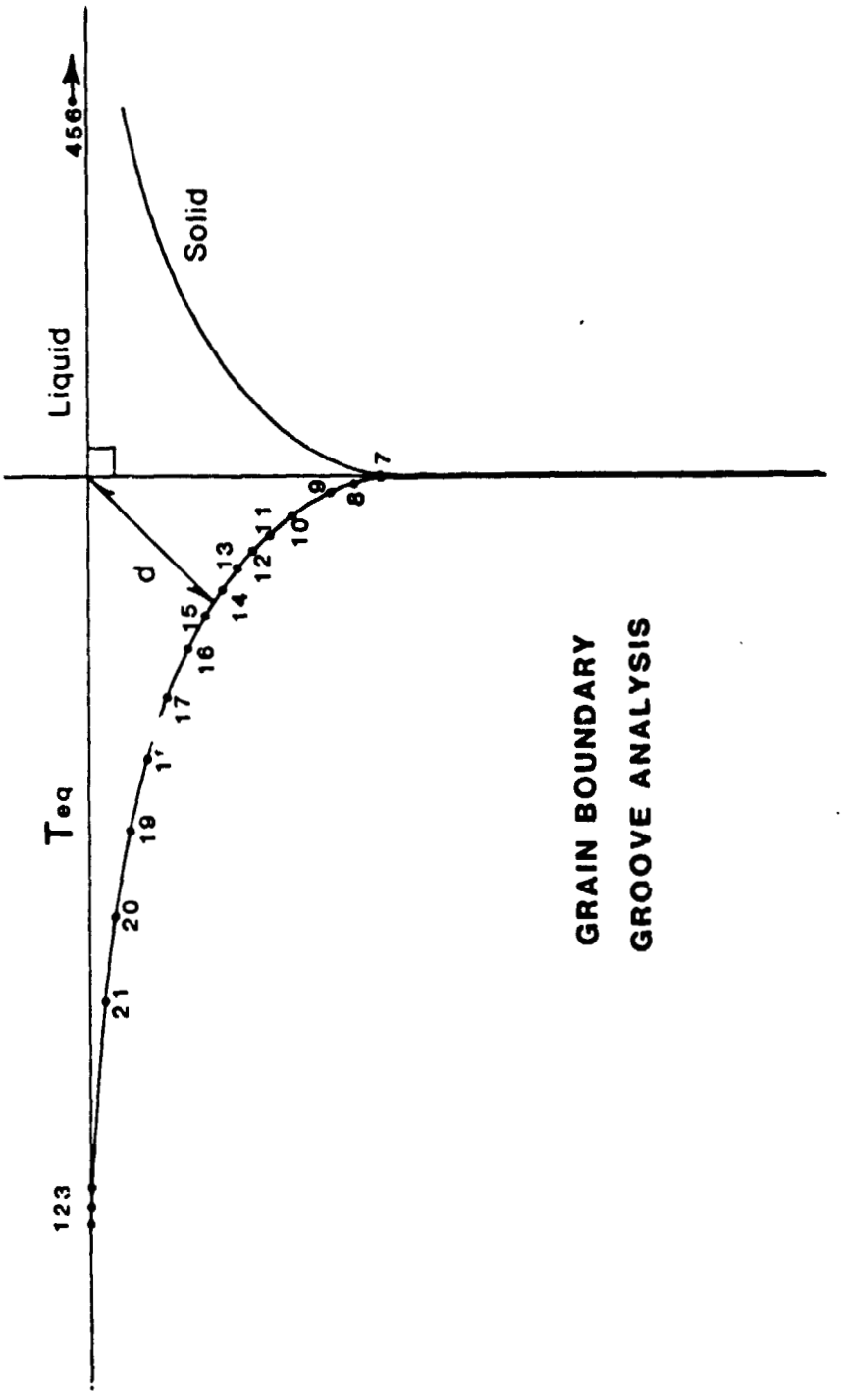
456
Liquid
Solid
d
Teq
123
7
8
9
10
11
12
13
14
15
16
17
18
19
20
21
GRAIN BOUNDARY
GROOVE ANALYSIS

Fig. 9.10

9.4.8 Eutectic Interface Analysis

From the inception of this work, it was believed that quantitative information could be obtained from the eutectic interface, as described earlier in section 8.2.3. Accordingly, a group of computer programmes were written to use the digitizer as the input device and systematically store the interface shape or other graphic information in the computer memory. The basic concept was to mark or trace out the curved interfaces and then to fit a polynomial to these points using a least squares regression procedure. The solid-solid interphase boundary was entered as a straight line. Therefore, three polynomials were needed for each trijunction. (See Fig. 9.11) The polynomial makes computer storage of the shape of the curve simple and the regression mooths out digitizing and quantification errors. The curved interfaces were foun be most adequately fit by a fourth order polynomial. (Third and fifth order did not reasonably fit at the end points.) Fifteen points along the curved interfaces, spaced by an experienced eye to produce the best fit, were used. Five points were used on the solid-solid interphase boundary.

The crossover point for the two curved polynomials was found by solving with Newton's Method [65]. Then, the derivatives of the curves were taken at this point. In this way, the angles at the trijunction could be measured. These are angles A, B and C in Fig. 9.11. The local radius of

curvature could be calculated and plotted from the polynomials. The original interface could also be reconstructed or enlarged for comparison to others.

Another program was written to use the digitizer to measure volume fraction and lamellar spacings of the eutectic. Lamellar spacing was measured by averaging the distances, point to point, from the centre of the minor phase, to the next centre of the minor phase along a line normal to the growth direction. Volume fraction was measured similarly, except the interphase boundaries were used to determine the average lamellar widths.

Fig. 9.11

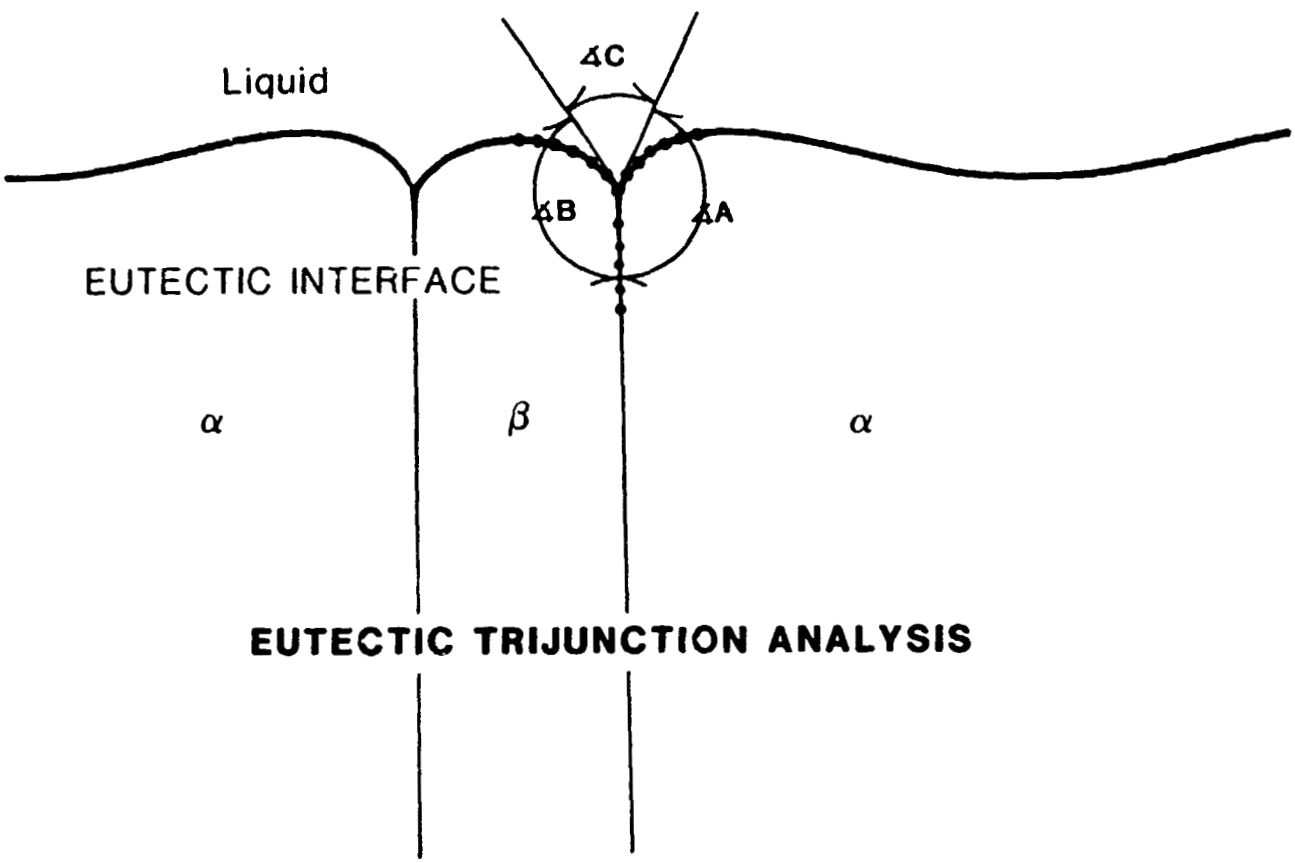
Liquid
∠C
∠B
∠A
EUTECTIC INTERFACE
α
β
α
EUTECTIC TRIJUNCTION ANALYSIS

10. EXPERIMENTAL OBSERVATIONS AND RESULTS

10.1 Organic Alloy System Measurements

Three system characteristics were needed which were not found in the literature. These are:

1. The phase diagram (section 10.1.1);
2. Variation of the enthalpy of fusion with composition (section 10.1.2);
3. Variation of the bulk solid density with composition (section 10.1.3).

This section summarizes the non-micrographic measurements made on the system, including the above data.

10.1.1 The Phase Diagram

The phase diagram was the most important information required. Preliminary information, obtained from cooling curves as described in section 9.4.4., indicated that the phase diagram was that of a simple binary type. The majority of the approximately seventy points determined for the diagram were measured using the DSC-2 differential scanning calorimeter. The phase diagram is shown in Fig. 10.1. The solid state transformations in these alloys could not be detected on the DSC-2 calorimeter.

The liquidus and solidus lines, as well as the eutectic isotherm, are least-squares polynomial regressions executed using the computer onto the appropriate set of data points for each line. The solidus compositions at the eutectic temperature, as well as the eutectic composition and temperature themselves, are taken from the intersections of the regressed curves. The regressed curves met at the eutectic point to within 0.1°C and 0.1 weight percent, giving the eutectic composition as 8.4 weight percent Hexachloroethane and the eutectic temperature as 83°C. It should be noted that the eutectic composition and temperature reported by Jackson and Hunt were 8.6 weight percent Hexachloroethane and 84°C respectively. The equations for the regressed curves are found in the Appendix.

Fig. 10.1

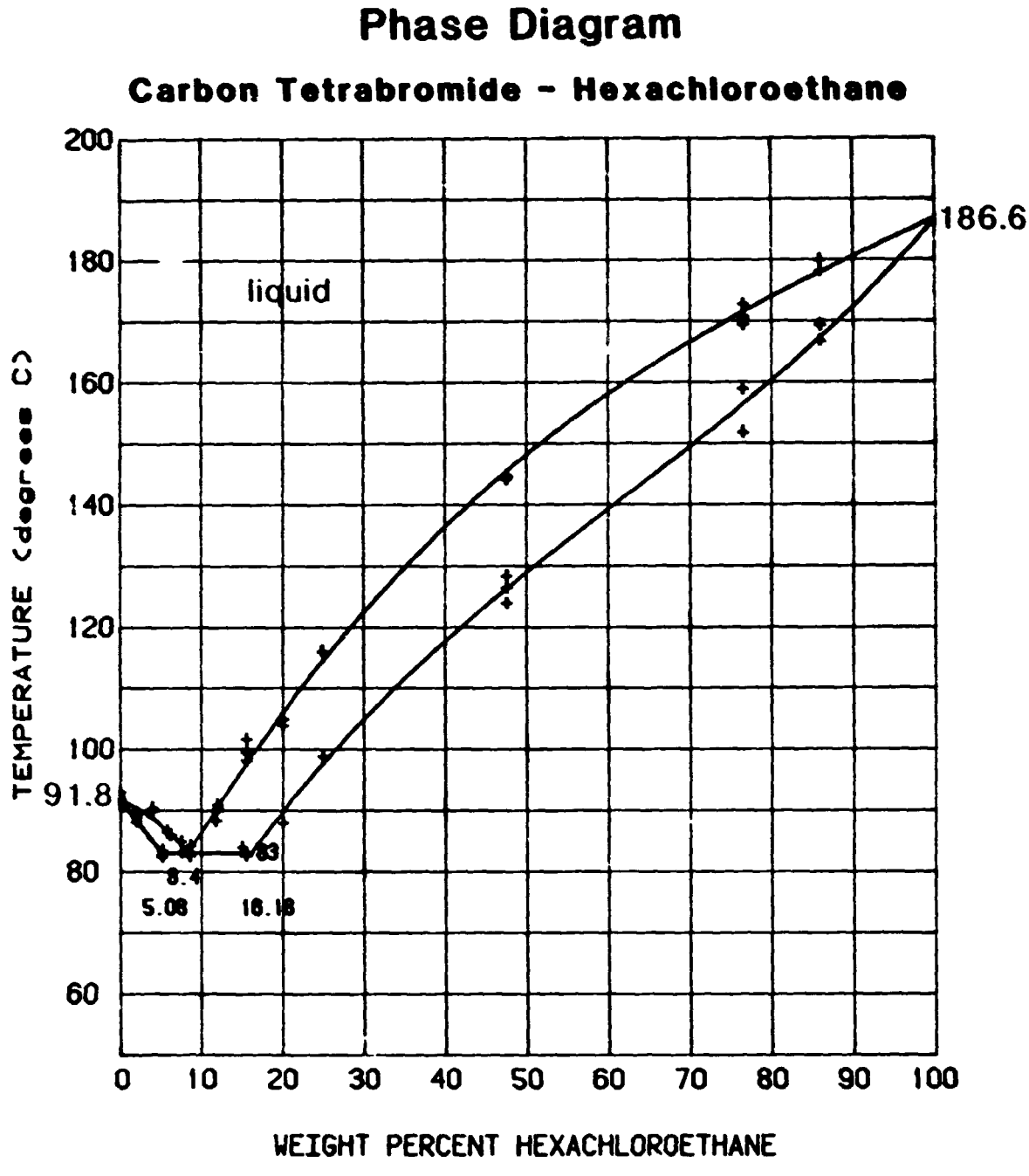
Phase Diagram
Carbon Tetrabromide - Hexachloroethane
liquid
186.6
91.8
5.08
16.18
TEMPERATURE (degrees C)
WEIGHT PERCENT HEXACHLOROETHANE
200
180
160
140
120
100
80
60
0
10
20
30
40
50
60
70
80
90
100

10.1.2 Enthalpy of Fusion

The total heat for the transformation from liquid to solid or solid to liquid was measured from the same DSC-2 charts for melting and for freezing used to obtain the phase diagram data (see section 9.4.6). The data are presented in Fig. 10.2. The curve shown is a fourth order polynomial regression of the data. The equation of the curve is given in the Appendix.

There was no resolvable difference between the total heat from crystallization and the total heat from fusion of the alloys. The reported data therefore include both values.

From the graph, it is clear that the variation of heat of transformation is not a straight line between the pure components of the alloy.

The total heat of transformation measured is given here for the freezing reaction of a single phase alloy in its component parts:

$$\Delta H_{total} = - X_1 \Delta H_f (CBr_4) - X_2 \Delta H_f (C_2Cl_6)$$
$$+ X_1 \int_{T_1}^{T_2} C_p (CBr_4 - solid)\, dT$$
$$+ X_2 \int_{T_2}^{T_1} C_p (C_2Cl_6 - solid)\, dT$$
$$+ \Delta H_{mix} (liquid)_{T_1}$$
$$- \Delta H_{mix} (solid)_{T_2}$$

where: ΔH_{mix} is the heat of mixing of the component to the alloy, X_1 and X_2 are the molar concentrations, C_p is the heat capacity at constant pressure, and ΔH_f is the heat of fusion of the pure material.

This summation accounts for the fact that alloys solidify over a freezing range. The heat of transformation was integrated over the temperature range $T_1 \rightarrow T_2$. The terms with C_p and ΔH_{mix} together contribute to the deviations from linearity between the pure component heats of fusion. The observation that no baseline correction was needed to make the heat of transformation measurement from the DSC-2 charts indicates that the ΔC_p of the alloys for the solid-liquid transaction is nil. From this, the heat capacity change from T_1 to T_2 is, as well, nil. Note that it is sufficient to know $\Delta C_p = 0$, even though the value for C_p (CBr_4) or the value for C_p (C_2Cl_6) is not known. The graph of Enthalpy of Fusion does not account for the fact that each alloy melted or solidified over a temperature range. As a consequence, the ΔH_{mix} components are not available.

In essence, the ΔH_{Total} above represents the difference in heat a molecule achieves as it changes from a crystal to a liquid or vice versa, by crossing the solid-liquid interface. It is this quantity of heat needed for the solution of the Gibbs-Thomson relation. The exact form for the heat required is ΔH_{fp}, the quantity of heat required to solve the more precise

binary Gibbs-Thomson relation given in the Appendix G. Within experimental error, the measured ΔH_{Total} represents this required heat.

Fig. 10.2

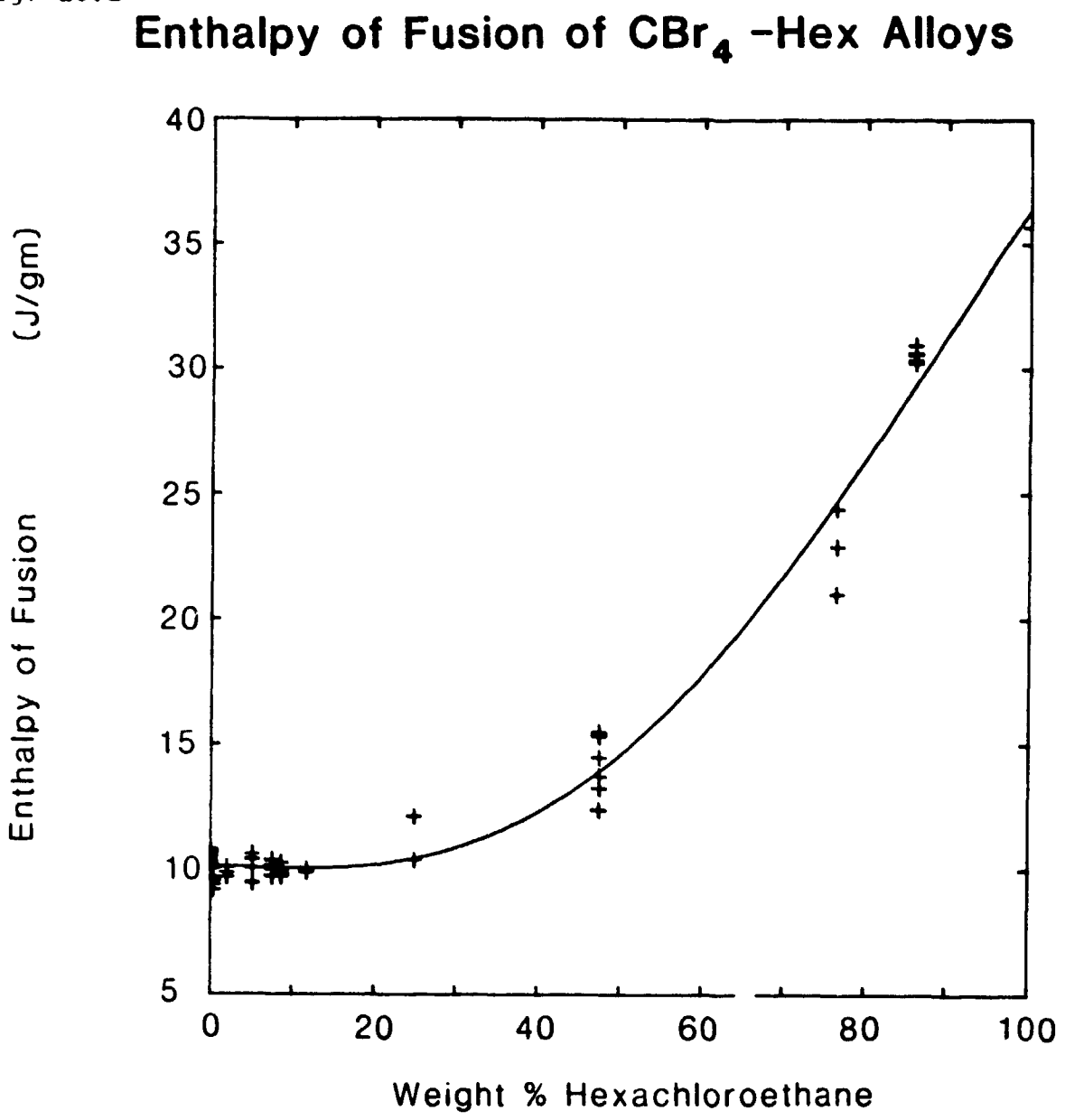
Enthalpy of Fusion of CBr_4 -Hex Alloys
Enthalpy of Fusion (J/gm)
40
35
30
25
20
15
10
5
0
20
40
60
80
100
Weight % Hexachloroethane

10.1.3 Density

The results of the density measurements are plotted for room temperature (23°C) in Fig. 10.3. A polynomial regression was used to fit the curve to the data points. The point for pure Hexachloroethane was obtained from the literature (see Table 8.4) since it was not possible to obtain a sufficiently large, void-free sample of pure Hexachloroethane for accurate density measurement.

The dependence of density on temperature was measured for a couple of alloys (one representing the α phase of the eutectic (5 w/o Hex), the other the β (16 w/o Hex.)). A linear dependence both above and below the solid state phase transformation temperature was observed, and was similar for the two alloys. This phase change occurs near 45°C for both α and β phases. The variation of density (ρ) with temperature, above the transformation temperature is approximately:

$$\frac{\partial \rho}{\partial T} = -1.6 \times 10^{-3} \text{ g/cm}^3 \text{ per degree}$$

The variation of ρ with temperature below the transformation temperature is approximately:

$$\frac{\partial \rho}{\partial T} = -1.85 \times 10^{-3} \text{ g/cm}^3 \text{ per degree}$$

The common and linear behaviour of the two alloys indicates that a calculated density of any alloy in the range zero to thirty weight percent Hexachloroethane can be obtained at the melting point of the alloy. This calculation was performed to provide the best density measurement for the

solution of the Gibbs-Thomson relation applied at grain boundary grooves.

Fig. 10.3

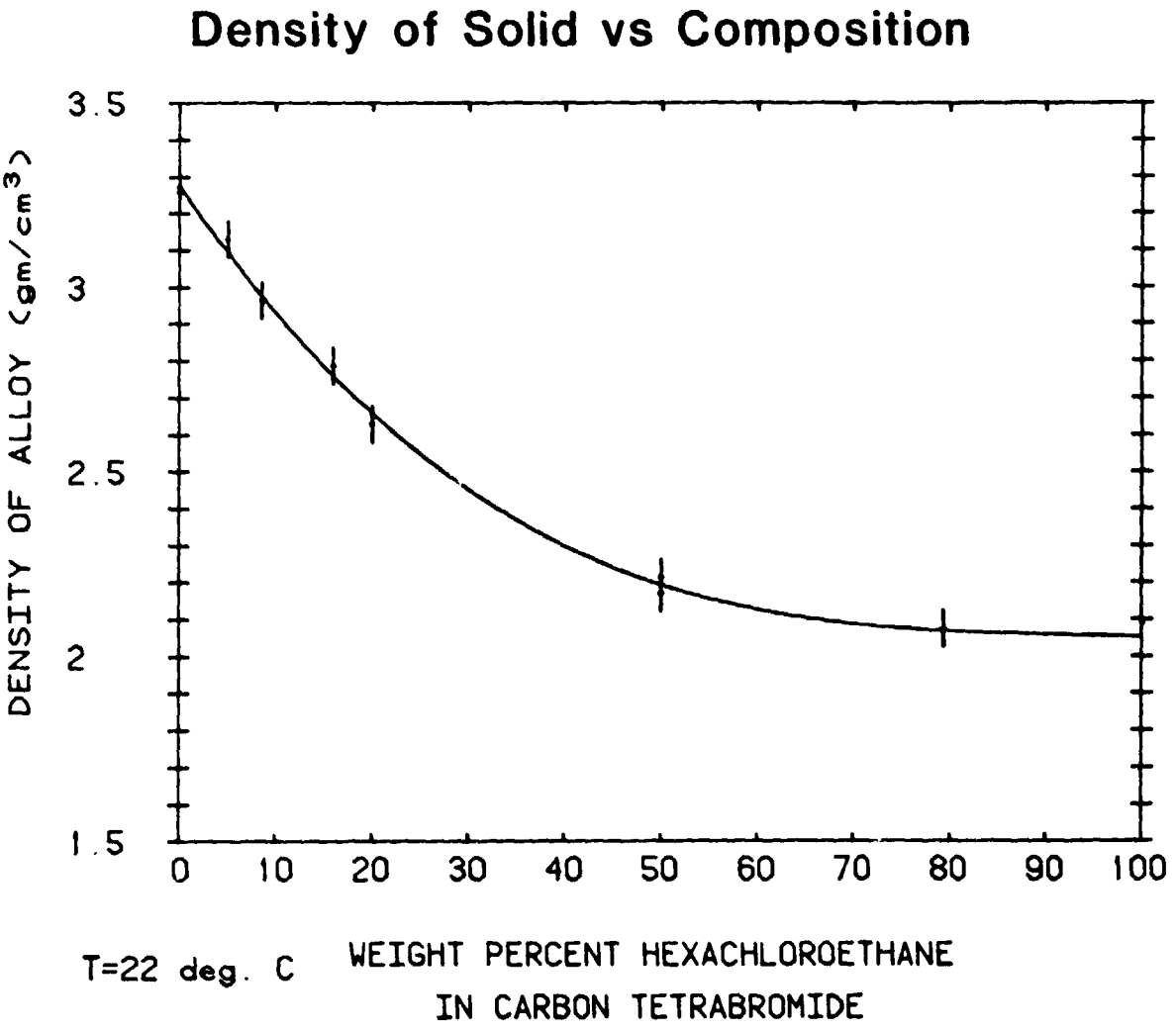

10.1.4 Entropy of Fusion

In order to solve the Gibbs-Thomson relation, the ratio of $\Delta H_f \rho/T_{eq}$ is required for each composition tested. For pure materials, this ratio (using proper units) is the entropy of fusion per unit volume: ΔS_f. The value of ΔS_f of pure CBr_4 and C_2Cl_6 are therefore obtained directly from the respective enthalpies of fusion as measured on the DSC-2. Since a eutectic reaction, by definition, occurs at an invariant point on the phase diagram, the definition for entropy of fusion was applied just as for the pure components.

In order to permit semi-automatic analysis of grain boundary grooves by computer, the terms above, ΔH_f, ρ, and T_{eq} were assembled as polynomials to form a single curve which may be called the entropy of fusion per unit volume vs. composition. See Fig. 10.4. The values for T_{eq} are from the solidus lines on the phase diagram. The polynomial terms for the curve are given in the Appendix.

Note that this calculation is not thermodynamically rigorous as terms like the entropy of mixing, which influence the system free energy, are not included in this derivation of "entropy of fusion". The simple calorimetric measurement of the heat of the solid-liquid transformation of the alloys is an experimental estimate of the heat required to solve the Gibbs-Thomson equation. In this application, the alloy behaviour is modelled as if it were a pure, single component material.

The application of the Gibbs-Thomson equation given earlier assumes that $\Delta G = 0$ for the equilibration of a pure solid-liquid interface. The addition of the second component to the interface requires the chemical potential change be zero and $\Delta G \neq 0$. As a result, the calculations performed here are a practical consequence of using the measured data using $\Delta G = 0$. The rigorous solution for a binary is given in Appendix G.

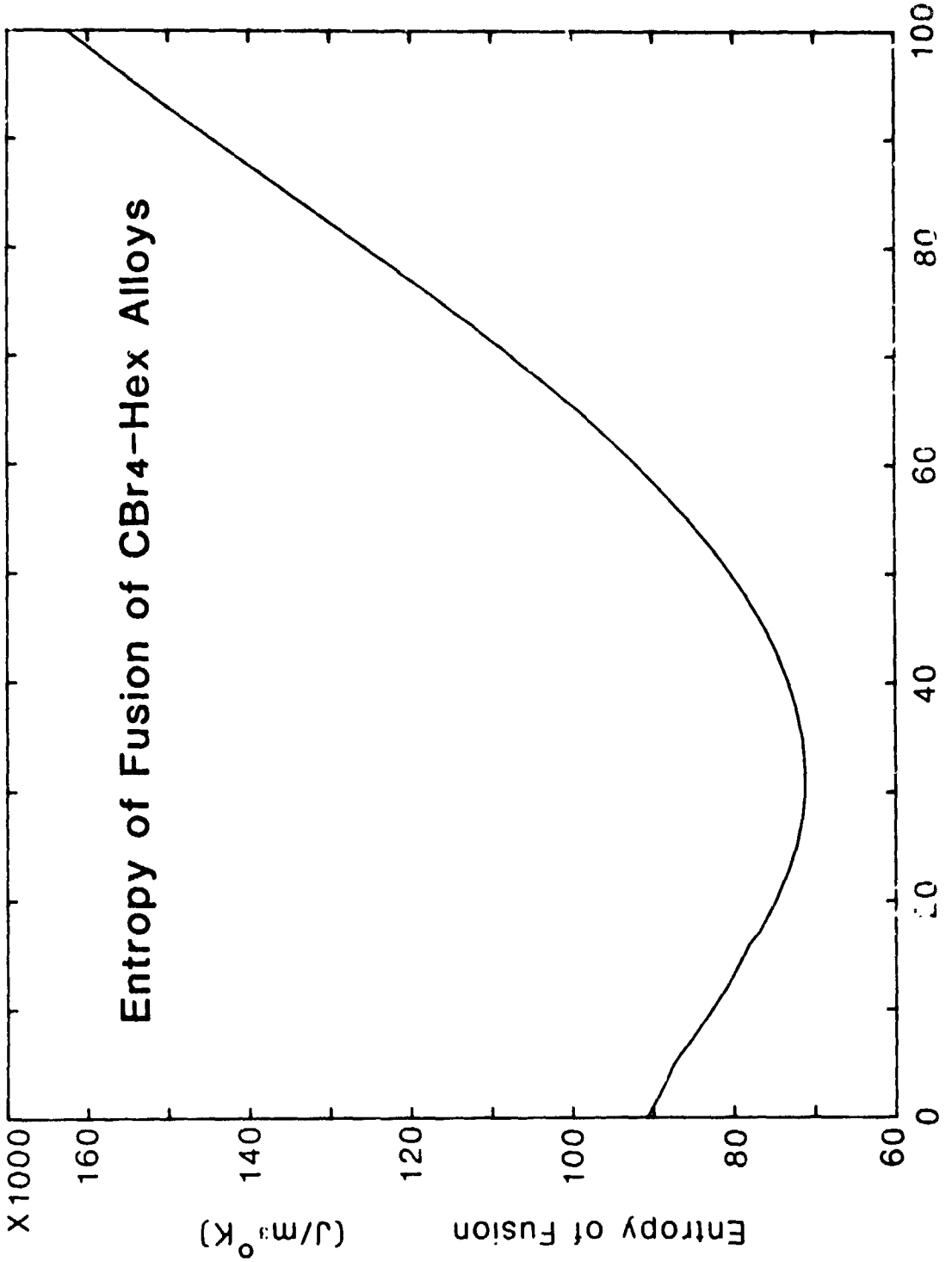
Entropy of Fusion of CBr4-Hex Alloys
X 1000
160
140
120
100
80
60
Entropy of Fusion
(J/mole °K)
0
20
40
60
80
100
Weight % Hexachloroethane

Fig. 10.4

10.1.5 Derived Values of Data

Measured data such as the phase diagram or density variation with composition were stored in the form of polynomials in the computer. Combinations of the polynomials can be solved for any composition. Many quantities which are frequently required for calculations were derived or interpolated from the polynomials. These quantities are summarized in Table 10.1. These are quantities which, of themselves cannot be measured. For example, some quantities are the density of the α phase of the eutectic, the slope of the liquidus for the α phase of the eutectic, or the Gibbs-Thomson coefficient for the α phase of the eutectic.

Table 10.1 Table of Selected Values of System Parameters

Densities (from fitted equation) in gms/cm^3

23°C $\rho_E = 2.9809$

$\rho\alpha = 3.091$

$\rho\beta = 2.7545$

$\rho_{CBr_4} = 3.2763$

$\rho_{Hex} = 2.0523$

Calculated Volume Fraction of Minor Phase - 0.3253±0.003 for 8.4 w/o
- 0.3451 @83°C for 8.6 w/o

Composition of α phase 0.0508 w/f Hex.
Composition of β phase 0.1618 w/f Hex. in CBr_4
Composition of eutectic 0.084 w/f Hex.

Equilibrium Melting Temperatures (measured)

Tm eutectic = 83°C
Tm CBr_4 = 91.8°C
Tm Hex. = 186.6°C

Phase Diagram Data

mα slope of liquidus (abs. val.)=	1.48168 °C/w/o	near eutectic
mβ slope of liquidus (abs. val.)=	2.164 °C/w/o	temp. and compos.
nα slope of solidus (abs. val.)=	1.6178 °C/w/o	@ eutectic temp.
nβ slope of solidus (abs. val.)=	1.7878 °C/w/o	@ Cα, Cβ

$k\alpha = \frac{n\alpha}{m\alpha}$ @ 100% CBr_4 = 0.3166

$k\beta = \frac{n\beta}{m\beta}$ @ 100% C_2Cl_6 = 0.4021

Other Data

$\gamma_{SL(\alpha)}$	8.0±2.0 (mJ/m^2)	L_E	3.0 x 10^7 J/m^3
$\gamma_{SL(\beta)}$	10.0±2.0 (mJ/m^2)	L_α	3.12 x 10^7 J/m^3 = approx. 10 J/gm
$\gamma_{SL}(CBr_4)$	6.1±1.25 (mJ/m^2)	L_β	2.79 x 10^7 J/m^3

10.2 Phenomenological Microscopic Observations

This section will deal with the observations which are best presented in descriptive terms. The subsections 10.2.1, 10.2.4, 10.2.7, 10.2.9, 10.2.10 and 10.2.11 deal with observations of morphological features commonly found in the organic which formed without outside intervention. The other subsections report a variety of observations concerned largely with the response of interfaces to external stimuli such as convection or quenching.

10.2.1 The Variety of Eutectic Interfaces

During the course of experimentation, a great many photomicrographs were taken of solid-liquid interfaces. Representative photomicrographs of eutectic interfaces, most growing in a planar fashion, are presented in this section to illustrate the variety of morphologies observed. They serve to supplement other photographs found in appropriate sections of the thesis. Dissimilarities in appearance among eutectic interfaces may be analyzed in terms of differences in certain features from one interface to the next. The uniformity of structure, variations of trijunction angles, local curvature on the interfaces, alignment of lamellae tips, and phase boundary angle with respect to the isotherms, are all considered important features.

A series of interfaces are shown in Fig. 10.5. The first group are representative of planar, uniform, eutectic interfaces with the expected periodicity of the shape or form of the solid-liquid interface from lamella to lamella. The second group are unusual for various reasons. Fig. 10.19 shows a "zero-velocity" eutectic interface and other eutectic interfaces of interest are shown in Figures 10.12 and 10.13.

One important feature of advancing eutectic interfaces is the development of negative curvature at the centers of the lamellae (near the tip). This is a concavity in the solid-liquid interface. A larger lamellar spacing and higher

growth rate increase the degree of this negative curvature. Only growing interfaces displayed the negative curvature, but the higher growth rates do not ensure negative curvature. This is shown by noting that the minor phase always tends to show positive curvature. With some care, an interface with negative curvature in the minor phase was prepared. This is seen in the middle micrograph, Fig. 10.5A. This interface was growing at steady state at approximately 0.15 micrometers/sec. and the large lamellae alloweo to develop. The growth rate was then increased to approximately 0.75 micrometers/sec. and, instantly, the negative curvature developed in the β phase lamellae. The first and third micrograph on the Fig. 10.5A are interfaces growing at steady state. The first is typical for this system. The third has slightly deeper concavity in the α lamellae. This alloy has some Oil Red dye in it which has a low distribution coefficient in CBr_4.

The second group of micrographs, Fig. 10.5B show a diversity of interface shapes. In the first micrograph of the group (upper left corner) the interface was growing in a coupled manner, but the addition of Azobenzene and the occurrence of low energy interfaces created the unusual interface profile. In this micrograph, as well, the undercooling of the pockets of liquid in the negative cusps of the lamellae was so severe that branches are forming and growing into these pockets. Two eutectic grains of a hypereutectic composition alloy are

Fig. 10.5A

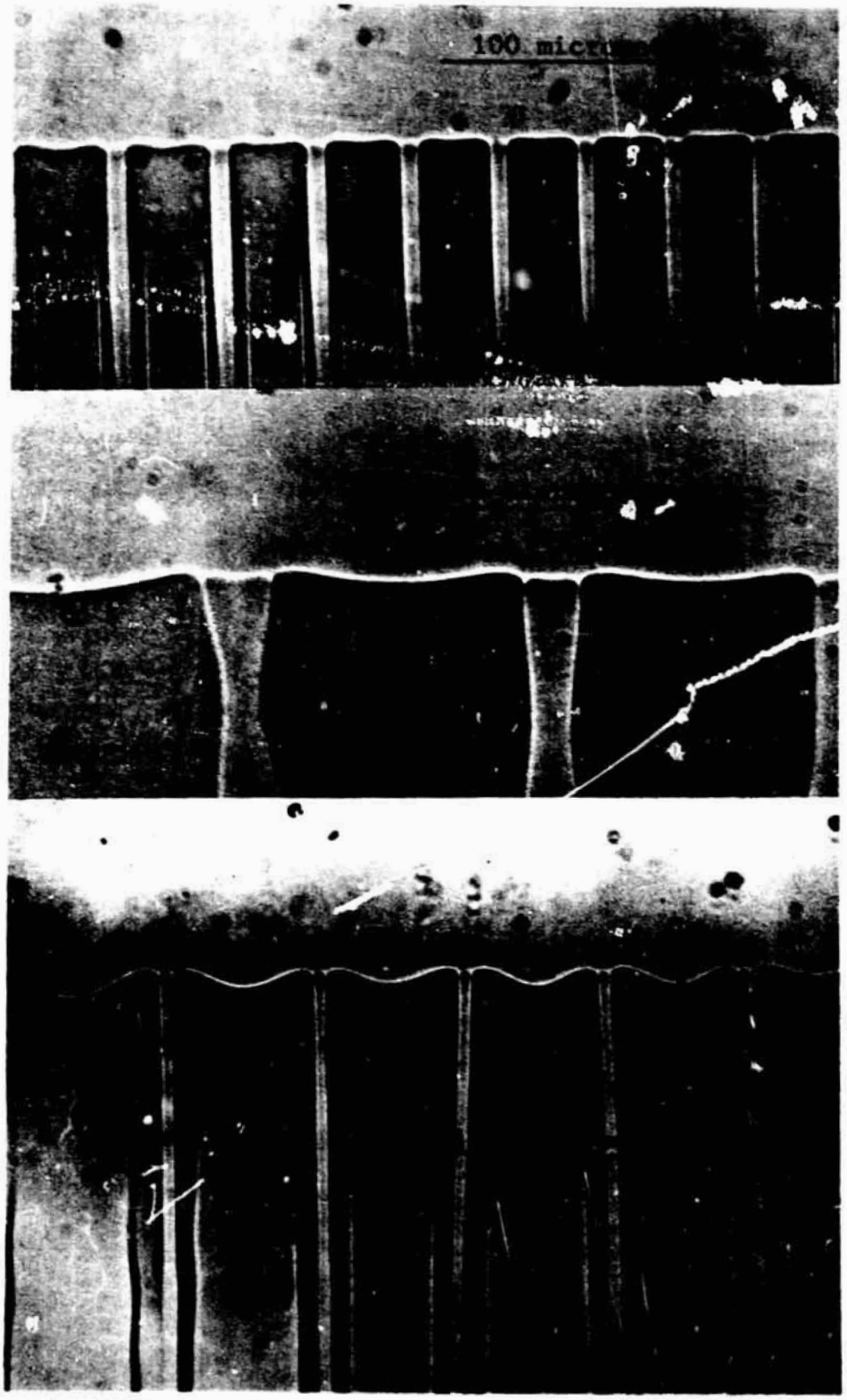

1. S27C2 G=24 degC/cm.,R=0.793 micrometers/sec.
2.S27C1 initial R=0.13,then raised to 0.8 micrometers/sec.
3.S33+Oil Red Dye impurity, 1.05 micrometers/sec.

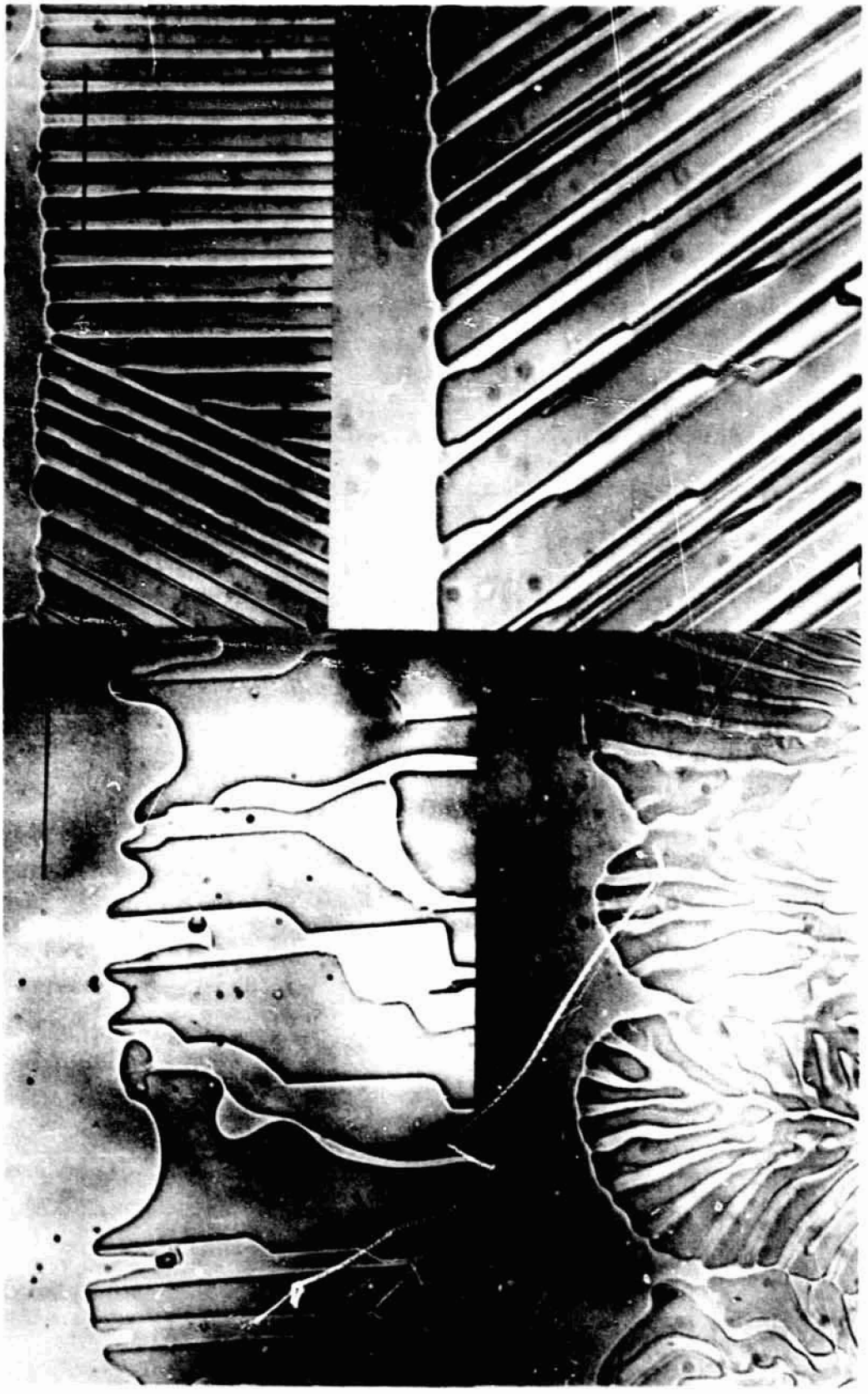

Fig.10.5B 100 micrometer markers
1. S9C1 0.529 micrometers/sec.; 2. S28C2 hypereutectic alloy.
3. S28C2 cellular interface; 4. S27C1 pure eutectic growing off-axis.

shown in the second micrograph in the group. The larger volume fraction of β phase is clearly shown as well as the overgrowth of one grain by another comprising of lamellae having lower interphase interfacial free energies.

The third micrograph in the Fig. 10.15B, shows a classic eutectic colony structure. Lamellar branching is also frequent in this micrograph.

The fourth micrograph in the set is a high magnification view of a very pure eutectic interface, but the phase boundaries between the lamellae show strong faceting and are considerably tilted with respect to the growth axis. Shallow trijunction cusps indicate that the phase boundaries are the "special" type, and the inflexibility of the lamellae to attain the "correct" volume fraction under these circumstances is also shown.

10.2.2 Convection Experiments

The effects observed when using the special convection cells were due wholly to forced convection phenomena. Due to the thin geometry of the cell and the viscosity of the liquid organic, natural convection effects were absent. Whenever impurity cells are considered in these cases, an addition of less than two weight percent Azobenzene was made. The results begin with pure and impure single phase alloys, then follow with eutectic interfaces. First, a description of convective behaviour will be presented.

The control of convection was direct and precise. The convection behaviour was easily observed since small dust particles or broken pieces of solidified organic in the liquid were seen moving with each application of the hydraulic forces. Flow was found to be smooth and uniform in velocity from tens of microns away from the interface right up the solid interface surface itself. Turbulent flow was never observed, nor were stagnant or boundary layers seen. For the isothermal cell construction, it is felt that if need be, the liquid ahead of one lamella could be shifted over, in plug type flow, to the next lamella.

Later, it was realized that such precise control was not necessary to observe the effects of convection on the interface. The results of the experiments, as well, were not significantly different when gentle versus forceful convection was used.

The third cell type for convection (see section 9.3.2) was used to replace pure liquid isothermally with impure liquid at a stationary single phase planar interface. The result was that the interface slowly receded and stopped at a point farther down the thermal gradient. The impure liquid could be considered corrosive to the pure solid. Where a grain boundary groove was present initially before convection, the shape of this groove did not change as the interface receded. Subsequent growth of the interface (at a rate which previously resulted in a planar interface) led to cellular breakdown.

The shape of a grain boundary groove in a "pure" alloy under isothermal convection conditions (convection cell type two, 9.3.2) did not perceptibly change its shape nor either melt nor grow.

Where the cell that was used was not the isothermal type, and a single phase alloy filled the cell, the convecting liquid replacing the liquid ahead of the interface would originate from a warmer part of the cell and cause the concommittant effects at the interface. This effect was melting back of the interface in the region near the barrier end where the flow was greatest.

The eutectic interfaces also melted back when the cell used was a simple (non-isothermal) convection cell. Secondary effects were observed as well. First, the major phase (CBr_4-rich) would recede more quickly than the minor phase.

Secondly, when the degree of convection was strong, the exposed fingers of the minor phase would weaken at their base (near the new position of the major phase interfaces) and swiftly be carried away as solid pieces after they were sheared off by the convective flow.

Isothermal convection of pure eutectic liquid at a eutectic interface is described next. Recall that considerable control of the convective flow was achieved, and that plug-type flow was observed in this type of experimental arrangement.

Regardless of the degree of convection, the only change at the slowly growing or stationary eutectic interface, was a slight "rounding" of the solid-liquid boundaries. The overall interface shape was made up of repeated convexity of the solid-liquid phase boundaries. (See Fig. 10.6) These observations were made on eutectic interfaces where the major phase width was less than approximately thirty micrometers. Larger lamellar widths were not observed under these conditions. The point of the above statement is significant since, as the lamellar spacing decreased, the change in interfacial shape upon the application of convection gradually became less perceptible.

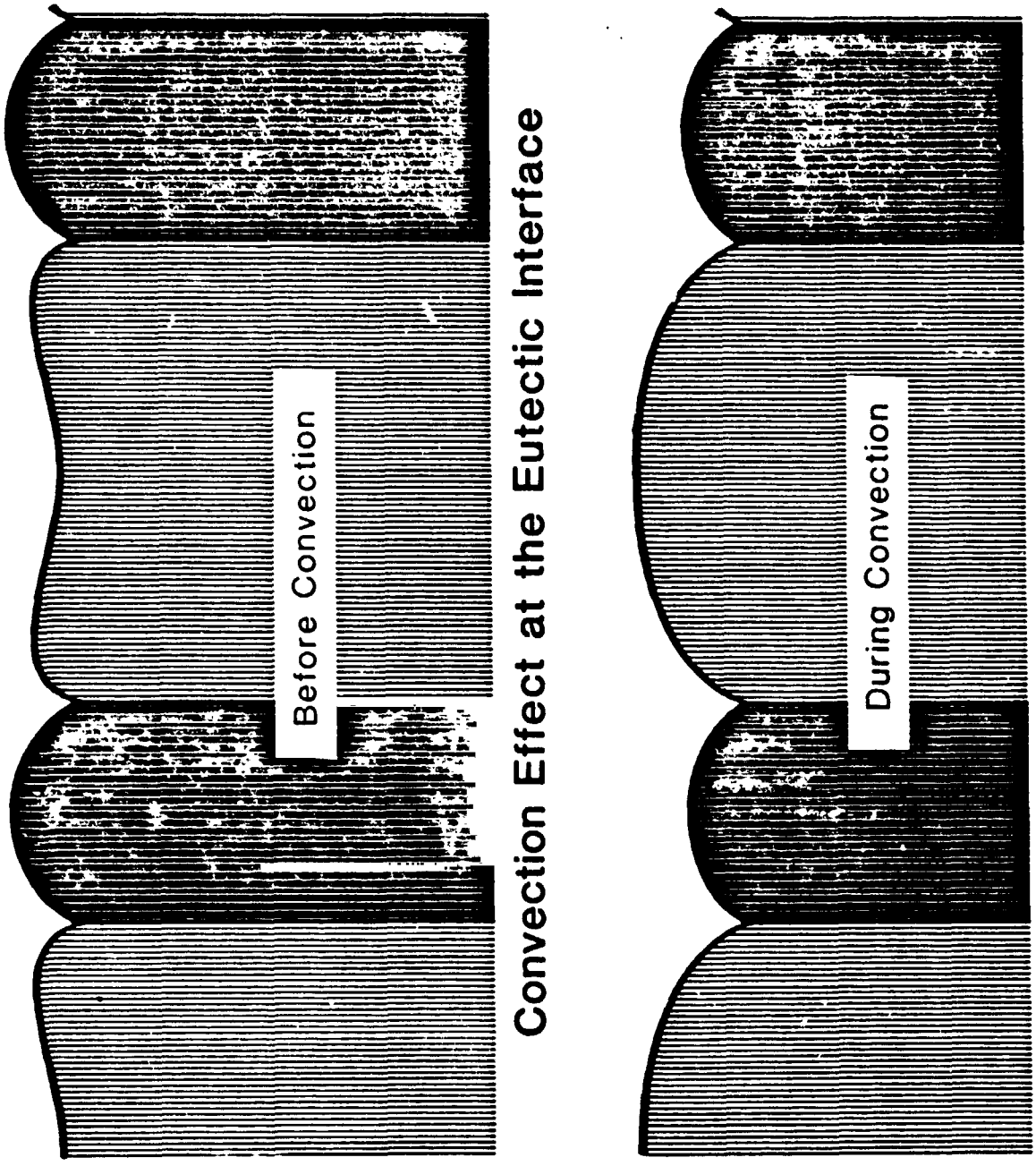
Convection Effect at the Eutectic Interface
Before Convection
During Convection

Fig. 10.6

10.2.3 Quenched Interfaces

The thermal transients introduced by quenching the liquid adjacent to a growing planar eutectic interface caused the formation of single-phase dendrites from the eutectic interface and the overgrowth of one phase by the other.

Rapid, strong quenches caused the formation of fine, single-phase dendrites, most of which originated from the CBr_4-rich phase. These dendrites grew in groups, distinguished by a common principal growth direction for the dendrites. Each group originated from a single eutectic grain. Wide lamellae of the CBr_4 phase often generated more than one dendrite stalk. If the lamellae of the minor phase were sufficiently wide, they too could generate dendrites, but these dendrites were always blocked by the other, faster growing CBr_4-rich dendrites. The dendrite groups from various eutectic grains were observed to be oriented at a variety of angles to the specimen axis, and rarely grew parallel to the eutectic lamellae from which they grew. A dendrite group could grow at a large angle from the eutectic growth axis and could block the growth of the dendrite group in the adjacent eutectic grain.

With the thermal transient source removed, the dendrite melted back completely in a few minutes. A second application of the quenching gas caused the same dendrite growth behaviour as in the previous thermal cycle, showing that the dendrite growth direction is unique for each individual eutectic

grain. These growth directions were presumably <100> directions, as the CBr_4-rich phase has the face-centred cubic structure. The fact that the dendrites were growing into a solute rich melt didn't alter the dendrite primary growth direction. [36] The dendrite primary arm spacing was always considerably smaller than the cell thickness. Dendrite growth did not appear to be influenced by the presence of the glass surfaces.

The severity of the quench could be controlled to give a wide range of cooling rates. A very mild quench was employed to study the initiation of the dendrites described above.

The mild quench caused the interface to advance in a similar fashion to the perturbations which develop at grain boundary grooves at planar single phase interfaces. An example of the development of these perturbations is shown in Fig. 10.9, for a single phase alloy. The trijunctions at the eutectic interfaces were the irregularities or singularities which initiated the breakdown. The sequence of events is depicted in Fig. 10.7 with micrographs and drawings. The CBr_4-rich phase, the major phase, overgrew the minor phase prior to the rapid dendritic growth from the solid. However, the overgrowth did not completely block the minor phase from growth but left a narrow channel through which the second phase could continue to grow.

The advance of the interface caused by a mild quench would recede in a few seconds to the original interface shape.

The local composition in the liquid under these circumstances may not have been upset sufficiently to prevent complete reversal of the quenching process to return the interface to its original state (as the temperatures return to the original values).

Fig. 10.7(a)

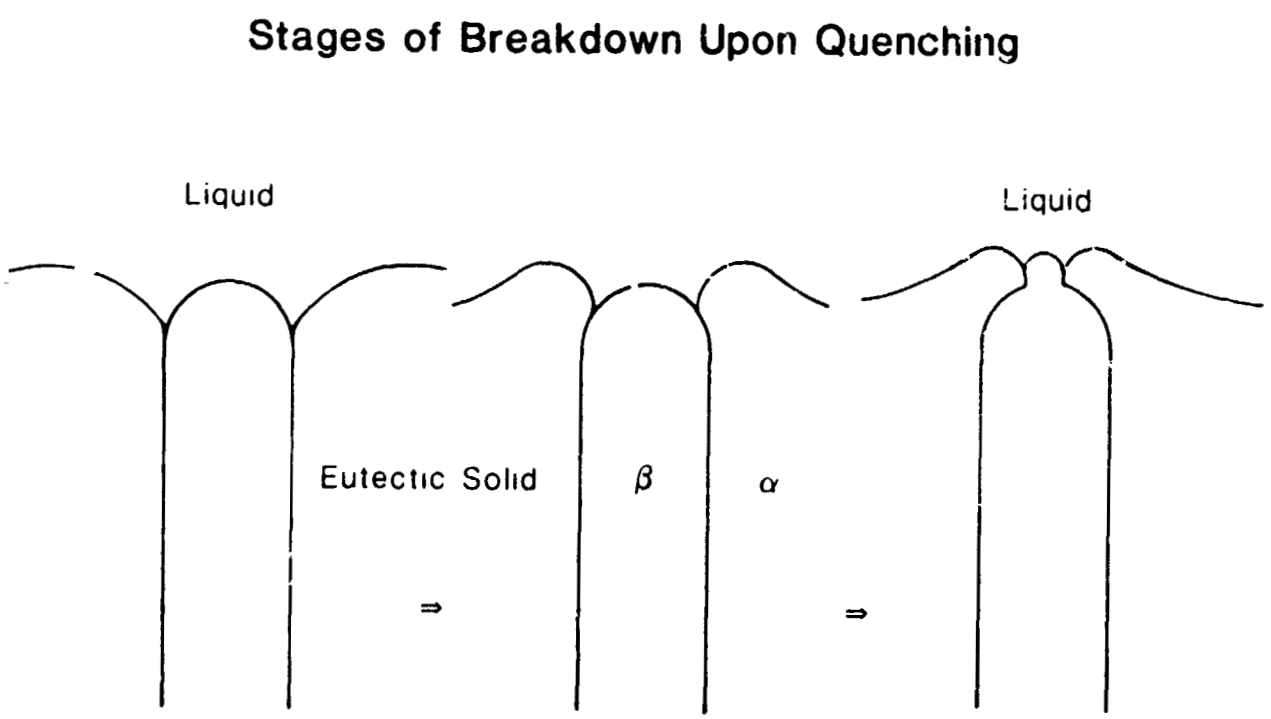

Fig. 10.7 (b) & (c)

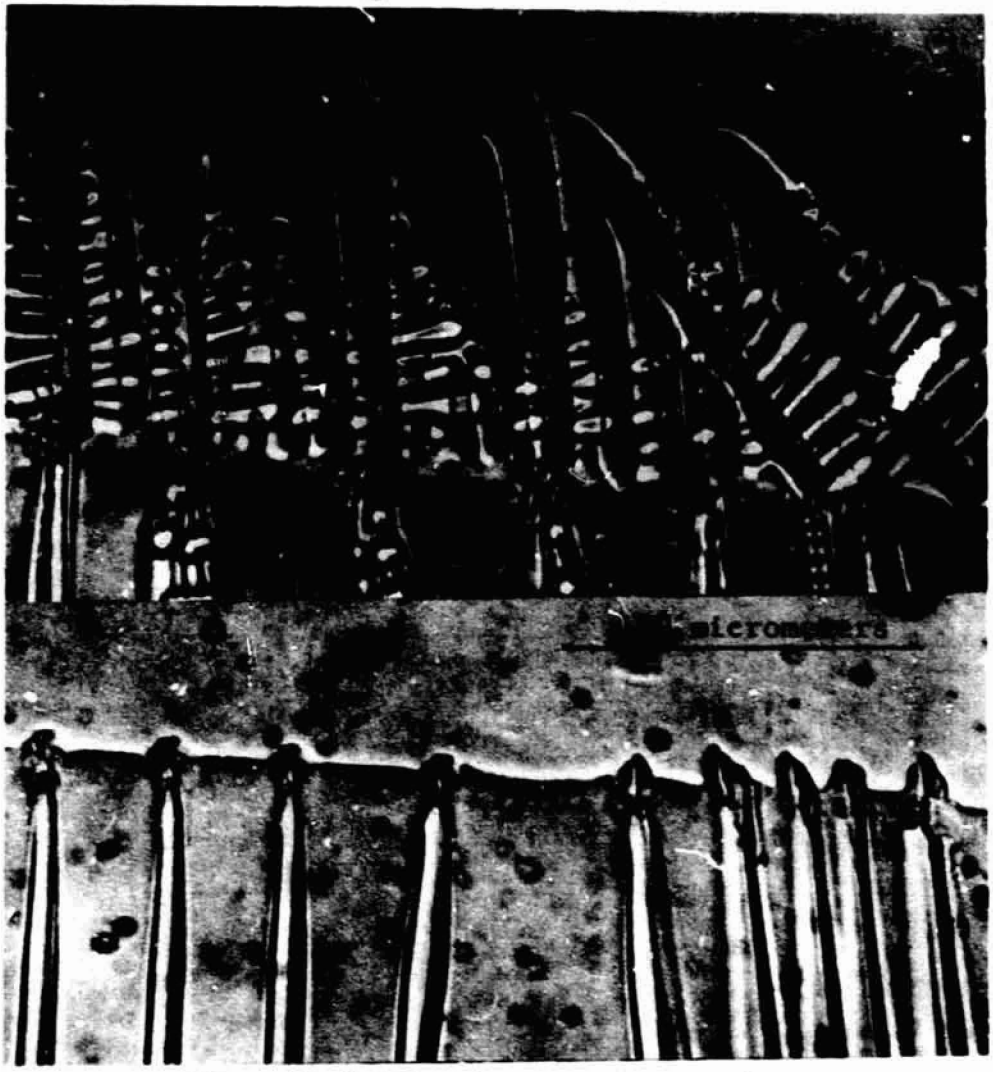

(c)
S12C2
Severe
Quench

(b)
Gentle
Quench

Fig. 10.8 Tilted View of Interface

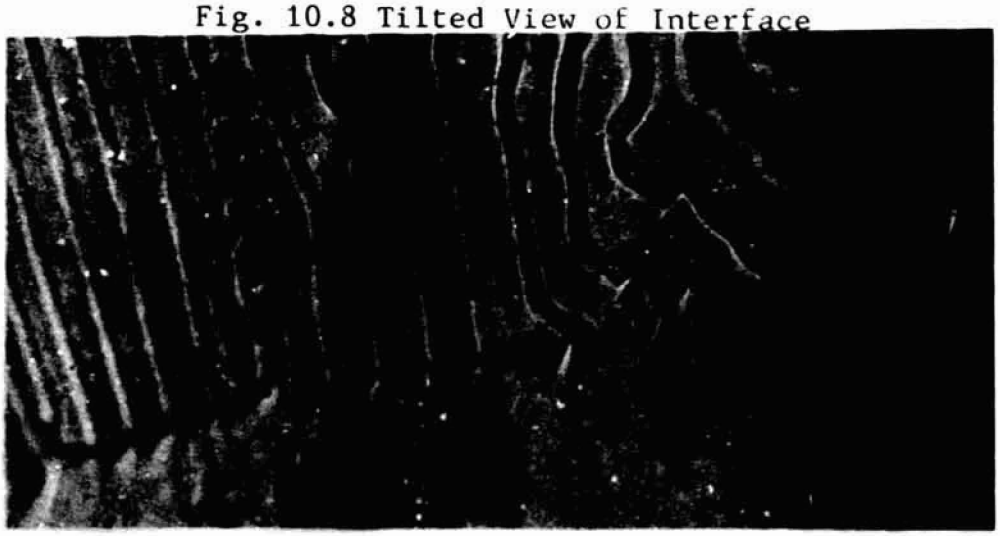

S12C3 2.0 micrometers/sec.

10.2.4 Angled View of Eutectic Interfaces

In order to determine the geometrical relationship between the solid-liquid interfaces and the glass surfaces of the cells, the microscope was remounted at an angle of approximately seventeen degrees from the vertical, so that the solid-liquid interface could be seen in perspective through the liquid. While observations were difficult owing to the limited depth of field of the objective lens (approximately two micrometers), photomicrographs of the interface revealed the features shown in Fig. 10.8 . An important observation is the virtually flat vertical face of the interface, without secondary curvature in the vertical axis. In addition, the phase boundaries tend to lie normal to the gla. ; surfaces. The photographs do not show the observed thin layer of liquid (melt) between the organic solid and the lower glass surface just behind the leading edge of the interface.

10.2.5 The Effects of Impurity Additions and Changes in Velocity of Growth on Single Phase Interfaces

The observations in this section describe the effects of changes in growth velocity on an interface in pure or impure CBr_4 as well as alloys of CBr_4 and C_2Cl_6. In particular, the shape of a grain boundary groove was monitored both with and without the development of morphological instabilities due to constitutional undercooling effects. The effects of constitutional undercooling on the morphology of a grain boundary groove have been extensively studied by others [7] and lead to changes characteristic of the cause (constitutional undercooling).

The first, simple experiment was to follow the changes, if any, of the grain boundary groove shape as the interface responded to various step changes in velocity from a standstill. The cell velocity was taken from zero to some constant value (e.g. five micrometers per second). When pure CBr_4 or an alloy made from pure CBr_4 was tested in this way, there was no visible change in the grain boundary groove shape, even for slow steady state growth up to speeds of the order of two to three micrometers per second. A similar observation was made by Jones and Chadwick in an ice-water-NaCl system. [13] They noted that small interface movements would not lead to shape changes at grain boundary grooves. After a period of steady growth of such an interface, there would be some change in the shape of the groove. The onset of the change in shape would occur more quickly when the velocity was set to a higher value. This

would be caused by the accumulation of the residual impurities or of the impurity products of degradation of the CBr_4 during growth. The changes in shape that were observed at this point were identical to those obtained when a third component was purposely added to an alloy. This effect is described next.

When otherwise pure alloys were doped with impurities such as Azobenzene and tested in the manner described above, there was little delay from the step change in velocity before a grain boundary groove shape change was observed. Fig. 10.9 shows a typical sequence with time, showing changes in a grain boundary groove resulting from a step change from zero to to 4.2 micrometers per second.

Observations of steady state growth of dilute alloys of C_2Cl_6 in CBr_4 were made as well. The stages of interfacial breakdown from the effects of constitutional undercooling were monitored.

The observations which follow were made for an alloy of 2.45 weight percent Hexachloroethane in CBr_4 , growing at 0.265 micrometers per second. At a velocity below this value, the interface was at all positions planar. Growing at this velocity, the interface was almost planar but a set of evenly spaced discontinuities formed, usually in one grain before another and starting, one at a time, from the discontinuity formed by an existing grain boundary. These discontinuities were spaced thirty to fifty micrometers apart and became invisible

approximately 150 micrometers behind the interface.

It is believed that the discontinuities described above are known as nodes. Nodes are the precursors of cell boundaries. [42, 7] The discontinuities observed caused no curvature at the solid-liquid interface (which would be characteristic of cell formation). Nodes form where rejected solute collects in periodically distributed pockets (without visible formation of interface curvature). When a slightly higher growth rate was applied, both the grain boundary groove and the solid-liquid interface near the nodes developed additional curvatures so that the interface became clearly cellular. At this stage, once steady state was reached, the cell boundaries and grain boundary grooves were indistinguishable from one another. This observation should be compared to the step change observation described earlier and shown in Fig. 10.9. The effects of constitutional undercooling were introduced more abruptly in the earlier case and the curvature of the grain boundary groove increased rapidly and caused full cellular growth to occur without the prior development of nodes. This (Fig. 10.9) form of breakdown is analogous to quenching the interface. (Blowing on the cell surface confirms this.)

There was a second purpose to study the planar-cellular breakdown process in dilute alloys. This was done to attempt a measurement of the diffusion coefficient in the

liquid of the solute using the constitutional undercooling criterion. Unfortunately, it seems the distribution coefficient of the unknown impurity in the CBr_4 is very much smaller than that for C_2Cl_6 in CBr_4 (which is greater than 0.3).

Fig. 10.9

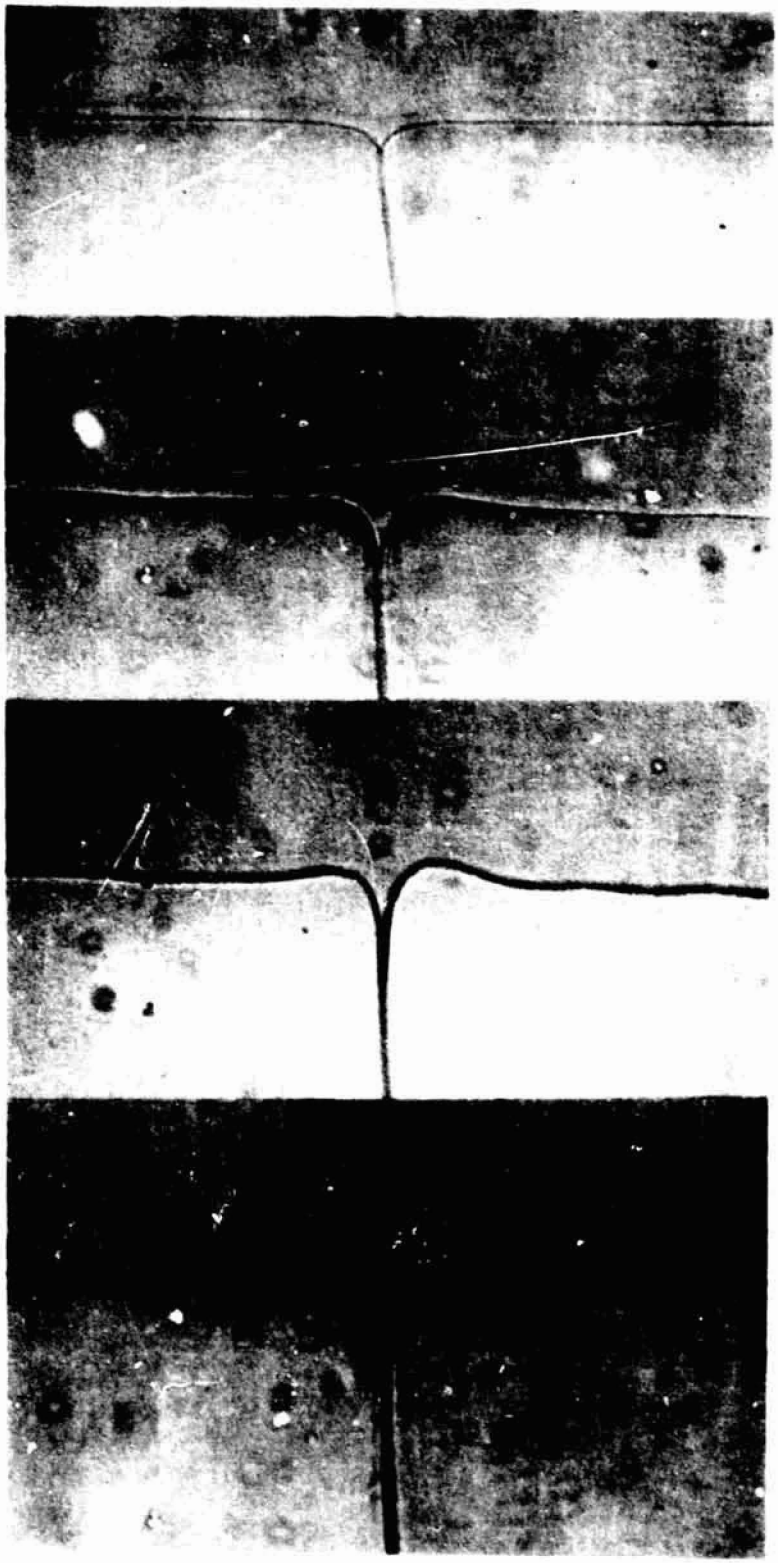

(a)
Zero
Velocity

(b)

(c)

(d)

Stages of breakdown of a Grain Boundary Groove
S16C2, R=0 to 2.5 micrometers/sec.

10.2.6 Combined Convection and Quenching

Quenching and convection could be done together when growing the organic alloy in a convection cell without the protective second coverglass. While various procedures were used, the most informative sequence involved a quench, followed by convection, then followed by another quench while convection was still in progress. The result of this sequence was as follows:

The first quench caused dendrite growth, as described earlier, each eutectic grain leading to a differently oriented set of dendrites. Convection at this time led to two observations. First, there was motion of small, foreign particles in the liquid well within the dendrite network, and even near the original interface, showing that forced convection was effective throughout the dendrite network. Second, large branches of the dendrites were seen to break off in the convection current and drift away in pieces while slowly melting.

The second quench caused the undetached dendrites to grow further, and the drifting pieces of dendrites to fasten themselves to the regrowing dendrites and continued to grow also. These dendrite pieces lodged themselves in random orientations in the newly formed solid, growing as separate eutectic grains.

These events exactly parallel grain multiplication in castings of single phase alloys. [7, 39] For the first time,

these observations have been made in a eutectic alloy. The dendrites, as finally solidified, were seen to be made up of two phases and thus could be classed as eutectic dendrites, although coupled growth was not maintained throughout their formation.

10.2.7 Nucleation Experiment

In this experiment, the cell, containing a fully molten eutectic alloy, was driven at constant speed toward the lower temperature end of the microscope stage. Some undercooling was achieved, and the nucleation event for the eutectic alloy was observed. As soon as the nucleation event was detected, the motor drive was turned off. The undercooled liquid solidified, and a solid-liquid interface was finally established on the equilibrium isotherm. The distance from this point, to the point of nucleation (most undercooled liquid), together with the known temperature gradient, permitted estimation of the undercooling attained.

In the experiments, the nucleation events were always the heterogeneous type, nucleation often occurring on the glue wall of the "V"-shaped end of the cell. In one cell, a nearly invisible dust particle consistently nucleated the alloy.

Fig 10.10 is a photograph of the television monitor displaying the view subsequent to the nucleation event. What was immediately evident was the single phase dendritic growth (apparently the α phase) in three mutually orthonormal directions. The dendrite arm which was directed towards the more undercooled liquid accelerated in growth rate as the dendrite tip entered progressively cooler liquid. Secondary dendrite arms formed and grew into the undercooled liquid. After approximately one second, the evolution of latent heat slowed the as yet still

single phase growth. Then, the other phase of the eutectic was observed forming between the arms of the dendrites. After this stage, coupled eutectic grew as colonies or grains.until the stationary equilibrium interface was formed.

The calculated maximum undercooling observed for these cells filled with eutectic was ~1.5 degrees.

Fig. 10.10

Nucleation of Undercooled Eutectic Liquid, T.V. sequence. Approximately 500 x.

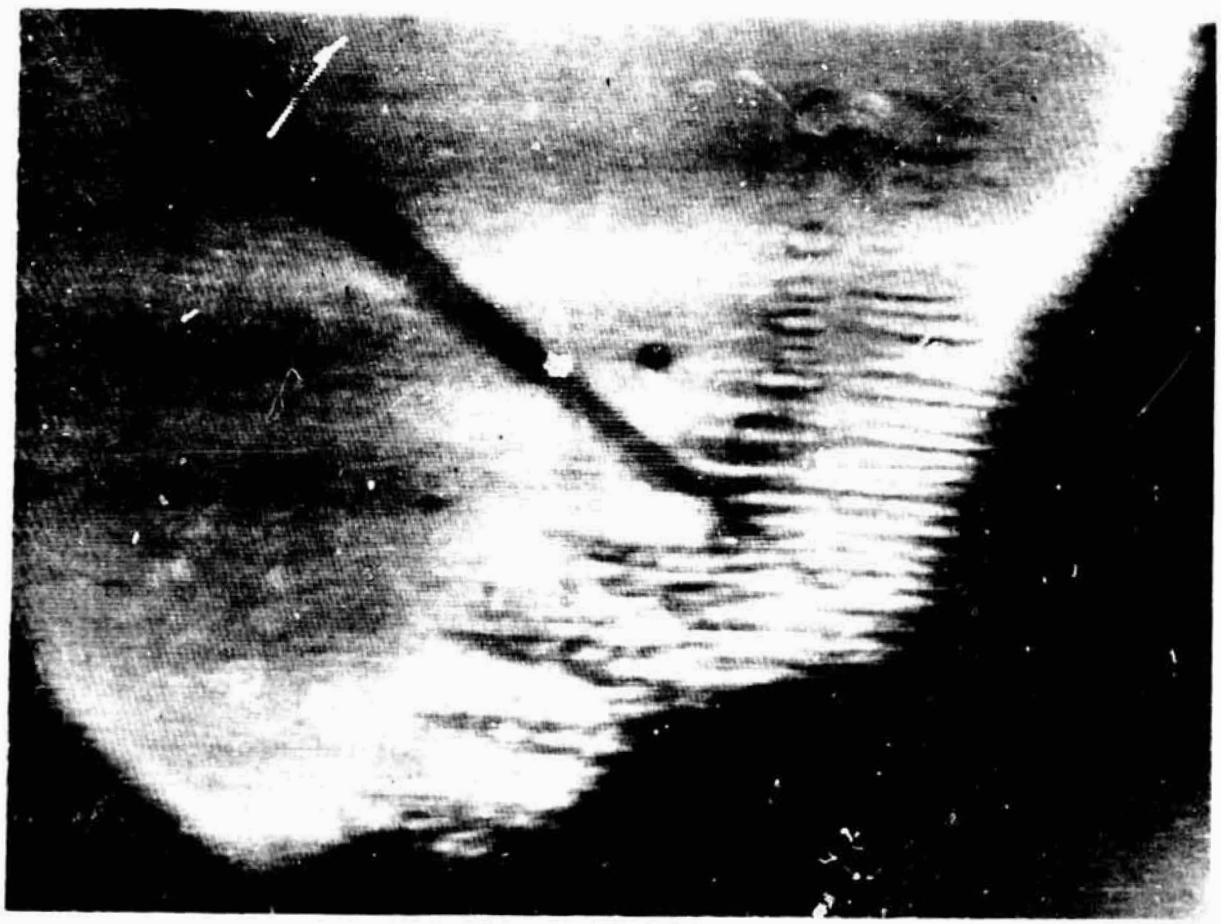

10.2.8 Double Alloy Cells

If growth was initiated in pure eutectic and continued into the impure eutectic liquid, there was little change of the interface shape on the scale of the lamellae. This was the case when the growth rate was kept very slow (e.g. R = 0.5 micrometers per second) to maintain a planar interface in the presence of the impurities. The only definite observation was the breakdown of the planar interface into a cellular interface at very low velocities (R<1.5 micrometers per second), and to eutectic dendrites at higher velocities.

Very little diffusion in the liquid occurred, which would mix the impure with the pure liquid. It was relatively easy to detect the transition by colour change of sample, since the impurity added (Azobenzene) is itself, yellow-orange in colour.

10.2.9 Thermomigration of Liquid Droplets

Observations of thermomigration of liquid droplets were made in single-phase alloy specimens prior to initiation of growth. In the cast solid near the interface, spherical droplets of liquid only a few micrometers in diameter were observed to form. In the temperature gradient present, these droplets migrated to the interface, to finally enter the bulk of the liquid. The depression in the solid-liquid interface that was formed when a droplet contacted the bulk liquid, filled in with solid rapidly, leaving no trace of the droplet.

On the average, the time elapsed from first contact of the droplet with the interface to the complete restoration of the interface shape, in a typical temperature gradient, was approximately ten seconds.

10.2.10 Low Energy Interphase Interfaces ("Special" Boundaries)

Across the width of a cell, a planar eutectic interface usually consists of several eutectic grains. This fact cannot be recognized by simply viewing a normal planar interface which is made up of high energy interphase boundaries, although the grains can be revealed by quenching to produce dendrites growing in a different direction from each grain. However, a distinct eutectic grain was frequently observed in which the interphase boundaries were aligned in a direction other than the growth direction as designated by the normal to the solid-liquid interface. Such a eutectic grain was growing with more stable, lower energy interphase interfaces ("special" boundaries). This lower energy is evident in the shallower cusps that develop at the trijunctions compared to the cusps or grooves at trijunctions which form with high energy interphase boundaries. A consequence of these eutectic grains made up of low energy interphase boundaries is the inflexibility of the interface to accommodate local variations of composition, or perturbations in growth rate, growth direction or volume fraction. These grains, because of their persistence in growing off-axis, eventually grow into other "lower energy grains" or cease growth at the sides of the cell. Such grains are easily detected at an interface if they grow-off axis. However, many grains with low energy interphase boundaries do grow alongside grains with high energy phase boundaries in the

cell axis. These can be identified by locating the very shallow or flat trijunction groove. A micrograph showing a group of low energy interphase interfaces growing off-axis to the heat flow is given in Fig. 10.11. The cell used in the micrographs was filled with an organic alloy made with CBr_4 that had not been purified. Other examples are found in Fig. 10.5.

Under conditions of low thermal gradients, using pure starting materials, another manifestation of the difference between high and low energy boundaries was observed, at the growing solid-liquid interface. Direct comparison of the position of the solid-liquid interface formed by eutectic growing with special boundaries and the position of the interface with high energy boundaries showed that the interface with the special boundaries grew with less undercooling. The local solid-liquid interface was seen to grow in advance of the surrounding interface when the former consisted of special boundaries and the latter consisted of high energy boundaries. Examples are shown in Fig. 10.12. The difference in undercooling must be small because this phenomena was only observed with a shallow thermal gradient (approximately 6.8 degrees/cm). From the interfaces in Fig. 10.12, the distance the low energy interface leads the high energy interface was measured and the relative temperature difference calculated. For the low R interface (0.65 micrometers/sec.) the temperature difference was 0.016°C and for the high R interface (4 micrometers/sec.)

the temperature difference was 0.036°C. The observation of this phenomenon was found to be masked by constitutional undercooling effects caused by impurities and higher growth rates. An extreme example of this was the observation of needle-like growth of one α and one β lamella side by side with the trijunction that formed at the tip showing almost no grooving. The interface nearby followed, but not in a fully planar manner. This behaviour could be induced in the purified eutectic alloys by growing at a speed greater than the planar-cellular breakdown velocity for the given thermal gradient. (There was always some residual impurity in all cells.)

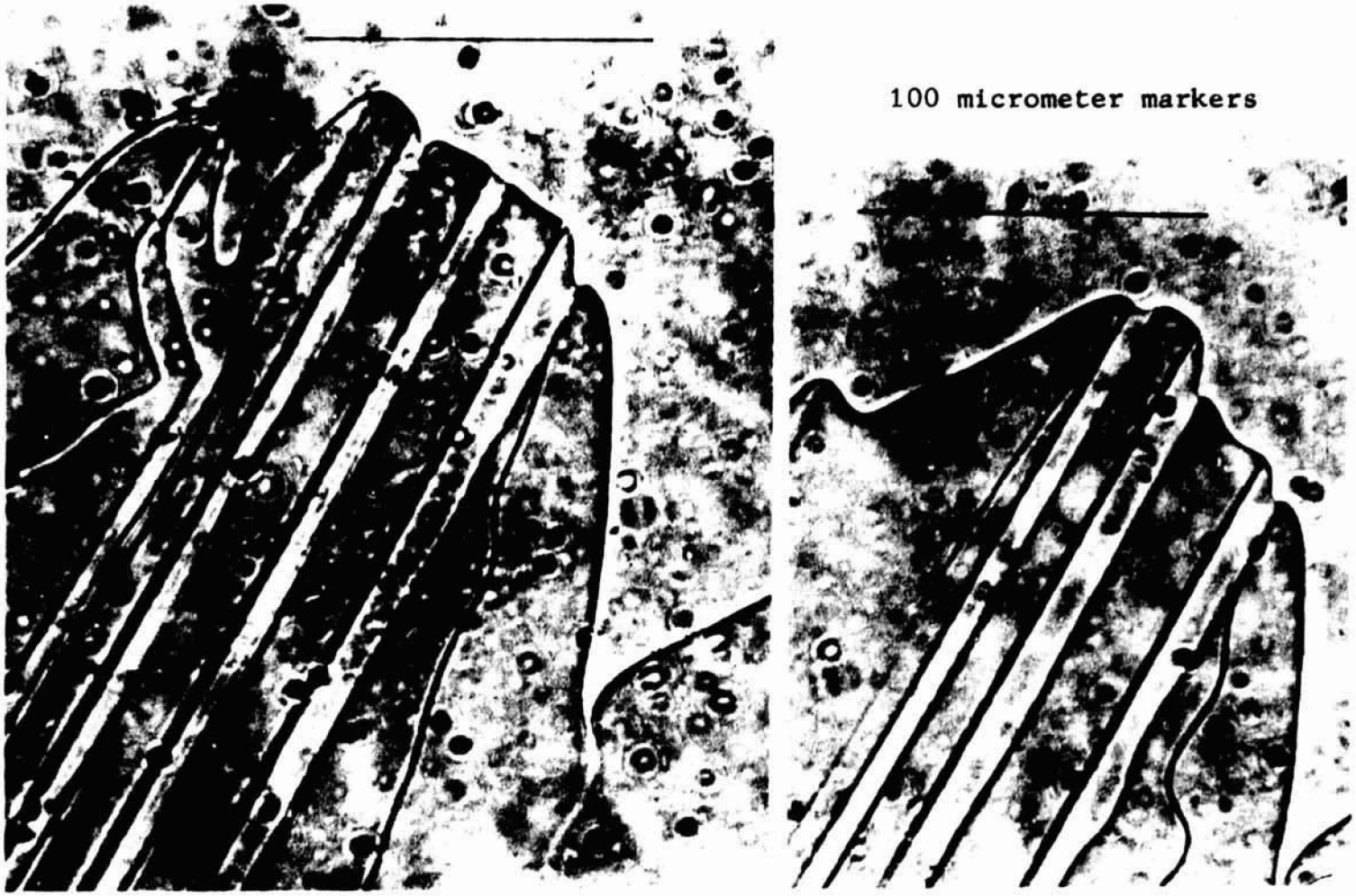

Fig. 10.11 (a) & (b)
Both micrographs: R=1.32 micrometers/sec., G= 6.8 degC/cm.

Fig. 10.12

Upper: S27C3 R=0.62 micrometers/sec., G=6.8 degC/cm.
Lower: same sample and G, R= 4 micrometers/sec.

10.2.11 Lamellar Spacing Development

During the experiments reported in this thesis, observations were made of the manner in which the eutectic lamellar spacing changes in response to a change in growth rate and of the development of a eutectic interface after nucleation in a fully liquid sample. These observations will be reported in this section.

Jackson and Hunt first observed using this organic alloy that when the growth rate was increased, the lamellar spacing became finer everywhere at the interface. The formation of several new lamellae did not occur by a nucleation mechanism but rather, a branch developed from the one phase and grew into the nearby pocket of undercooled and solute enriched liquid ahead of the neighbouring phase. [2]

It was observed in this work that the minor phase would generally branch to eventually consume the solute and liquid in the pocket formed by the negative curvature in the major phase lamella (formed after the change in R was made). The branch stems from the side of the minor phase at nearly right angles to the interphase boundary plane. The branch usually developed in a region up to approximately fifty micrometers behind the leading edge of the interface. This is because there is a thin film of liquid between the lower surface of the solid eutectic and the glass surface. The branch can follow this liquid to the enriched pocket which had

developed spontaneously from the growth rate increase. On rare occasions a branch was observed to develop as described above except that the branch did not follow the liquid film to the solute pocket, (as was more often the case) but rather, an opening was formed in the lamella through which the branch penetrated. Examples of these branches can be found behind some interfaces in Fig. 10.5; for example in the colony structure shown, a few branches can be located. Branches such as these have been observed in deeply etched metal eutectic alloys. [40, 43] The solidified morphology would reveal perforated lamellae at the branch. This mechanism for the reduction in lamellar spacing was the only one observed. For small changes in growth rate, only a few minor phase lamellae branched. These were generally adjacent to a slightly oversize major phase lamella. When the growth rate change was large, nearly every major phase lamella developed a deep negative curvature into which branching occurred by the minor phase. A planar interface then continued to grow, with the new lamellar spacing. Splitting of the minor phase was rarely observed.

The mechanism by which the lamellar spacing increased when the growth rate was reduced was observed during the development of zero velocity interfaces. (See section 9.2) A quick reduction of interface velocity would eventually cause many major phase lamellae to thicken and join together to reduce their numbers. The sequence of events was as follows. First, a reduction in R occurs. For low growth rates, the minor

phase lamellae would recede slightly from the interface front. At higher growth rates, the relative position of the major and minor phases would not change significantly. Then the process of elimination of minor phase lamellae began. The neighbouring major phase lamellae about a minor phase lamella would edge up the sides of the exposed solid-liquid interface of the minor phase until the two major phase lamellae joined, terminating growth of the minor phase lamella. As the interface continued to grow, the lamellae in the vicinity adjusted their widths until steady state growth was again achieved. The result of a reduction in R is shown in Fig. 10.13.

The development of a polyphase morphology from a liquid could not be observed directly until the transparent organics were studied. The generation of hundreds of lamellae has not been observed before. The genesis of a planar eutectic interface has been studied here for two conditions. The simple case of growth from a partially melted solid readily yields a composite interface. The cast eutectic alloy always had some β phase within the α phase matrix in contact with the melt. Under these circumstances, β phase nucleation is not a pre-requisite for growth. The random arrangement of lamellae quickly adjusts to a regularly spaced eutectic as growth proceeds. Combinations of the lamellar spacing change mechanisms direct the lamellae into an orderly interface.

The nucleation (See section 10.2.6) experiment provided

the means of observing the genesis of a eutectic interface from the liquid. As noted earlier, the first solid to form from a fully molten specimen was a single phase dendrite of the carbon tetrabromide phase. After the supercooled liquid was consumed by forming the dendrite, the remaining liquid between the dendrite arms transformed to the second phase which grew on the dendrite arms. The result was the periodic structure of the eutectic. Continued growth of the interface would include the alignment of the solidification front to the isotherms and of the simultaneous adjustment of the lamellae to the interface velocity and local growth direction. Groups of lamellae were observed, at times, to grow in a curved path (forming an elbow) until the steady state unidirectional growth along the cell and heat flow direction began. Approximately one side of one dendrite stalk would develop into one eutectic grain. Sequential, repeated nucleation of one phase on another was never observed.

Fig. 10.13

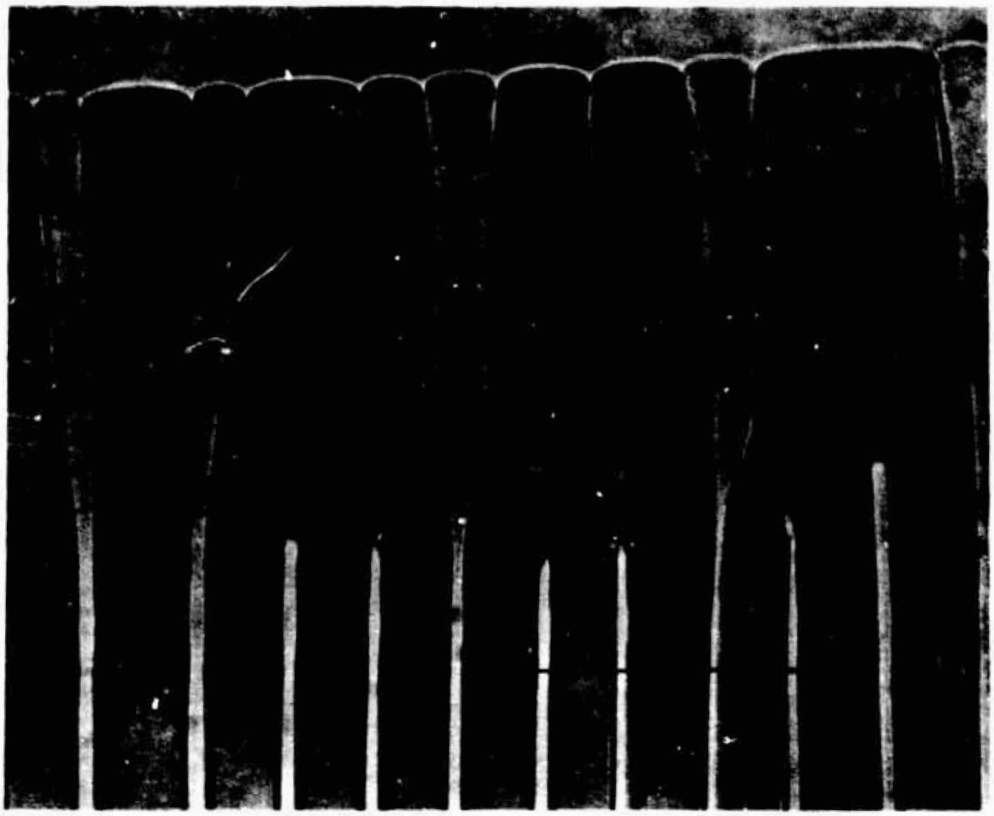

S31C2 R=0.13 micrometers/sec., G=25 degC/cm.

100 micrometer markers

Fig. 10.14
S12C3 melting interface, G approx. 25 degC/cm.

10.2.12 Controlled Melting of an Interface

The Temperature Gradient Microscope was as well suited to the performance of controlled melting experiments as to controlled growth. Depending upon the rate of melting, the interface shape was sometimes radically different from that for a growing interface. For example, for melt rates of less than one micrometer per second, the eutectic interface was indistinguishable from a growing one. Up to rates of two to three micrometers per second, the distinguishing feature of a melting interface was the constant positive curvature where, during growth, regions of zero or negative curvature had been ovserved. These differences between melting and freezing interface morphology depended upon the initial lamellar spacing and thus growth rate. Finer lamellar spacings reduced the apparent differences in morphology of the interface between growing and melting.

At higher rates of melting (e.g. over six micrometers per second) the interface curvature developed to a form very unlike any observed during growth. Fig. 10.14 shows an interface melting at a high rate. The sharpened nature of the minor phase is very characteristic of these melting interfaces. Where the melt rate was even greater, such as ten micrometers per second, the minor phase extended well into the liquid and formed a long, wedge-shaped remnant of the lamella. The sides of the wedge appeared to be flat and the tip sharp. The major phase,

even under these conditions, attained a constant positive curvature of the interface. It seems that the melting process was not totally controlled by the local temperature. This statement can be made from the knowledge of the similarity of thermal conductivity of the solid and liquid and that the heat of fusion for both phases is nearly the same. From this, it is apparent that the wedge of minor phase melts at a rate that is not determined by the local curvature nor by the local temperature gradient.

10.2.13 Other Observations

Observations which were not consequences of a systematic series of experiments are presented in this section. One such observation was the appearance at the eutectic interface of a grain boundary groove cusp within a lamella. While grain boundaries within the minor phase were rare, the extraordinarily large CBr_4-rich lamellae were sometimes "split" by a grain boundary which would propagate in a stable manner. The appearances of these grain boundary grooves were similar to the trijunction cusp shapes when the growth velocity was low. However, as the growth rate was increased, the grain boundary cusp deepened, relative to the trijunction cusps.

The grain boundary within the lamella constitutes the eutectic grain boundary, and quenching the interface caused dendrite growth in different directions from either crystal about the grain boundary. The neighbouring lamellae of the same grain produced dendrites growing out in the same direction. Fig. 10.13 shows two grain boundaries at a eutectic interface.

In this micrograph, a chronological record of the sequence of events is preserved. The reduction of the growth rate from 0.53 micrometers per second to 0.13 micrometers per second caused some α lamellae to overgrow the β lamellae, but when doing so, some misorientation between the thicker, slower growth rate lamellae led to the formation of the grain boundaries. Close examination will show that the two grain boundaries originate at

prior β phase lamellae. In addition, note that the volume fraction of β phase did not readjust itself immediately after the reduction in the number of β lamellae, but rather did so over an extended period of time and growth.

On one occasion, a test was performed to ascertain if the lamellar spacing would continue to increase with decreasing speed of freezing to the lowest attainable speed. This organic eutectic and the apparatus were uniquely suited to this task. The rate of growth was gradually reduced until a growth rate of 0.53 micrometers per second was achieved where to this time, the lamellar spacing smoothly increased. Then, the growth rate was reduced by half, to 0.265 micrometers per second. For the first several minutes, the lamellar spacing remained the same. Without altering the spacing, the minor phase then began to send out branches near the interface within a thin layer of liquid which often remains against the glass. The branches formed periodically on either side of each minor phase lamella. When a branch reached the midpoint of the major phase lamella tip, then a new minor phase lamella began to grow, now the full thickness of the cell, as the others. Eventually, the lamellar spacing for the interface was half that for the faster growth rate of 0.53 micrometers per second. There was, in addition, a difference in morphology of the lamellae. Instead of plano-parallel lamellae growing normal to the interface, there was a gentle weaving back and forth of each of the minor phase lamellae.

Off-eutectic compositions could support coupled growth if the compositions were not excessively hyper or hypoeutectic. It was difficult to obtain a planar interface made up of lamellae for hypoeutectic compositions. For example, an alloy containing 7.5 weight percent Hexachloroethane could only grow in a coupled manner if the growth rate was high enough (R>1 micrometer/sec.), otherwise planar single phase growth resulted. Hypereutectic alloys up to 11.5 weight percent Hexachloroethane were readily grown in a coupled manner without a velocity restriction.

The addition of small amounts of impurity (Azobenzene, Benzil, Cyclohexanol, Succinonitrile, Oil Red (Samples #6, 9, 14, 15, 18, 19) from 0.1 to 0.3 weight percent did not cause significant changes to the eutectic interface morphology when the interface was grown as a planar one. The addition of the impurities did, however, increase the difficulty of maintaining a planar interface in the presence of constitutional undercooling. Lower growth rates were always needed. Changes to the morphology did occur when constitutional undercooling induced interfacial breakdown occurred. The rejection of impurities was confirmed in two ways. The coloured impurities, Benzil, Azobenzene and Oil Red all were observed to collect at the interface, causing a sharp band of colour to develop at the interface. The Succinonitrile impurity had such low solubility in the solid eutectic, that it was observed to precipitate at the eutectic interface. When Succinonitrile was added to pure CBr_4 (sample

S22) Succinonitrile collected in the liquid at the single phase interface and precipitated in the liquid prior to being engulfed by the solid. The interfaces both were of the planar type as this phenomenon occurred. In addition, there was no perceptible difference between these interfaces and those which were otherwise pure.

10.3 Results of Micrographic Analysis

10.3.1 Solid-Liquid Interfacial Free Energy Variation With Composition

The results compiled for the measurements of $\gamma_{\alpha L}$ and $\gamma_{\beta L}$ vs. weight percent Hexachloroethane, are presented in Fig. 10.16. Several important points that relate to this graph will be noted in this section, including modification to the application of the Glicksman and Nash method, a comparison with the Bolling and Tiller analysis, reasons for the limited range of composition covered and an estimate of the accuracy of the method. Changes in γ_{SL} of pure CBr_4 due to the addition of small quantities of various other organic materials are also reported.

During the course of performing the experimental measurements, some limitations of the Glicksman and Nash method, as outlined earlier in section 8.2.2, became evident when the method was applied to this experimental arrangement. One limitation, which will be discussed later in the thesis (section 10.3.4 and in the Appendix) was found when the parameter $\delta>0.22$. The second limitation, which applies to this section, was found by experience and requires that $\delta>0.06$. This limit, which arises from the difficulty of reading a computer-generated curve in the Glicksman and Nash paper near one end of its range, was important when the grain boundary groove spacings became exceptionally large, as they often did. It was discovered that for $\delta<0.06$,

the Bolling and Tiller type analysis would give an equivalent answer. This stems from the fact that the Bolling and Tiller analysis assumes that the groove under study is isolated (such that for Glicksman and Nash, $\delta \to 0$).

Under nearly all circumstances, the grain boundary grooves observed were over one hundred micrometers apart. For such spacings, an imprecise value of γ_{SL} was given by strictly applying the Glicksman and Nash method. A systematic and justifiable correction was devised. The solution to the problem was found by applying the Glicksman and Nash method to measure the γ_{SL} from a hypothetical Bolling and Tiller grain boundary groove, drawn with preselected values for γ_{SL}, G and ΔS_f. When the groove spacing (2λ), required in the Glicksman and Nash method, was selected to fall in a particular range, the measurement was found to regenerate the preselected value of γ_{SL} to within an accuracy of a few percent. This experiment not only cross-checked the methods but showed how the convenient Glicksman and Nash method might be implemented in an amended form. From the cases where the experimental grain boundary groove spacing was small enough to apply the unmodified Glicksman and Nash method, and from test measurements with computer generated Bolling and Tiller shapes, a value of spacing (2λ) was obtained by trial and error methods that could be applied to all measured d values for the special cases where $\delta < 0.06$. A single value of δ was found ($\delta = 0.06$) where the

two methods would overlap.

The first step in finding the value of γ_{SL} was to compile the measurements of d from the grain boundary grooves which were formed in the same (±1.5°C/cm) temperature gradient. This places the grooves on an equivalent basis which was only possible because of the common value of G used. These measurements are plotted in Fig. 10.15. Over fifty separate measurements were compiled in this figure. The plot shows graphically the observed increase in groove dimensions (d) as the concentration of C_2Cl_6 was increased. The application of the selected value of δ to the data permitted the calculation of the γ_{SL} for each point and resulted in the graph of γ_{SL} vs. composition presented in Fig. 10.16.

Changes in γ_{SL} caused by adding an impurity to CBr_4 were tested by making dilute alloys of CBr_4 with less than one weight percent of various other organic materials added. All alloys were observed with the same thermal gradients. The measurements obtained from these observations were treated in the same manner as those for the other grain boundary grooves. The d measurements are plotted in Fig. 10.15. The interfacial energies were calculated using the entropy of fusion for pure CBr_4. The changes in interfacial energy of the impure CBr_4 can be seen from Fig. 10.15 by comparing the values of d. Note that some values differ considerably (and some not at all) from that for pure CBr_4. A table of the calculated interfacial

energies is given in Table 10.2.

Note that metastable single phase grooves could be formed when the alloy composition was sufficiently off-eutectic. Note as well that the technique presents γ_{SL} at the fusion temperature of the alloy.

The cell design and the apparatus used limited the range of alloy compositions that could be studied. The higher temperatures required for high Hexachloroethane concentrations caused rapid cell deterioration. Included in Fig. 16 are data points for Hexachloroethane concentrations over 18 weight percent. These specimens were not prepared by the author, and all were equilibrated in steeper temperature gradients (46 to 77°C/cm). The alloy compositions studied were limited to less than forty weight percent C_2Cl_6.

After summing the individual contributions to the error of the method of measurement, an estimate of the accuracy of the measurement method was set at plus or minus twenty percent, while the precision of each measurement is good to within less than plus or minus ten percent in the worst case.

d vs Concentration Hexachloroethane

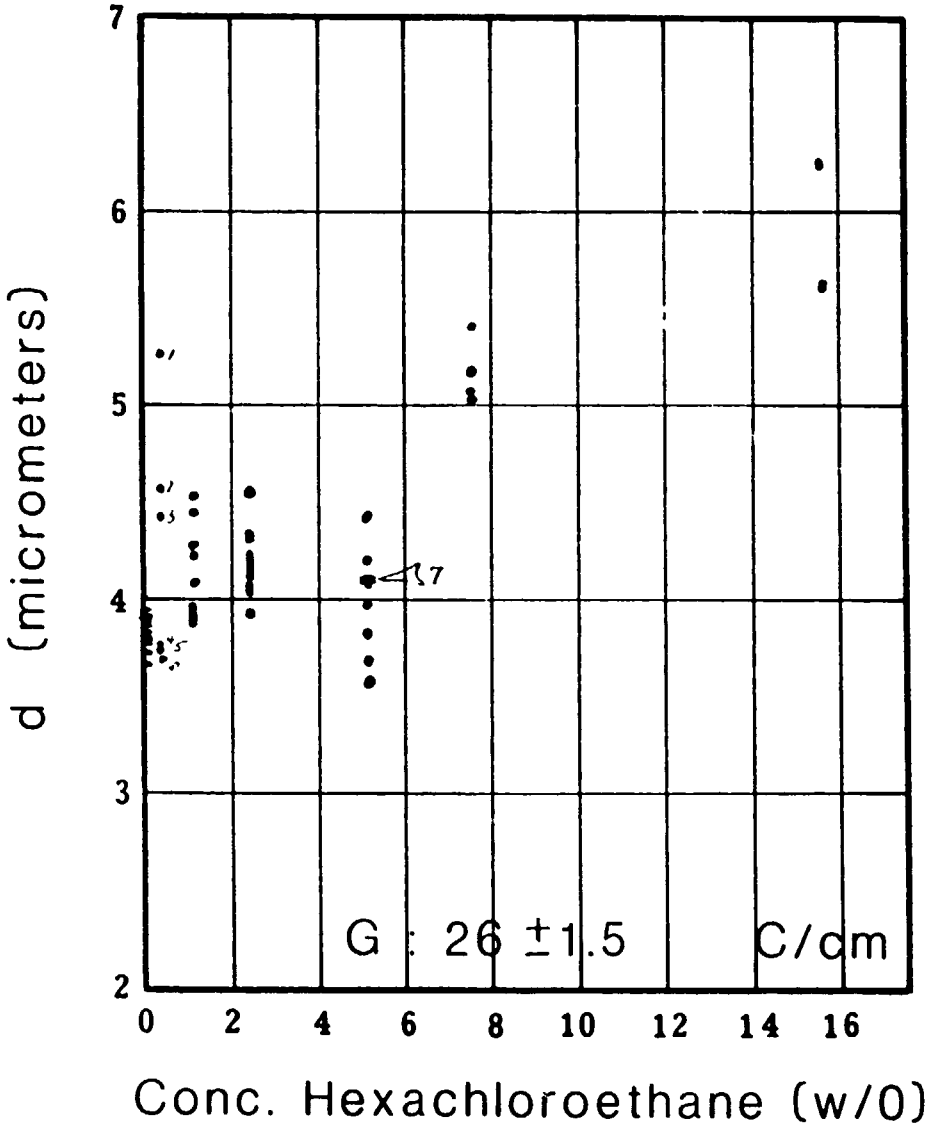

Fig. 10.15

1. 0.27 W/0 Camphene in Carbon Tetrabromide, 2. 0.36W/0 Cyclohexane
3. 0.518 W/0 Azobenzene, 4. 0.009 W/0 Azobenzene, 6. 0.334 Succinonitrile
5. 0.4 W/0 Hexachloroethane, 7. d measured from major phase of eutectic interface.

Fig. 10.16

Plots of Measured Solid-Liquid Interfacial Free Energy vs Concentration of Hexachloroethane of Each Phase of the System

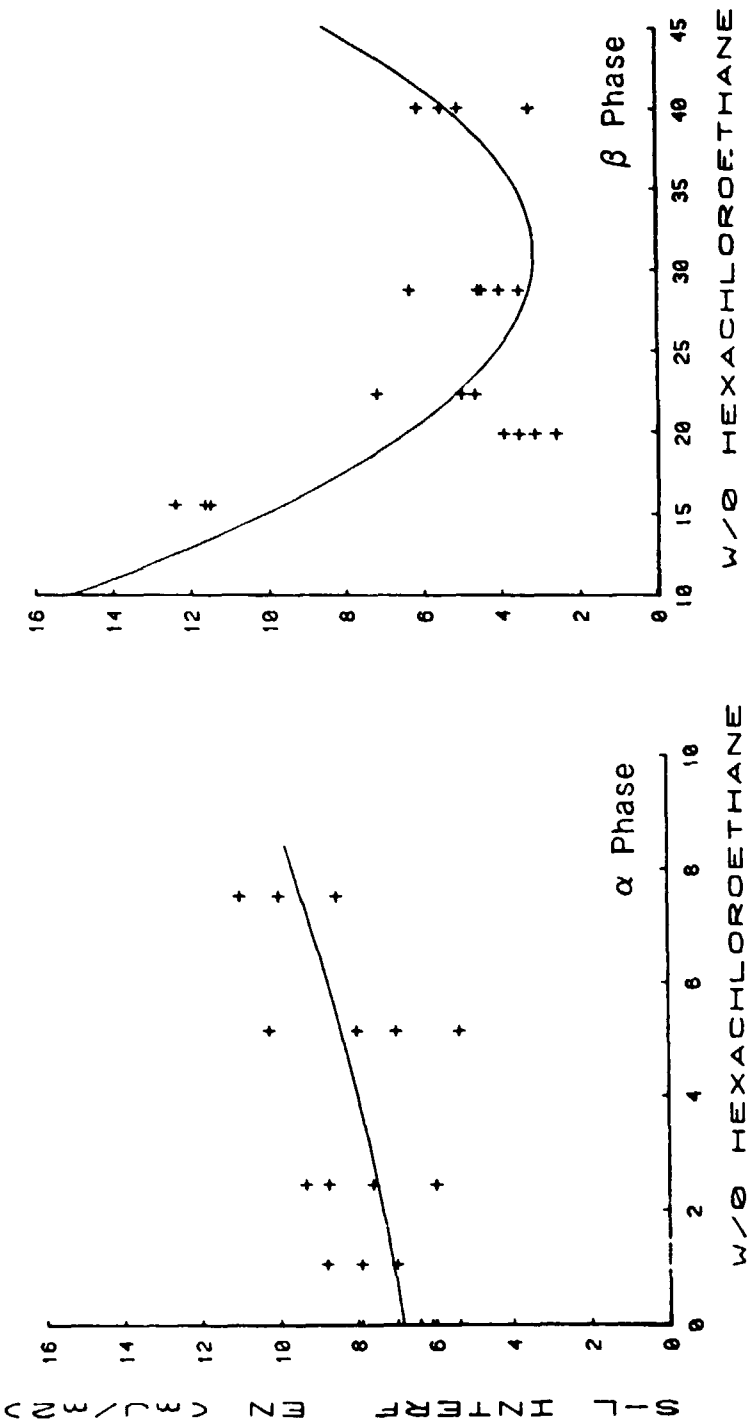

Table 10.2 Solid-Liquid Interfacial Energy of Impure Carbon Tetrabromide

d (μm)	Alloy	Composition	γ_{SL} (mJ/m^2)
3.703 (1 pt)	S22	0.334 w/o Succinonitrile	5.75
4.569 (8 pts)	S23	0.3613 w/o Cyclohexanol	8.83
5.273 (7 meas)	S24	0.2774 w/o Camphene	11.78
4.443 (8 meas)	S16	0.5168 w/o Azobenzene	8.29
3.883 (4 meas)	S11	0.009 w/o Azobenzene	6.36
3.74 (2 meas)	S20	0.315 w/o Hexachloroethane	(for comparison) 6.1

10.3.2 Lamellar Spacing/Growth Rate Relationship

Organic eutectic (specimen identification: S27C1) made of very pure components was grown in a fixed temperature gradient (6.8°C/cm) at various velocities. From photographs of the interface, growing at steady state at each velocity, the interlamellar spacings at the growth front were measured, using the digitizer. The average spacing is plotted vs. $1/R^{1/2}$ in Fig. 10.3.2. There were five points added at the origin for the fitted line. The slope-squared of this plot, when forced through the origin, is $9.61 \times 10^{-16} m^3/sec$. This value is known as A^2 in Chadwick's version of Tiller's formula. [28]

$$\gamma_{\alpha\beta} = \frac{\varepsilon A^2 (C_E - C\alpha) L_E \rho_E}{8 T_E D \left[\frac{1}{m\beta} - \frac{1}{m\alpha}\right]}$$

when:

A = slope described above

ε = constant (here = 1 [28])

C_E = eutectic composition

$C\alpha$ = composition of α phase

L_E = latent heat of fusion of eutectic liquid

ρ_E = density of eutectic liquid

T_E = eutectic temperature

D = diffusion coefficient in liquid

$m\alpha$, $m\beta$ = slopes of α and β liquidus lines

This formula may be used to calculate $\gamma_{\alpha\beta}$ from the data presented elsewhere in this thesis and from the measurement of A.

From a log λ vs. log R plot, the calculated slope was -0.473. This value comes very close to the accepted value of -0.5.

Irregular lamellae such as those with low energy phase boundaries were omitted from the measurements. Two interfaces used for the measurements are found in Fig. 10.12.

Fig. 10.17

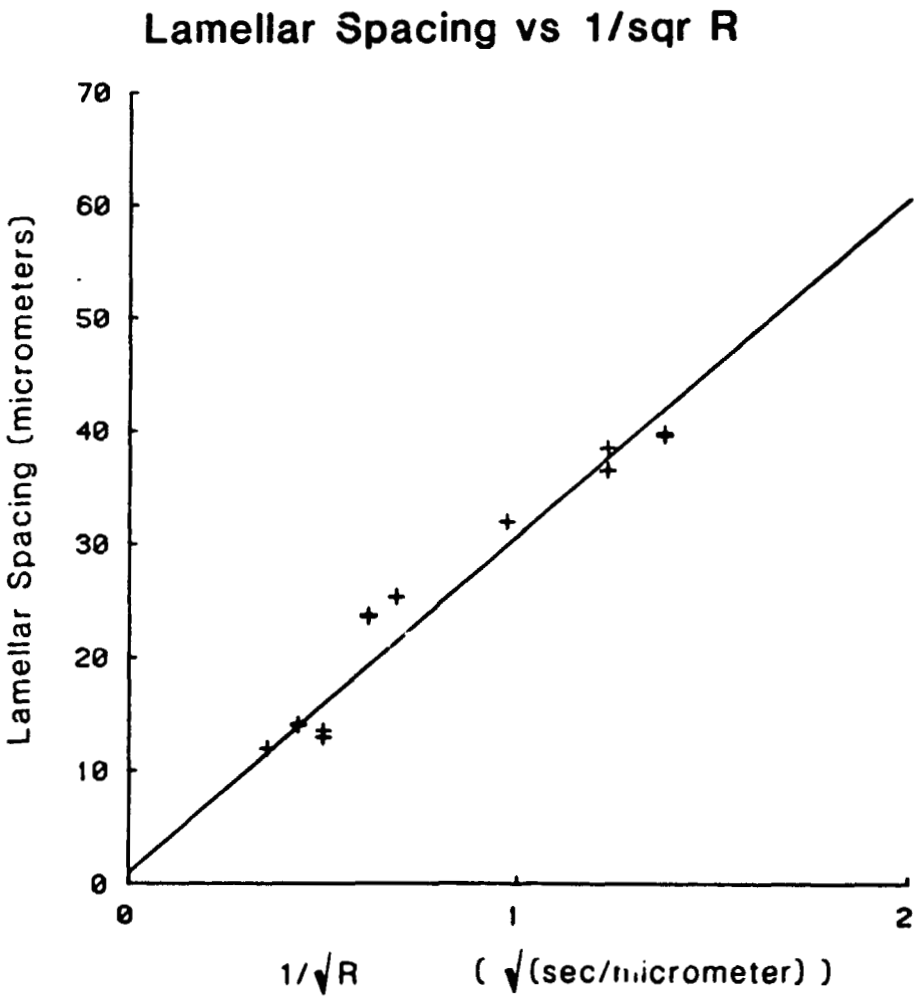

10.3.3 Measurement of $\gamma_{\alpha\beta}$ and the Torque of the α-β Phase Boundary

Measurement of $\gamma_{\alpha\beta}$:

Measurement of the dihedral angles which are developed at the eutectic trijunctions, as indicated in Figure 10.18, permits calculations of the solid phase boundary interfacial free energy from the two solid-liquid interfacial energies, using the relationship:

$$\gamma_{\alpha\beta} = \gamma_{\alpha L} \cos A + \gamma_{\beta L} \cos B \qquad [63]$$

where the terms are as defined previously (see Fig. 10.18). The measured values for $\gamma_{\alpha L}$ and $\gamma_{\beta L}$ are 8 and 10 mJ/m^2, plus or minus 2.0 mJ/m^2, respectively. These values are assumed to hold for every eutectic trijunction.

The measurement of the $\gamma_{\alpha\beta}$ relies on the knowledge that the $\gamma_{\alpha L}$ and $\gamma_{\beta L}$ are isotropic. Only with this knowledge, can the equation above be used with confidence.

Measurement of Interfacial Torque:

Equilibrium of the force balance was assumed both for the case in which the interface was growing and for zero velocity trijunctions. The two angles, A and B in Fig. 10.18, measured from both growing and stationary interfaces, cluster around one pair of values when typical high energy interface boundaries are considered. The angles measured are listed in Table 10.3. With the angles and interfacial energies presented, an unresolved

force component needs to be taken into account even for the high energy phase boundaries (see Fig. 10.18a). This will be shown to be due to the torque associated with the α-β interface. Low energy or "special" interphase boundaries were also observed (see Figs. 10.11 and 10.12). These boundaries can intersect the solid-solid interface with little or no visible cusping. To accomplish this, other forces are needed to counteract the asymetrical γ_{SL} of the two phases. Again this force is due to a significant interfacial α-β torque term. (See Table 10.3)

A brief discussion on the nature of interfacial torques is presented below.

When two crystalline phases are assembled to form a single, common interface, the relative orientations of the crystals and the orientation of the interfacial plane between the crystals are defined by five parameters (five degrees of freedom). The misorientation between the crystals accounts for three degrees of freedom and the orientation of the phase boundary plane for the remaining two degrees of freedom. Interfacial anisotropy is the variation of γ with the orientation of the boundary at constant misorientation between the phases. If there is no variation of interfacial energy with the orientation of the boundary plane, then the interface is said to be isotropic. Interfacial energy does not depend on orientation for isotropic interfaces; for such interfaces the γ-plot (the polar diagram of

γ as a function of interfacial orientation, θ) is spherical. At any particular orientation the torque is equal to the local slope of the γ-plot, $d\gamma/d\theta$, which for isotropic interfaces is zero. When interfacial energy is anisotropic, the γ-plot is no longer spherical and in general the torques are not equal to zero. One would expect low-energy or special boundaries to be situated at a cusp on a non-spherical γ-plot and in such cases the interfacial torque can be thought of as a force which resists rotation of the interface from its preferred low-energy orientation. For boundaries which are not in the cusp orientation on the other hand, the torque acts so as to rotate the boundary toward the plane of lowest γ. Torques have been experimentally observed to act on twin and grain boundaries [88-90]. Very little is known about torques at interphase boundaries [91]. To date, the method of torque measurement presented in this thesis is the first of its kind.

The convention for expressing interfacial energies and torques in this thesis follows that developed by C. Herring [66, 63]. A more recent treatment would be that followed by Cahn and Hoffman [67, 68] using vector thermodynamics. This treatment reduced to that of Herring under the conditions cited here. The expression Herring derived which describes the equilibrium geometry of the interfacial junction is:

$$\sum_{i=1}^{3} (\gamma_i \nu_i + \frac{\partial \gamma_i}{\partial \nu_i}) = 0$$

(please refer to Fig. 10.18b)

$$T_i = \frac{\partial \gamma_i}{\partial \nu_i} \qquad T_i \perp \nu_i$$

where:

γ_i is the interfacial free energy

ν_i unit vector in the interface plane, normal to the line of intersection (in three dimensions)

T_i interfacial torque vector.

$\gamma_{\alpha L}$ and $\gamma_{\beta L}$ have been experimentally shown to be isotropic so that no torques act on the solid-liquid interfaces. (see Section 10.2.9) However, since a full vectorial balance of forces at the trijunction was not possible with only γ terms, a residual force must exist and this would have to be, by inspection (Fig. 10.18b), the out-of-plane vector: T_i in the diagram. The magnitude of this vector may be calculated by resolving the interfacial tensions onto the axis normal to the interphase interfacial plane. This imaginary axis is the direction vector that contains the torque. Thus, the horizontal components of the solid-liquid surface tensions are balanced by the torque of the interphase boundary, which acts normal to the boundary plane. Note that interfacial torque does not alter the $\gamma_{\alpha\beta}$ calculations using the equation, since the only $d\gamma/d\theta$ term which acts in this system is perpendicular to the direction of the $\gamma_{\alpha\beta}$ force.

The magnitude of this torque must be higher at the trijunctions formed with special interphase boundaries because the dihedral angles are shallower (larger).

Calculations and Data: next page

Table 10.3 lists the data and results of calculations for the measurement of $\gamma_{\alpha\beta}$ and the phase boundary torque. The results show the calculations for high energy interphase boundaries separately from those for special boundaries. For the angles encountered, and using the measured values for $\gamma_{\alpha L}$ and $\gamma_{\beta L}$, the maximum uncertainty in the individual measurements of $\gamma_{\alpha\beta}$ would be plus or minus 4.0 mJm^{-2}, given that there is (at most) a two degree uncertainty in each angle measurement. The maximum uncertainty in the torque values quoted is plus or minus 1.4 mJm^{-2} obtained from the uncertainty of each solid-liquid interfacial free energy measurement. These limits apply to the accuracy of the individual measurements. The reproducibility of the measurements was plus or minus 0.6 mJm^{-2} for both the phase boundary energy and for the torque.

Fig. 10.18a

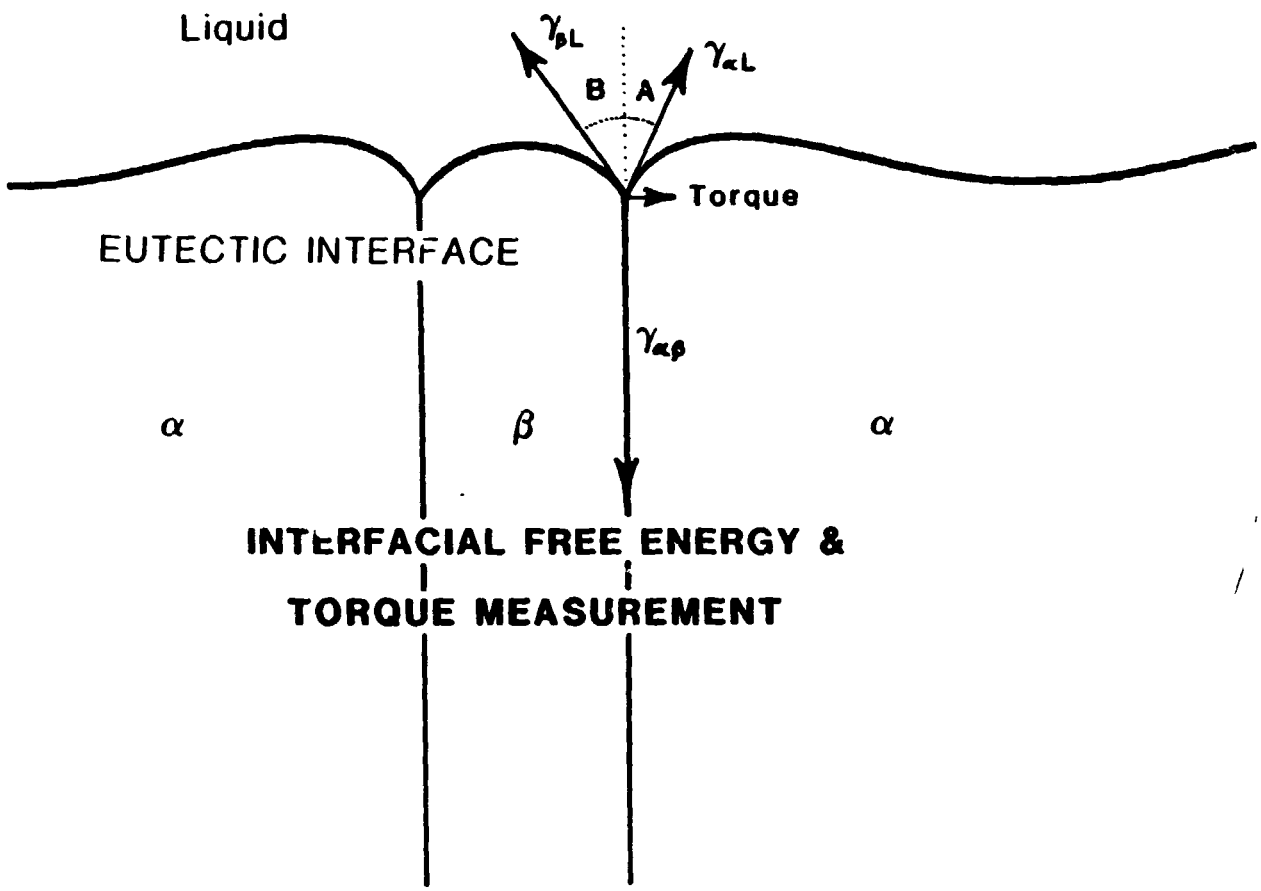
Liquid
$\gamma_{\beta L}$
$\gamma_{\alpha L}$
B
A
Torque
EUTECTIC INTERFACE
$\gamma_{\alpha\beta}$
α
β
α
INTERFACIAL FREE ENERGY &
TORQUE MEASUREMENT

Fig. 10.18b

HERRING'S TRIJUNCTION ANALYSIS

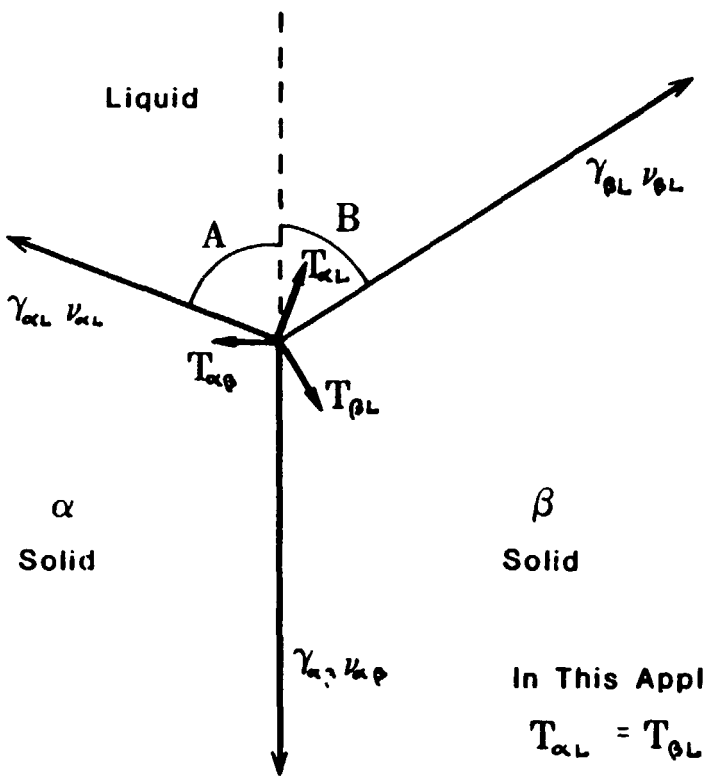

In This Application:

$T_{\alpha L} = T_{\beta L} = O$

Table 10.3

Calculations of $\gamma_{\alpha\beta}$ and Interfacial Torque

	Angle A (degrees)	Angle B (degrees)	Angle C (degrees)	Horizontal Component - α (mJ/m^2)	Horizontal Component - β (mJ/m^2)	Torque (mJ/m^2)	$\gamma_{\alpha\beta}$ (mJ/m^2)
Random High Energy Phase Boundaries Zero Velocity Interfaces							
1.	63.8	59		-3.53	5.15	1.618	15.75
2.	63.7	55.4		-3.54	5.67	2.133	15.40
3.	55.5	54.5		-4.53	5.80	1.27	14.73
4.	57	55		-4.35	5.73	1.378	14.90
5.	71	70		-2.60	3.42	0.81	16.96
6.	53.5	28		-4.75	8.82	4.07	11.12
7.	45.5	45.9		-5.6	6.96	1.35	12.88
Gr[illegible]ing Interfaces							
1.	68.1	54.1		-2.98	5.86	2.87	15.52
2.	46.7	50		-5.48	6.42	0.94	13.48

cont'd....

Table 10.3 (continued)

	Angle A (degrees)	Angle B (degrees)	Angle C (degrees)	Horizontal Component - α (mJ/m^2)	Horizontal Component - β (mJ/m^2)	Torque (mJ/m^2)	$\gamma_{\alpha\beta}$ (mJ/m^2)
Special Phase Boundaries, Growing Interfaces							
1.	145	98.82	116.19	-4.59	9,882	5.29	8.09
2.	129.25	72.29	158.47	-6.19	9.52	3.33	2.01
3.	123.33	64.33	172.34	-6.68	9.01	2.32	0.06
4.	121.71	93.89	144.41	-6.80	9.97	3.17	4.88
5.	110.68	91.09	158.23	-7.48	9.99	2.51	3.01

Angle Geometry for Table on previous page

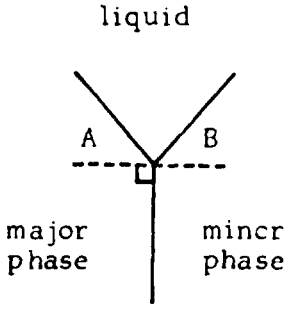

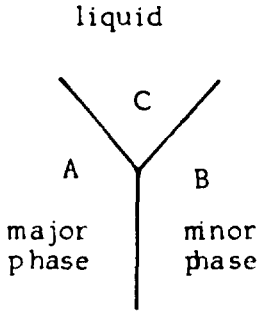

Angle Geometry for Table on this page

10.3.4 Interfacial Free Energies of the Lamellar Phases Against Liquid as Measured From the Eutectic Interface

The morphology of this organic eutectic requires the use of two different methods to measure the solid-liquid interfacial energies of the two phases directly from the interface. The method used to measure the γ_{SL} for the major (α) phase is the Glicksman and Nash grain boundary groove technique. An analysis developed specially for this eutectic system by the author for the measurement of the γ_{SL} of the minor (β) phase is also described later. Neither method should be applied to a growing eutectic interface because there are contributions to the interfacial undercooling from other causes. Therefore, the best interface to use for measurement of the interfacial energies is a zero velocity eutectic interface as described in section 9.2, where the major phase has a wide region of zero curvature. Such an interface is shown in Fig. 10.19. One can obtain the interface temperature for such an interface where the curvature is zero at some point.

The solid-liquid interface of each phase in the eutectic was treated separately, as a portion of a grain boundary groove (where the other portion would have been of the same composition). The difference between a high energy α-β phase boundary and a random, high angle grain boundary, amounts for this purpose, to a difference of interfacial energies. The response to this difference would be an angle change to balance

the interfacial forces. Other than this angle change at the base of the cusp, the overall solid-liquid interface shape would not be affected by replacing a random, high energy grain boundary by a random, high energy α-β phase boundary. This is important because the shape is used to measure the γ_{SL}.

It was possible to develop a region of zero curvature on the solid-liquid interface of the major phase. This region identified the eutectic isotherm. The curvature at the cusp could therefore be measured with the Glicksman and Nash method, and the interfacial energy calculated. The groove spacing was taken as the α-β phase boundary spacing for one lamella.

Under these circumstances, where a region of zero curvature was available, the interface contour matches that for an equivalent grain boundary groove interface. To illustrate this point, an interface profile was drawn using Bolling and Tiller's equation for the grain boundary groove shape on the Figure 10.19 using the measured interfacial energy and composition data. Some eutectic interface measurements of the α lamella solid-liquid interface are presented together with the grain boundary groove data in Figure 10.15 for comparison to the separate measurements of γ_{SL} of single phase alloys.

Measurement of the minor phase solid-liquid interfacial energy using the Glicksman and Nash method was not possible for this eutectic, for the following two reasons.

First, there usually was no region on the interface of the minor phase where there was zero curvature. This makes determination of the location of equilibrium isotherm line uncertain. Second, the Glicksman and Nash method is not usable for the boundary spacings as small as the width of the minor phase lamellae. The value of d (see Fig. 8.4 for definition) measured for the minor phase (using neighbouring minor phase lamellae tips to outline the isotherm) was of the same order of magnitude as the boundary spacing $\delta = d/\lambda \approx 1$. This places the value of δ outside the range where the Glicksman and Nash method could be applied.

From the author's experience and from calculations made with various combinations of parameters, the useful range of δ for the Glicksman and Nash method is $0.06<\delta<0.22$. The following will deal with the lower limit only. It is unlikely that the lower limit will be exceeded when the Glicksman and Nash method is applied to equilibrated grain boundary grooves. If a pair of grain boundaries were so close to one another that $\delta \geq 0.06$, then, under normal circumstances, the boundaries unite by lateral migration to form one grain boundary groove. Such grain boundary migration has been observed in the organic alloy studied. The migrating boundary does not remain normal to the interface, and thus should not be measured. On the other hand, the phase boundaries present in the eutectic, while normal to the interface, cannot migrate, so that the

small groove spacings for the minor phase are stable. Therefore the Glicksman and Nash method cannot be applied to the minor phase.

From observations of interface profiles when grain boundary grooves come close to one another, such as just prior to merging, it is seen that the shape of the solid-liquid interface approaches an arc of a circle between the boundaries. Examination of the interfaces of the minor phase in the eutectic showed this was often the case as can be seen in Fig. 10.19. Also, as the lamellar width decreases, the radius of curvature of the solid-liquid interface decreases accordingly. At a given interface, whether growing or not, there was also observed a variation of the degree of depression of the minor phase with respect to the imaginary line formed by the α lamellae tips. The variation depended upon the lamellar width. As the lamellar width lessened, the β phase solid-liquid interface became more depressed.

The observations reported above are in accord with the Gibbs-Thomson relation (section 8.1.2) since interfaces with a greater curvature were equilibrated at lower temperatures. An attempt was made to estimate the interfacial energy based on these observations by applying the Gibbs-Thomson relation and knowledge of the temperature gradient. The radius of curvature for each lamella was assumed to be the half width of that lamella.

Zero Velocity Eutectic Interface

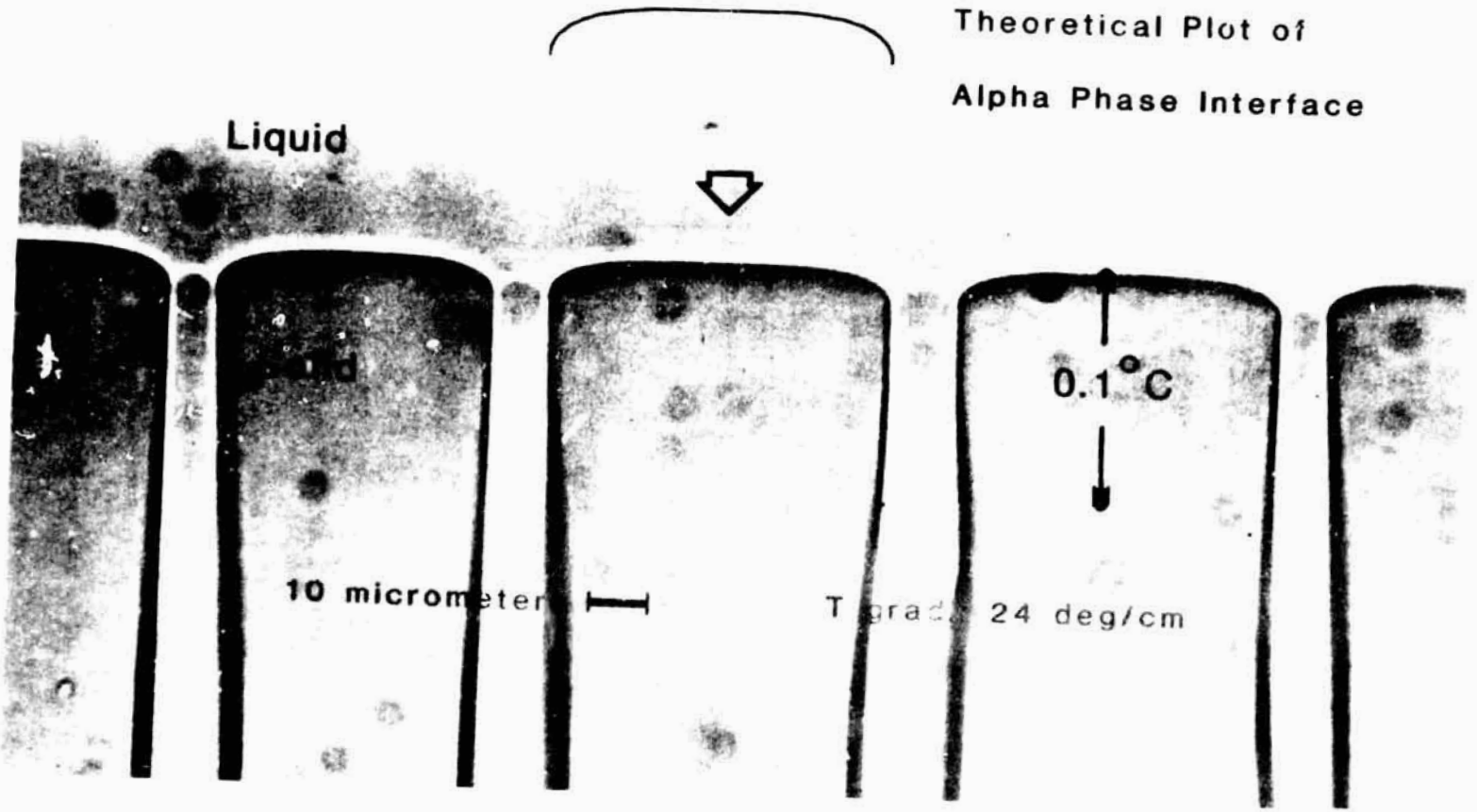

Fig. 10.19

Theoretically, a single measurement of the phase depression and the corresponding lamellar width as well as knowledge of the temperature gradient, is all that is needed to measure $\gamma_{\beta L}$, as long as the interface is stationary. One can then obtain knowledge of the position of T_E where the interface has zero curvature. If the interface is growing, however, some other means of measuring the undercooling (from T_E) which caused the depression, is required. This is because the position of T_E is indeterminate and there are unquantified contributions to the interface undercooling.

An alternate approach was found which alleviates the latter problem. Advantage was taken of a eutectic system property. There is a small, measurable variation in the lamellar widths across an interface. With a change in the β phase lamellar width, it was observed that a corresponding change in the degree of depression occurred as well. See Fig. 10.19. It was observed, as well, that when one plots these measurements, one against the other, a linear relationship develops. A plot such as this is presented in Fig. 10.20 where the depression distance was converted to a relative undercooling and curvature was calculated by dividing two with the lamellar width or, alternatively: $\kappa = 1/S\beta$. The data for the plot were obtained from three micrographs of a zero velocity eutectic interface (like the one in Fig. 10.19). The slope of this plot is $m = \Delta T/\kappa$. (See Fig. 10.20) The Gibbs-Thomson r ation was

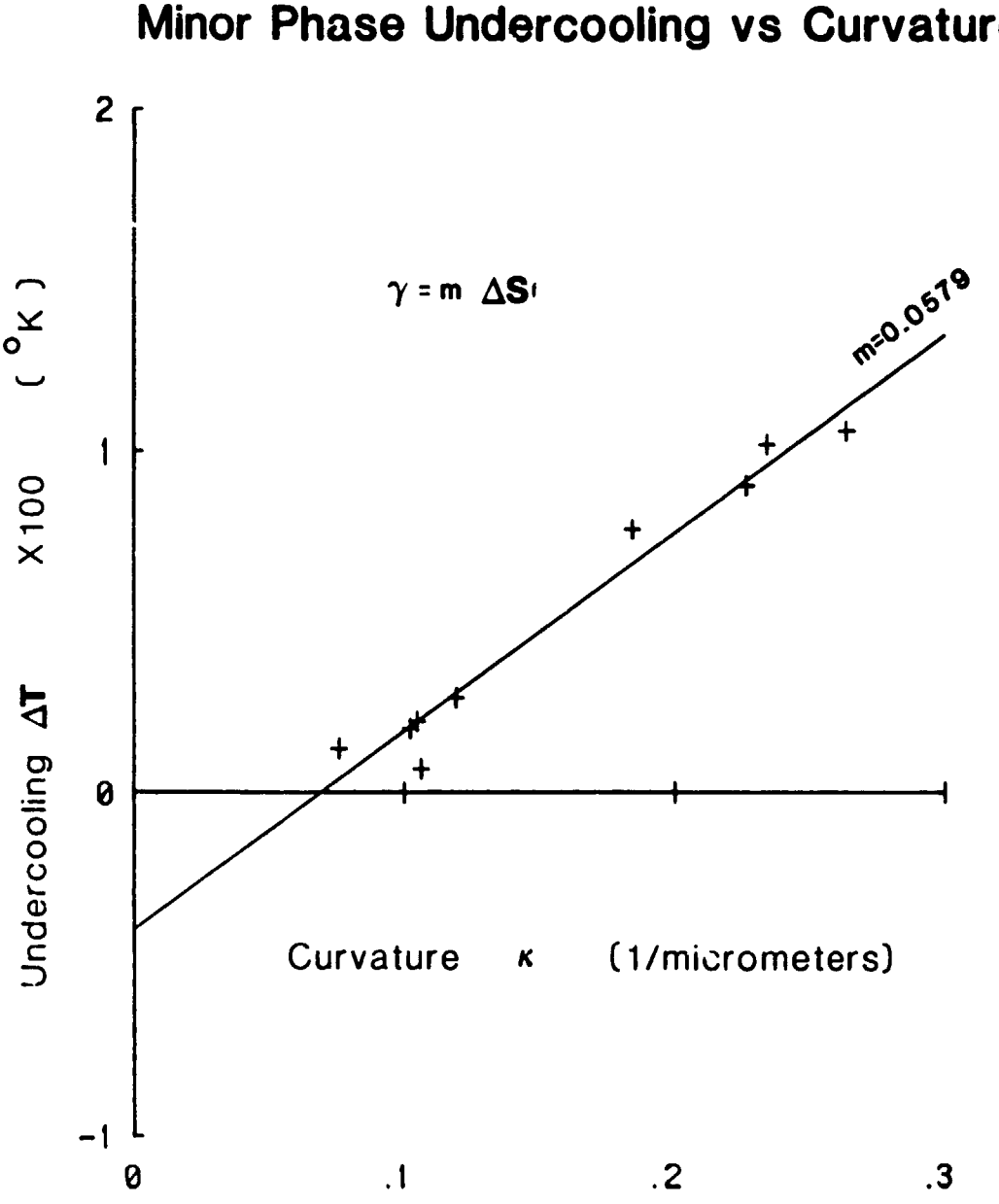
Minor Phase Undercooling vs Curvature
$\gamma = m \Delta S_f$
m=0.0579
Undercooling ΔT X100 (°K)
Curvature κ (1/micrometers)
2
1
0
-1
0
.1
.2
.3

Fig. 10.20

rearranged so that a slope could be used to obtain $\gamma_{\beta L}$:

$$\gamma_{\beta L} = \frac{\Delta T}{\kappa} \Delta S_f = m \Delta S_f$$

The equation of the line shown in Fig. 10.20 and that of another, where the interface was growing is given in the Appendix. Choosing the value of 77,000 $J/m^3 deg.K$ for the entropy of fusion yields an interfacial energy of 4.5 mJ/m^2 for the zero velocity interface and a value of 1.1 mJ/m^2 for the interface which was growing at 0.529 micrometers/sec.

The quality of the measurement depends on the strength of the assumption of circular arcs for the minor phase solid-liquid interfaces. Notice that only a relative undercooling is sufficient when knowledge of the variation of the lamellar widths is obtained. The absolute undercooling is not, therefore, required.

10.3.5 Results from Thermocouple Cells

A group of observations was made with the thermocouple cells. One observation is the discovery that the eutectic solid and melt have nearly the same thermal conductivity. Degradation of the organic alloy with time was monitored from the freezing temperature of the alloy with time. Finally, the results from the attempt to measure interfacial undercooling are presented.

The observations indicated that the thermal response of the interface was accurately recorded. The fine wire thermocouples used did not visibly alter the heat flow in the surrounding organic. This was observed by noting that the shape of the solid-liquid interface was not affected by the presence of the thermocouple wire. In addition, the transit of the interface over the thermocouple bead was easily observed and the interface was, again, not affected by the thermocouple. Also, by using transparent organics one can confidently know that the temperature recorded is that of the interface.

There was no visible change in the slope of the temperature vs. time trace (for any growth rate) as the interface was passed over the thermocouple bead. This shows that the thermal conductivity of the eutectic solid is the same as the liquid.

The thermal response of the organic material (to thermal transients) in the cell was observed using these

thermocouple cells.

When the cell velocity was abruptly changed, the immediate thermocouple response as observed on the temperature-time charts, proved that there was little or no thermal lag within the cell. Consequently, for the velocities of the interface encountered experimentally, the interface temperature that was measured was at all times dependent on the interface composition or, alternatively, the organic has the same thermal gradient impressed upon it as the surroundings. Thermal lag was detected at velocities higher than approximately ten micrometers per second.

The attempt to measure the undercooling of the growing interface was not successful. Instead, a variation of interface temperature with time was found. Repeated passes of the interface over the thermocouple resulted in continuously descending interface temperatures. Over a period of four hours, with repeated growing and melting, the interface temperature would drop over 1.3 degrees Celsius. This effect was confirmed by finding the interface position relative to the apparatus when the thermocouple bead contacted it. This was done by counting the motor revolutions during growth (using the mounted digital counter) and then again during the return (melting back) of the cell to prepare the interface for another pass. From knowledge of position only, the interface temperature was known to ±0.15°C for several consecutive runs. From the knowledge

of the number of motor revolutions, the position the cell moved was calculated. The exact location (±40 micrometers) of the thermocouple is therefore known just as the interface passes over it. The position was noted on each freezing cycl of the interface. The position of the interface (when it contacted the bead on each cycle) progressively moved to the cooler regions of the apparatus. The interface temperature change after several cycles was calculated from the position and coincided with the temperature change measured by the thermocouple. The only explanation for this behaviour, is that the organic itself was becoming impure with time. This could be due to the extended period the cell was held at high temperatures and the catalytic effect of the bare thermocouple upon the breakdown of the organic.

One cell was cycled repeatedly until the growing interface temperature was constant (but not representative of pure eutectic). A few more cycles at various growth rates (from 1.3 to 5.3 micrometers per second) showed no variation of interface temperature with growth rate to within ±0.05°C. The consequence of these measurements is that the interface undercooling should be less than 0.05 degrees Celsius for velocities up to five micrometers per second.

10.3.6 Volume Fraction Measurements

From the series of photographs used to measure the lamellar spacing, the volume fraction of the minor phase was measured. (See 10.3.2) This resulted in a measure of the variation of volume fraction with growth rate.

The measurements are plotted in Fig. 10.21. A line was fitted to the data and the equation is listed in the Appendix.

Unlike the lamellar spacing measurements, the precise measurement of volume fraction relies upon precise selection of the phase boundary location. Phase boundaries can be tilted very slightly from the optical axis, and are sites for optical diffraction. These effects reduce the precision to which the phase boundary spacings can be measured.

Other irregularities, such as lamellae which have low energy interphase boundaries, were omitted from the measurements as these phases do not adjust their lamellar spacings and therefore their local volume fractions remain abnormal. The local variation of lamellar width requires that as large a number of measurements be made from as many lamellae as possible.

Fig. 10.21

Volume Fraction of Minor Phase vs Growth Rate

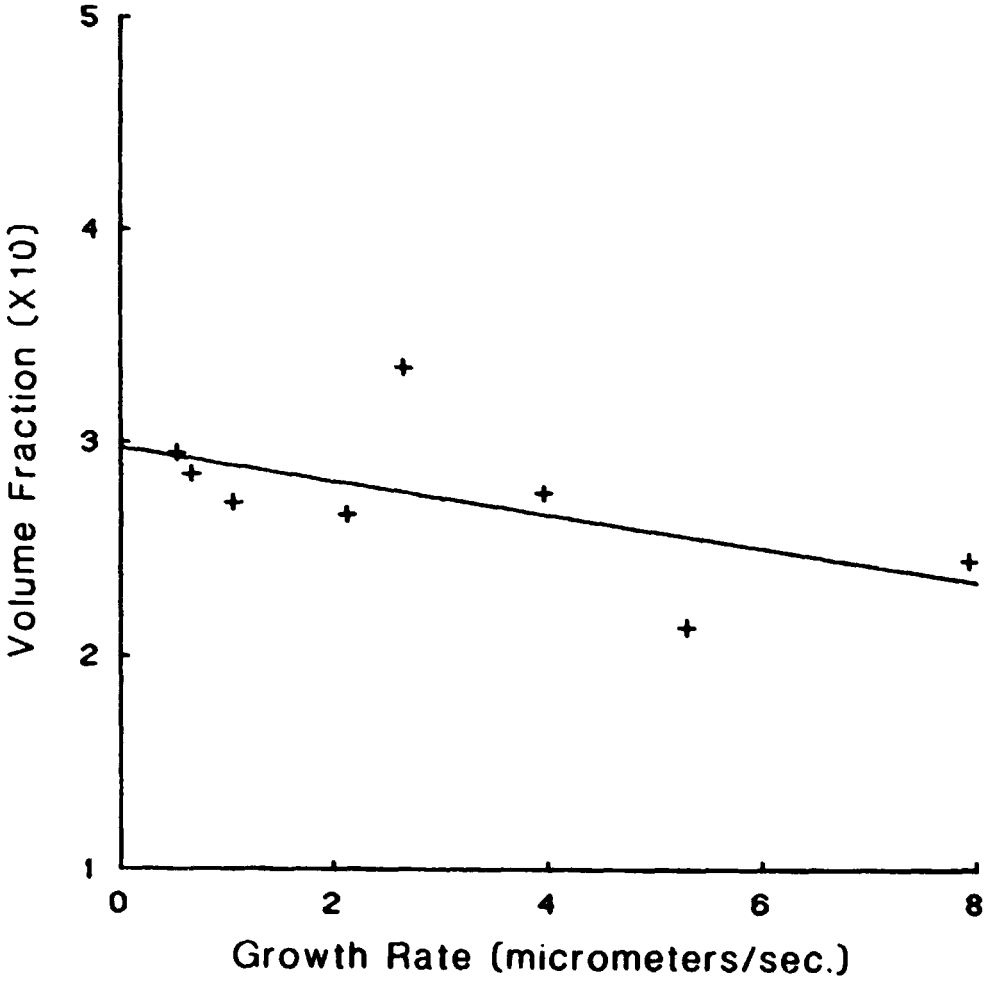

11. DISCUSSION

The discussion that follows is divided into three parts; the first deals specifically with the measured properties of the organic alloys of Carbon Tetrabromide and Hexachloroethane, while the second part deals with the interpretation of the experimental observations and measurements, as they relate to lamellar eutectic growth. For both of these sections, the results are examined in the light of the current understanding of the field. The third part is a theoretical discussion of eutectic growth.

The points of interest in the first part (section 11.1) are a discussion of the phase diagram and of the interfacial free energy data obtained for the interface.

In the second part (section 11.2), an examination of the interfacial phenomena at the growing organic eutectic solid-liquid interface will be given, based on the experimental observations. The emphasis in this section is placed on the contributions to interfacial undercooling, ΔT_R, ΔT_D and ΔT_γ, and on the importance of the interfacial free energies encountered at the eutectic trijunctions.

The third section (section 11.3) is a general discussion of eutectic growth theory emphasizing differences from the past ideas on the subject.

11.1 Discussion of the Carbon Tetrabromide-Hexachloroethane System

Most of the information needed to analyze the solidification behaviour of a material has been measured for the system: CBr_4 - C_2Cl_6. The two most significant items found were the phase diagram for the system and the solid-liquid interfacial free energies for single phase alloys in the composition range of interest, extending from approximately zero to twenty weight percent C_2Cl_6 in CBr_4.

11.1.1 The CBr_4 - C_2Cl_6 Phase Diagram

The overall form of the phase diagram was known prior to the thermal analysis from a specially prepared organic alloy cell constructed by Jackson and Hunt, when they first discovered the system. [2] Within one cell they placed side-by-side nearly pure CBr_4 and C_2Cl_6 and allowed these two bands of material to interdiffuse along a central line in a temperature gradient. In so doing, a pseudo phase diagram was generated, as could be seen by observing the shape and orientation of the solid-liquid phase boundaries formed as a result of temperature variation along one axis of the cell and composition variation along the other. Thus, in one cell, the slopes of the liquidi and the eutectic tie line were observable. [2] The thermal analysis carried out in the present study resulted in a phase diagram which appears much as the pseudo phase diagram. [2] From the pseudo diagram, however, the exact placement of the solidus lines and of the limits of solid-solubility could not be made. This problem was made more difficult by the fact that the pseudo diagram did not extend from zero to one hundred percent C_2Cl_6, and that the compositions were not known, even approximately. What is important is that the placement of the measured lines or boundaries on the phase diagram is similar to the phase boundary placement in the composition range of interest as depicted by the special "binary" cell of Jackson and Hunt.

11.1.2 Interfacial Free Energies of CBr_4

The use of Carbon Tetrabromide as a model for metal solidification has raised interest in measuring its properties. As a result, some material properties (see Table 8.1) have been obtained for pure CBr_4 which permit comparison of the measured interfacial energies here with those obtained by other methods.

In the literature, there is reported one measurement of γ_{SL} for CBr_4, obtained using grain boundary groove techniques. [11] Apparatus required for the observation of the groove and to generate the temperature gradient was similar to those listed earlier and first reported by Jackson, Hunt and Brown. [61] Two types of analysis were applied, the Bolling - Tiller type, which yielded a value for γ_{SL} of 16.5 mJ/m^2 and the Glicksman - Nash type, which gave a range of values from 10 to 20 mJ/m^2. [11] These values are comparable to those obtained from homogeneous nucleation experiments. [11] The higher γ_{SL} values reported in this paper, compared to that found in the present study, may be due to the use of a higher measured value for the entropy of fusion, (see Table 8.1). Details of how the methods were applied were not available from the papers.

Comparison of the measured γ_{SL} to the value obtained empirically from the heat of fusion can also be made. The empirical relation:

$$\gamma = k \frac{L}{N^{1/3} V^{2/3}}$$

where: k = empirical constant

γ = interfacial energy

L = heat of transformation

N = Avagadro's Number

V = molar volume

has been evaluated for metals and other materials for the interfacial energies between solid and vapour, solid and liquid and liquid and vapour, by using the heat of sublimation, fusion and evaporation respectively. The constant k, has the values 0.15, 0.46 and 0.15 respectively for the three cases above, when applied to metals [69]. The interfacial energies estimated in this way for CBr_4 are:

γ_{SV} = 41 mJ/m^2 (ΔH sublime from Table 8.1)

γ_{SL} = 9.02 mJ/m^2 (measured ΔH_f)

γ_{LV} = 37 mJ/m^2 ($\Delta H_{evap.}$ from Table 8.1)

A great deal of confidence cannot be placed in these relations since different constants can be found using different sources for the "measured" values of the interfacial energies. It does appear, however, that the value of the solid-liquid interfacial energy of CBr_4 derived in this way, coincides sufficiently well with the values measured in the present work that the material can be considered to behave in metallic manner.

The applicability of the grain boundary groove technique to the measurement of γ_{SL} has been well established by others, [10-12, 14, 16] for the case of pure, single component materials, using stationary, well equilibrated grooves. As mentioned before, one purpose of the work described in this thesis was to establish the applicability of the measurement technique to alloys and to investigate the measurement under conditions where the interface may be growing ($R<8$ micrometers/sec.). The experiments performed here (and the results described in sections 10.2.5, 10.3.1, 10.2.8) indicate that when constitutional undercooling effects and thermal transients are absent, measurements made on a growing solid-liquid interface will yield a constant value for interfacial free energy with no indication of change as growth progresses. The absence of a visible change in grain boundary groove shape during slow growth of the planar interface verifies this. Slow growth of an alloy was possible without a change in grain boundary groove

shape, and interestingly, only when cellular breakdown occurred could a change in shape from a stationary interface be detected. This statement is a consequence of careful visual examination of the grain boundary groove as the growth rate was changed, and is not the result of performing a detailed computer-aided analysis. However, differences were clearly visible among the shape of stationary grain boundary grooves for alloys of different compositions. It was the quantification of these changes which resulted in the plot of the variation of γ_{SL} vs. weight percent C_2Cl_6 shown in Fig. 10.16.

This discussion of changes in the interface shape has a major significance if segregation of a trace of impurity were to occur in such a way that a change in the interfacial free energy resulted from the adsorption of this impurity to the interface. The segregation would occur in such a way that the system energy were reduced. This type of segregation and its development has been observed at grain boundaries in a solid, and on liquid-vapour interfaces. [87] The analogous effect at solid-melt interfaces has not been as well documented. [87] At no time was any effect of such segregation to the interface observed during the course of an experiment. The effect, if it occurred, would have caused a change in the shape of the grain boundary groove as the segregation would have increased during the initial stages of equilibration. This should be contrasted with the measurements of γ_{SL} of CBr_4 with small amounts of various organic solutes. (see section 10.3.1 and

Table 10.3) What is important to note, and is clearly visible from the data, is that the different types of impurity led to a wider variety of values for γ_{SL} (impure) than would be obtained from normal scatter of γ_{SL} for any alloy. In addition, the quantity of solute added was very small (<0.4 weight percent). The large range of γ_{SL} for the various impurities observed cannot be accounted for by assuming that the concentration of the impurity in the solid or liquid at the interface was close to the value one would take as the bulk value. One could only account for such large changes in γ_{SL} from the "pure" value if a mechanism is found which permits a large local change in the composition of the interface with respect to the solute. One mechanism has been explained earlier, that of adsorption of the solute to the interface. However, this would probably stabilize γ_{SL} by giving constant interface composition, due to adsorption. Another mechanism would be the equilibrium partitioning of the solute one would expect if the distribution coefficient for the solute in CBr_4 were significantly different from 1 ($k<<1$; $k>>1$). The condition is stronger if growth were to occur as well. This latter mechanism could be used to explain the difference in γ_{SL} (CBr_4 - Azobenzene) where the concentration of Azobenzene was very different between the two alloys tested. The smaller the distribution coefficient, the greater the magnification of the local solute concentration in the liquid at the interface. The small change in γ_{SL} (from the "pure" CBr_4 value) found when Succinonitrile was added may

be explained when one considers that this organic is not soluble in solid CBr_4 (as observed by its precipitation from the growing interface of the alloy tested). An abrupt change in $\gamma_{SL}(CBr_4)$ as one adds C_2Cl_6 is not expected because the distribution coefficient has a value close to unity ($k \approx 0.4$).

As experience was gained with forming and measuring grain boundary grooves, slight variations from ideal groove shape (which were readily quantified) were detected by eye, through the microscope or from photographs. For example, many grooves were asymmetrical because the grain boundary was a few degrees off from the normal to the interface isotherm. By its very nature, the Glicksman and Nash technique is sensitive to these shape deviations. Since little information is needed in the Glicksman and Nash procedure to perform the measurement, the "quality" of the groove with respect to how well it meets the idealized conditions set by the geometry of the measurement is very important. It seems clear that the precision of the measurement would be reduced if the whole groove profile was used for the analysis. One method in which this is possible is the Bolling and Tiller analysis, but in that case, γ_{SL} must be isotropic and the grooves isolated from one another. Another more generally applicable method, is the one first suggested by Arbel and Cahn. [37] The whole groove profile is used and, in addition, the measurement permits a quantification of the degree of interfacial anisotropy. A modification of the method

permits the measurement to be made also for a solid-melt combination in which the thermal conductivities are unequal.

Some success was obtained by the author in performing a non-linear regression of the equation of a grain boundary groove, as derived by Bolling and Tiller, onto a set of digitized coordinates taken from a photomicrograph of a grain boundary groove. This method should improve accuracy, but would apply only when the interfacial energy is isotropic and the thermal conductivities of solid and melt are nearly equal. The potential for an improved precision of the measurement is demonstrably clear for either of these other methods.

As stated before, all the methods except that of Arbel and Cahn require that the solid-liquid interfacial free energy be known to be isotropic. This was not a mere assumption in the present work (as it has been for others). Experimental confirmation of the interfacial isotropy was obtained from the observation of perfectly spherical liquid drops formed in the cast solid near the solid-liquid interface. (see Section 10.2.9) The observation corroborates the initial assumption that the γ_{SL} would be isotropic based on the crystal structure and behaviour of the organic materials. Isotropy of properties is usually found with materials having a cubic crystal structure, like a metal. The plasticity and low entropy of fusion of the organics used would further lead one to expect the solid-liquid interfacial energy to be isotropic.

11.2 Growth of the Carbon Tetrabromide-Hexachloroethane Eutectic

This portion of the discussion will cover two aspects of eutectic growth in the system Carbon Tetrabromide-Hexachloroethane. The first subsection will deal with experimental observations of the effects on the solid-liquid eutectic interface which influence the undercooling of the interface. Means of quantifying the contributions to the interfacial undercooling will be discussed. In the second subsection, a discussion of the influence on interface morphology by the three interfacial free energies, $\gamma_{\alpha L}$, $\gamma_{\beta L}$ and $\gamma_{\alpha\beta}$ will be made.

Most of the experimental observations were limited to a great extent by the inability to reduce the effects of constitutional undercooling caused by the impurities which could not be removed and by the products of the degradation of the CBr_4 which slowly formed during the period of an experiment. The majority of the experiments were performed in a temperature gradient of approximately 25°C/cm. It was at first believed this value represented a reasonably shallow gradient. Near the end of the work, experiments were performed with an even lower value of G, ~7°C/cm. Much useful data resulted with the application of this very low G because the effects of alloy degradation were postponed as the melt was not so elevated in temperature.

11.2.1 Eutectic Interface Undercooling

Although the attempt to measure the undercooling of the growing eutectic interface with the micro-thermocouples was complicated by the degradation effects mentioned previously, it seems clear that the actual interfacial undercooling of this eutectic is very small, under the growth conditions used. Measurements performed during the course of this study permit the calculation of interface undercooling using equations from the Jackson and Hunt analysis, [8, 88] for comparison with the observations made using the thermocouple cells. Jackson and Hunt give:

$$\Delta T = K_1 \lambda V + \frac{K_2}{\lambda}$$

where:

$$K_1 = \frac{m\alpha m\beta Co P (1+\zeta)^2}{(m\alpha + m\beta)\ \zeta D \pi^3}$$

$$K_2 = \frac{2(1+\zeta)}{(m\alpha + m\beta)} \left[m\beta a\alpha \sin\theta_\alpha + \frac{m\alpha a\beta \sin\theta_\beta}{\zeta} \right]$$

$\zeta = S\beta/S\alpha = 0.479$

$Co = Co^{\alpha} + Co^{\beta} = 11.1$ weight percent

$a\alpha = \gamma_{\alpha L}/\Delta S_f(\alpha) = 8.0 \times 10^{-5}$ mmK

$a\beta = 11.4 \times 10^{-5}$ mmK

$P = 0.03$ (Jackson and Hunt parameter)

$\lambda = 7.5 \times 10^{-3}$ mm

$V = 8 \times 10^{-3}$ mm/sec

$\theta_\alpha = 65°$ $\theta_\beta = 55°$

$D = 2 \times 10^{-3}$ mm^2/sec

The only value required that was not measured, or known precisely from other sources, was the diffusion coefficient, here taken as a representative value for liquid diffusion. The undercooling calculated using the Jackson and Hunt formula is approximately 0.01 degrees K for the growth rate of eight micrometers per second and for the maximum recorded growth rate in this work, the undercooling would attain a value of only approximately 0.05 degrees K. Such a low value appears to have been below the limit of measurement with the thermocouple cells. In other systems, notably metallic ones, measured interfacial undercoolings in excess of several degrees have been reported: systems with faceting phases show the highest values of undercooling, while those in which both phases are non-faceting show the lowest maximum undercoolings in the group. [24] This latter observation appears to be consistent with the calculation above.

An alternate type of calculation, not reported elsewhere, is the estimation of the interfacial undercooling from the measured variation of volume fraction (V_f) with growth rate. The measured variation is plotted in Fig. 10.21. This calculation is unconventional, but the precision of some of the measurements performed justifies its application. It is based on the assumption that, if solidification of the eutectic occurred at a temperature below the equilibrium eutectic temperature, the compositions of the solid and liquid formed at that temperature would be those represented on the phase diagram by extensions of the solidus and liquidus lines to the

appropriate degree of undercooling. In this way, it is possible to find the compositions of the two phases which solidify for any selected value of undercooling. The differences in composition would, in the CBr_4 - C_2Cl_6 system, result in a similar change in the respective densities of the phases and, therefore, in the volume fraction of one phase relative to the other, e.g., the volume fraction of the minor phase, $V_f(\beta)$. Using the computer, a series of calculations was made, for small values of undercooling, in order to obtain the variation of $V_f(\beta)$ with undercooling. The calculations employed the lever rule, with the "fulcrum" of the lever fixed for all undercoolings at the eutectic composition. For small undercoolings (<1 degree) the calculated variation of $V_f(\beta)$ with temperature was -0.04 $V_f(\beta)$/°C; the theoretical value of $V_f(\beta)$ at the equilibrium temperature is 0.3238. At the velocity of 8 micrometers/sec., the corresponding undercooling would be approximately 1.5 degrees, based on the measured $V_f(\beta)$ value for that growth rate. Although it is difficult to establish a precise slope for the line in the graph, there clearly is a general downward trend. The decrease in $V_f(\beta)$ as R increased occurs despite the fact that the growth rate changes were not made in a consecutive order. Thus, while the accuracy of the measurement of interface undercooling is questionable, there is experimental support for the applicability of the method.

Another ramification of the above method is the consideration that the undercooling sustained by the freezing

interface may not be wholly due to the mechanisms for undercooling mentioned in section 8.1. It is conceivable that a small amount of impurity could reduce the freezing temperature of the interface and also affect the volume fraction of the system. This effect may occur if the eutectic valley from the binary eutectic to the ternary eutectic point drops in a direction which forces the compositions of the two major phases in the binary to deviate sufficiently to cause the volume fraction change. Higher growth rates may cause more rejected solute to collect at the interface and further cause the V_f to deviate. Unfortunately, for the case cited, the possible impurity effect serves to mask the measurement of interfacial undercooling by other mechanisms.

A relative interfacial undercooling was shown by the slight advance of a section of eutectic interface intersected by "special" low energy boundaries over a neighbouring section intersected by "random" high energy phase boundaries. Two relative undercoolings were measured, as shown in Fig. 10.12 for two growth rates. In section 10.3.3 a measure of the $\gamma_{\alpha\beta}$ of some "special" boundaries is given. The values of $\gamma_{\alpha\beta}$ were significantly smaller than those for the random, high energy boundaries, Table 10.4. As the interfacial energies of the "special" boundaries are low in value, the contribution to interfacial undercooling is similarly small among them. Effectively, the interfacial undercoolings caused by "special"

boundaries are equivalent.

Since there is no evidence to suggest that the interfacial energy of a phase boundary (particularly a "special" boundary) varies with the conditions under which it is formed, such as the conditions for Fig. 10.12, then the cause for the two different relative undercoolings (for Fig. 10.12) must originate in the character of the interface with higher energy phase boundaries. That is to say, for the higher of the two growth rates, the interface with the higher energy phase boundaries grows with a greater undercooling relative to the "special" boundary interface.

The contributions to the undercooling of the "higher energy" interface must stem from mechanisms which allow the contributions to the undercooling to vary with R. These mechanisms include the contributions: ΔT_R, ΔT_γ and ΔT_D. (Little difference is expected from ΔT_K.) The finer lamellar spacing characteristics of the higher growth rate increases the curvature on each lamella, increases the number of high energy phase boundaries and the higher R decreases the time for diffusion, although the diffusion distance is as well reduced. The relative undercoolings, calculated from the imposed temperature gradient, were found to be 0.0364 degrees and 0.0162 degrees for the higher and lower R respectively. Thus, the difference in undercoolings is 0.0202 degrees for these two growth rates. The equation given in section 8.1 for ΔT_γ was used to calculate

the relative contribution to the undercoolings from the phase boundaries for the two lamellar spacings of the "high energy" interfaces. The calculated undercoolings using $\gamma_{\alpha\beta}$ = 14 mJ/m^2, ΔS_f = 8 x 10^{6}J/m^{3}K and λ_1 = 13.5 x 10^{-6}m and λ_2 = 37 x 10^{-6}m, are respectively 0.026 and 0.0095 degrees. The relative difference is 0.0165 degrees. In comparison to the measured relative difference of 0.02 degrees one would expect that the remaining contribution of the undercooling would originate from ΔT_R and ΔT_D which together (0.01 degrees) have a similarly small contribution to the increased undercooling of the higher R interface.

The relative importance of the interfacial energy balance at the trijunction, compared to the contribution to the undercooling from the solute, ΔT_D, in determining the shape of the interface can be illustrated by utilizing "special" boundaries. A eutectic grain made up of "special" type phase boundaries can form and grow in the axis of the cell along the heat flow direction. Such an interface would appear as a straight solid-liquid interface with the phase boundaries intersecting normal to this interface and doing so without forming significant cusps at the trijunctions. The interface just described would be growing without any undercooling due to curvature, as there is no curvature, and the interface would be truly isothermal. Interfaces such as those described above, have been observed during growth of the organic eutectic in some eutectic grains. An example of an interface with an impurity addition and with low energy interphase boundaries growing along the cell axis is the first micrograph of Fig. 10.153. This interface does have

negative curvature which was induced by the contribution to the undercooling: ΔT_D. Therefore, under these circumstances, all the visible interfacial curvature is that which was required to counter the undercooling due to the collected solute. In this case, an impurity addition with a low distribution coefficient further accentuated the undercooling in the lamellae. A pure eutectic was observed to display negative curvature in this way as well. The contribution to the undercooling may then be quantified simply by measuring the depth of the liquid pocket in the center of a lamella and applying the known temperature gradient. This measurement was performed for the impure interface shown in Fig. 10.15B, and the largest undercooling measured in this was was approximately 0.075 degrees. The contribution to this figure of the impurity alone is not know It should be noted that the amount of undercooling depended on the lamellar width. However, once a lamellar width is established with special boundaries, it is not likely that the lamellar spacing could adjust to changes in growth rate. One of the purposes of the micro-thermocouple cells was to measure ΔT and by calculating ΔT_R from the shape measurements, a value of ΔT_D would have been obtained. By the direct observation of the negative curvature on the interfaces where there are "special" boundaries, and therefore little or no ΔT_R, one could calculate the ΔT_D which caused the negative curvature.

Tiller's formula [28] as presented in section 10.3.2, was used to calculate $\gamma_{\alpha\beta}$ and D using the measured values from

other portions of this work. With the values selected from these measurements and the value for D set to 2 x 10^{-5}cm^2/sec., the calculated value for $\gamma_{\alpha\beta}$ was determined to be 15 mJ/m^2. Since $\gamma_{\alpha\beta}$ was measured independently, a value for D could be calculated using the same equation. A representative value of $\gamma_{\alpha\beta}$ (for a random, high energy phase boundary) was selected as 13.5 mJ/m^2 and the remaining parameters retained. The calculated value for D was found to be 2.18 x 10^{-5}cm^2/sec. The resemblance to the "accepted" value for D of 2 x 10^{-5}cm/sec. is not surprising as the calculated value for $\gamma_{\alpha\beta}$ is, as well, very close to the independently measured value.

Two types of experiments were performed which showed directly the importance of ΔT_D in determining the shape of a growing eutectic interface. In one set of experiments, stationary solid-liquid eutectic interfaces were produced. According to eutectic growth theories (8.1), the contribution to the interfacial undercooling from the cross-diffusion, in the liquid adjacent to the interface, of the components of the eutectic phases is due to the growth of the interface, and corresponds to a periodic variation in the solute composition distribution in the liquid with a period equal to the lamellar spacing. The periodic variation of the solute in the liquid and the associated undercooling variation at the interface cannot exist at a stationary interface. Nevertheless, under the condition of zero interface velocity, the characteristic eutectic interface shape was observed. This shape did not differ significantly

from the shape of a slowly growing interface. Jackson and Hunt state that interface curvature observed at a eutectic interface is due to the compensating curvature contribution to the undercooling needed to offset the constitutional undercooling. (section 8.1) From the zero velocity interfaces, one can only observe the curvature due to the interaction of the interfacial energies in the temperature gradient.

The isothermal convection experiments were devised in order to separate the ΔT_D from the overall interfacial undercooling by sweeping away the solute layer, in the liquid isothermally, at a growing solid-liquid interface. The conclusion from the observed effects is that, even for a growing interface, the overall contribution of the ΔT_D component to the interfacial undercooling is small. This was demonstrated by the return of the interface to a shape similar that it would attain if it were a stationary interface. It is interesting to note as well, that the time required by the interface to adjust itself is very small. This is emphasized further when observing the melting interface at slow melt rates. At the slower rates, the interface profile was similar to that for a slowly growing or stationary interface. The resemblance was closer when the rate of melting approached zero. It seems then, that for slowly growing, slowly melting or stationary interfaces, the contribution to the interface shape due to ΔT_R resulting from the interaction of the interfacial energies and the temperature

gradient is greater than that due to ΔT_D.

The contribution to interfacial undercooling by ΔT_D was found to increase as growth rate increased. This was found by decreasing the growth rate at a moderate rate such that the lamellar spacing didn't have the opportunity to change. In this way, the comparison was fair. The faster growing interface would have negative curvature developed in the midsection of the major phase lamellae. As the growth rate was changed, and the solute boundary layer permitted to diminish by diffusion into the liquid, the major phase would become less concave at the tip, until a region of zero curvature was formed in the middle. Little change was observed to occur on the minor phase lamellae. Then, as the growth rate decreased further, the interface would be everywhere convex in much the same was as the second diagram in Fig. 10.6. Eventually, the slowly growing interface would be indistinguishable from a stationary one.

There are, therefore, two conditions under which a portion of the eutectic interface can show zero curvature. One is the case of a stationary interface, provided that the lamellae are sufficiently wide. The other is as described above, where some positive curvature from the interaction of the interfacial energies and the temperature gradient is balanced by the slight negative curvature caused by the solute buildup at the interface in the midsections of each lamella. In order that the slight positive curvature be present at zero velocity, the lamellae must be adequately narrow.

Since the degree of positive curvature can now be calculated using interfacial energy data, the observed reduction of the positive curvature at a growing interface could be used to quantify the local value of ΔT_D. For comparison, a calculation is presented here to compare ΔT_R and ΔT_D where ΔT_R was calculated using the lamellar width and applying the Gibbs - Thomson relation, and the ΔT_D was calculated for the interface conditions using the Jackson and Hunt equations. These conditions are given in Fig. 11.1 for an interface growing at one micron/sec. To further enhance the ΔT_D, a smaller value for D was selected. $5 \times 10^{-6} cm^2/sec$. Note that the concentration variation is plotted for the second component (B) in the liquid. The average composition of the liquid at the interface is 6.1 weight percent C_2Cl_6. This is a consequence of the Bo term (plane wave term) in the equation. The eutectic alloy composition was set to 8.4 weight percent C_2Cl_6 in CBr_4. The ΔT_D was found to be a maximum of 0.013 degrees and ΔT_R an average value of 0.235 degrees. The value for ΔT_D will increase at a faster rate than ΔT_R as R increases. However, for the growth rates encountered in this work, $\Delta T_D < \Delta T_R$.

A thermal transient of undercooling was introduced in the quenching experiments. When the undercooling was sufficient, single phase dendrite growth occurred. The dendrite tip radius was observed to be much smaller than the typical lamellar interface radius and growth was faster. The initial breakdown of the lamellae to dendrites occurred at the phase boundaries in an

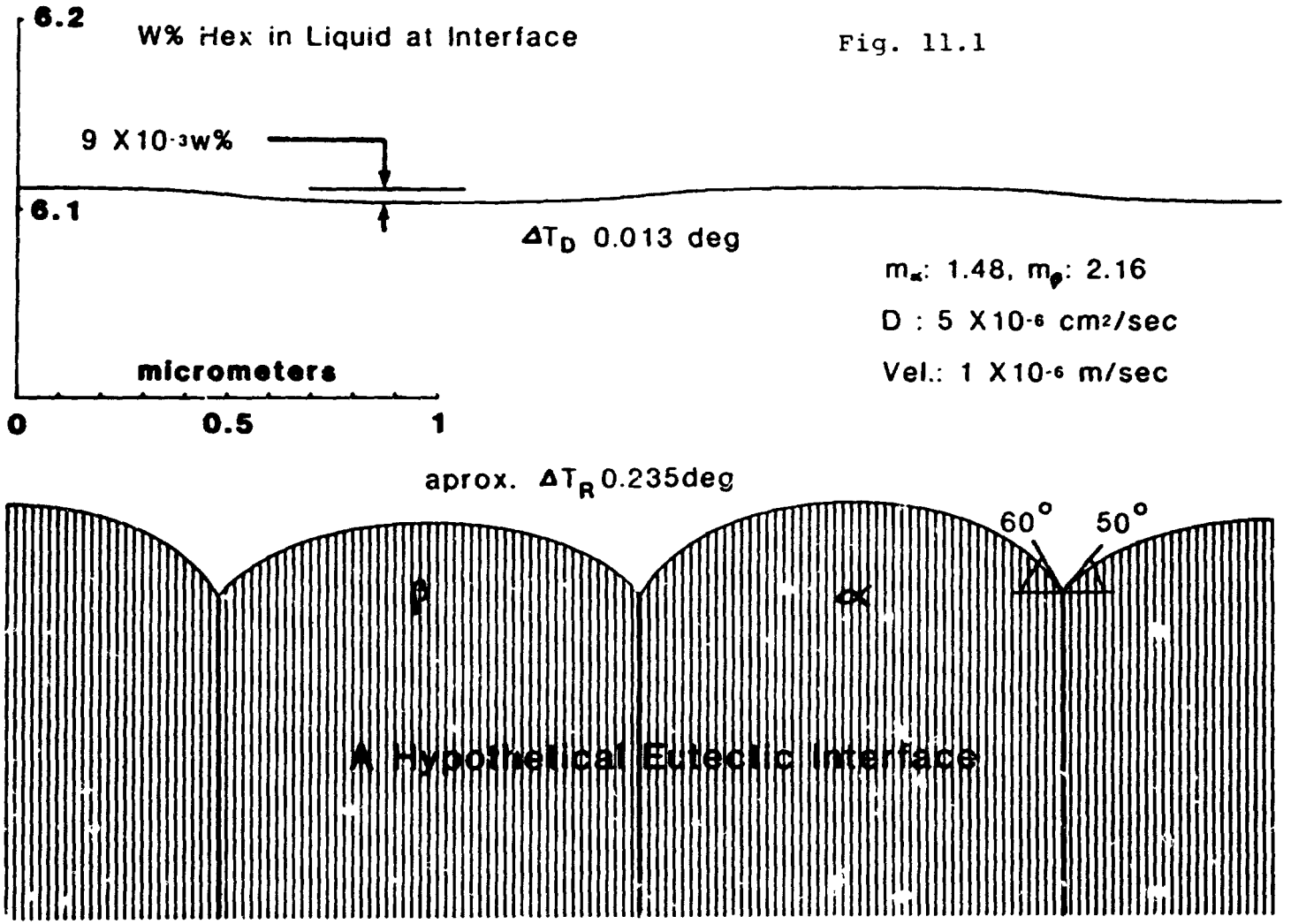
6.2
W% Hex in Liquid at Interface
9 X10-3w%
6.1
ΔTD 0.013 deg
mα: 1.48, mβ: 2.16
D : 5 X10-6 cm2/sec
Vel.: 1 X10-6 m/sec
micrometers
0
0.5
1
aprox. ΔTR 0.235deg
60°
50°
β
α
Hypothetical Eutectic Interface

Fig. 11.1

analogous manner to the breakdown of a grain boundary groove. The point of inception of the dendrite was on the interface where the interfacial undercooling due to local curvature was high. The sharper local radius of curvature allows the interface to grow faster locally. The driving force for faster growth is greater still because the region of higher curvature on the major phase is situated directly adjacent to the liquid enriched in solute just in front of the minor phase interface. Notice that the constituent rejected by the minor phase is causing this liquid to be a rich source of constituent for major phase growth and so little additional undercooling (contributed by the gas jet) was required to cause this liquid to be consumed by the major phase as is shown in Fig. 10.7. This can be seen when one considers that the liquid in front of the minor phase is undercooled more with respect to the major phase when the quench causes the decrease in temperature. This process did not occur to the exclusion of the minor phase. It appears its radius of curvature also decreased dramatically and a small lamella of minor phase was still present even after the quench. The dendrite growth process rejected the constituent needed by the minor phase (although in smaller amounts since the growth rate was so high) to continue to grow. In this way, no mechanism of renucleation of the minor phase would be required at an interface such as this which has an almost single

phase structure. Renucleation of the minor phase after this sort of thermal transient was at one time believed to be a necessity for the continuation of coupled growth after the transient.

11.2.2 Interfacial Energies at the Eutectic Interface

Some discussion has already been presented regarding interfacial energies, mostly with respect to CBr_4. There were some problems encountered when measuring γ_{SL} from the eutectic interface for each phase. The problems were solved since the variety of interfaces produced, and the ability to generate a stationary eutectic interface made it possible to modify the methods, as described elsewhere. The measurements do show the influence of the interfacial free energies upon the eutectic interface morphology.

While the value of $\gamma_{\alpha L}$ measured from the eutectic interface fell within the range predicted from the γ_{SL} vs. composition plot, the value of $\gamma_{\beta L}$ measured directly from curvature of the β lamellae (without using the Glicksman - Nash method) fell below the expected value based on the single phase measurements. However, the accuracy of the value of $\gamma_{\beta L}$ measured from the eutectic interface is not expected to be high, so that the result is considered to be in agreement with that from single phase measurements. The apparent linear relationship between undercooling and calculated curvature (Fig. 10.20) may not be correct over a larger range of curvature. This will be discussed in section 11.3.

It is clear from the many observations made that a eutectic trijunction profile shares the shape of two grain

boundary grooves. The similarity can be seen directly in Fig. 10.13. This figure also shows that a eutectic grain boundary can exist coincident with a phase boundary, or in this case, as a grain boundary included within a lamella. This has not been observed elsewhere. This statement is further substantiated by the observation of the dendrite growth directions at a quenched eutectic interface.

From the angles formed between the phase boundaries at the trijunction, and the measured solid-liquid interfacial energies, the interphase interfacial free energy was calculated. In order that the force vectors be balanced in all directions, it was necessary to introduce the interfacial torque term. The phenomenon of the torque in the eutectic phase boundary parallels that in certain grain boundaries and twin boundaries. The higher interfacial torques were found for the lower energy "special" boundaries as compared to the random, high energy phase boundaries. The torque was always found to act in the same direction (Fig. 10.18). The estimation of the torque would not have been as simple to perform if the solid-liquid energies were not confirmed to be isotropic. Although there is an observed variation among the values for torques and for interfacial energies, the values fall into two groupings. Some interphase interfaces show high interfacial energies and low torques, while the "special" boundaries have low interfacial energies and high torques.

The measured undercooling from the nucleation cell was only ~1.5 degrees. The theoretical homogeneous nucleation undercooling for pure CBr_4 should be approximately seventy degrees. Since heterogeneous nucleation occurred in the experiment, no interfacial energy estimate can be made.

11.3 The Eutectic Interface (Theory)

Two types of solid-liquid interface will be considered in this section. The first will be a pure eutectic interface. Emphasis will be placed on the formulation of a eutectic interface based strongly on interfacial energy arguments. The hypothetical solid-liquid interfaces are assumed to be isotropic. Secondly, an impure solid-liquid eutectic interface will be considered.

In an earlier section (section 10.3.4) a Bolling and Tiller plot of the equation for a grain boundary groove was drawn. It had a shape similar to the shape of the solid-liquid interface of the major phase lamella, Fig. 10.19. This was done to show how the solid-liquid interfacial energy for a eutectic phase could be used to actually draw an interface given only the temperature gradient and entropy of fusion. If the lamellar width is sufficiently large, the unmodified application of the Bolling and Tiller equation could then be used to draw a solid-liquid phase boundary for a lamella for a stationary interface, $\Delta T_D = 0$. The calculated curve is duplicated and reversed so that the portion of the curve which approaches the isotherm is aligned and connected to the same portion of the reversed curve. The distance between the roots of the cusps is then adjusted by bringing the curves closer to or farther from one another, to give the required lamellar width. The same approach can be taken for the minor phase as well, provided that

the lamellar width is sufficiently large that there is some portion of the interface with zero curvature. This situation was rarely encountered for the minor phase in the organic eutectic studied. Higher growth rates also caused the lamellar spacing to become sufficiently small that no portion of the solid-liquid interfaces of the phases would show zero curvature at zero velocity. In order to accommodate such narrow lamellar widths, the degree of overlap between the two Bolling and Tiller curves must be increased until the portions of the curves with positive curvature interact. As the curve is a representation of undercooling at the interface, an interface shape can be drawn using additivity of the undercoolings from each of the curves where they overlap.

The shape of the final curve obtained by adding the two grain boundary groove profiles is much like a section of a circle. The interface shape then would look like a minor phase solid-liquid interface such as those in Fig. 10.19. As the cusp halves on each end of the generated interface profile are brought closer together to represent finer lamellar widths, the radius of curvature of the circular section diminishes. The position of these curves also moves farther from the isotherm for the original grain boundary grooves. This is a consequence of the increased value for the undercoolings which are being added. The maximum undercooling that can be obtained by adding the two groove shapes would be found when the two cusps coincide at zero lamellar width. At this point, the undercooling is

exactly twice the value for a single grain boundary groove. (By reversing the procedure, an estimate of the solid-liquid interfacial energy of the lamella and its melt could be made in the manner described in section 10.3.4. There, a measurement of the lamellar tip depression as a function of lamellar width was used to otbain $\gamma_{\beta L}$ by using the Gibbs - Thomson relation.)

A pair of grain boundary groove profiles were constructed mathematically in the computer and the "lamellar width" reduced. The depression of the tip of the hypothetical lamella was followed as the grooves overlapped and the undercoolings added. It was found that as the hypothetical lamellar width was decreased linearly, the tip of the hypothetical lamella receded from the original isotherm for the grain boundary grooves. At first, with the cusps well apart from one another, the rate of recession was slow, and as the cusps approached closer, the rate of recession increased. Although the variation of tip depression with lamellar width was non-linear, during the initial stages (where the cusps were farther apart) a nearly linear relationship was found. Therefore, when the minor phase undercooling was plotted against curvature in Fig. 10.20, the almost linear relationship that was found would correspond to the nearly linear relationship between tip recession and lamellar width observed from the computer calculations. The consequence of this latter observation is simply that if the lamella, for which one wishes to draw an interface profile, were narrow, a suitable shift in the position of the final shape away from the isotherm

for zero curvature would be required.

From the volume fraction and from the relationship of lamellar spacing to R, the actual lamellar width of each of the two eutectic phases can be obtained. Knowing the solid-liquid interfacial free energies of the two phases and the temperature gradient, one can then fit curves such as those described above to these lamellar widths. This was done and is presented in Fig. 11.2. Until now, the dihedral angles at the trijunction and the contribution to interfacial undercooling from ΔT_D were ignored. The Bolling and Tiller equation, as presented in section 8.1.2. would suffice if the dihedral angles formed at the base of the cusps were near zero degrees.

As stated in section 8.1.2, the interfacial energies of the two solid-liquid interfaces and the grain boundary must cause the angles formed at the junction to reach equilibrium values. As pointed out in the earlier text, the angles for eutectic trijunctions were considerably larger than zero. In order to attain a finite dihedral angle at the root of a cusp formed using the Bolling and Tiller equation, a portion of the cusp may be removed such that the tangent for the free end of the remaining cusp has the required angle. The required angles can be calculated from the three interfacial energies, $\gamma_{\alpha L}$, $\gamma_{\beta L}$, and $\gamma_{\alpha\beta}$ if the interphase boundaries are all assumed to be isotropic.

The required sequence of α then β lamellae may then

Fig. 11.2

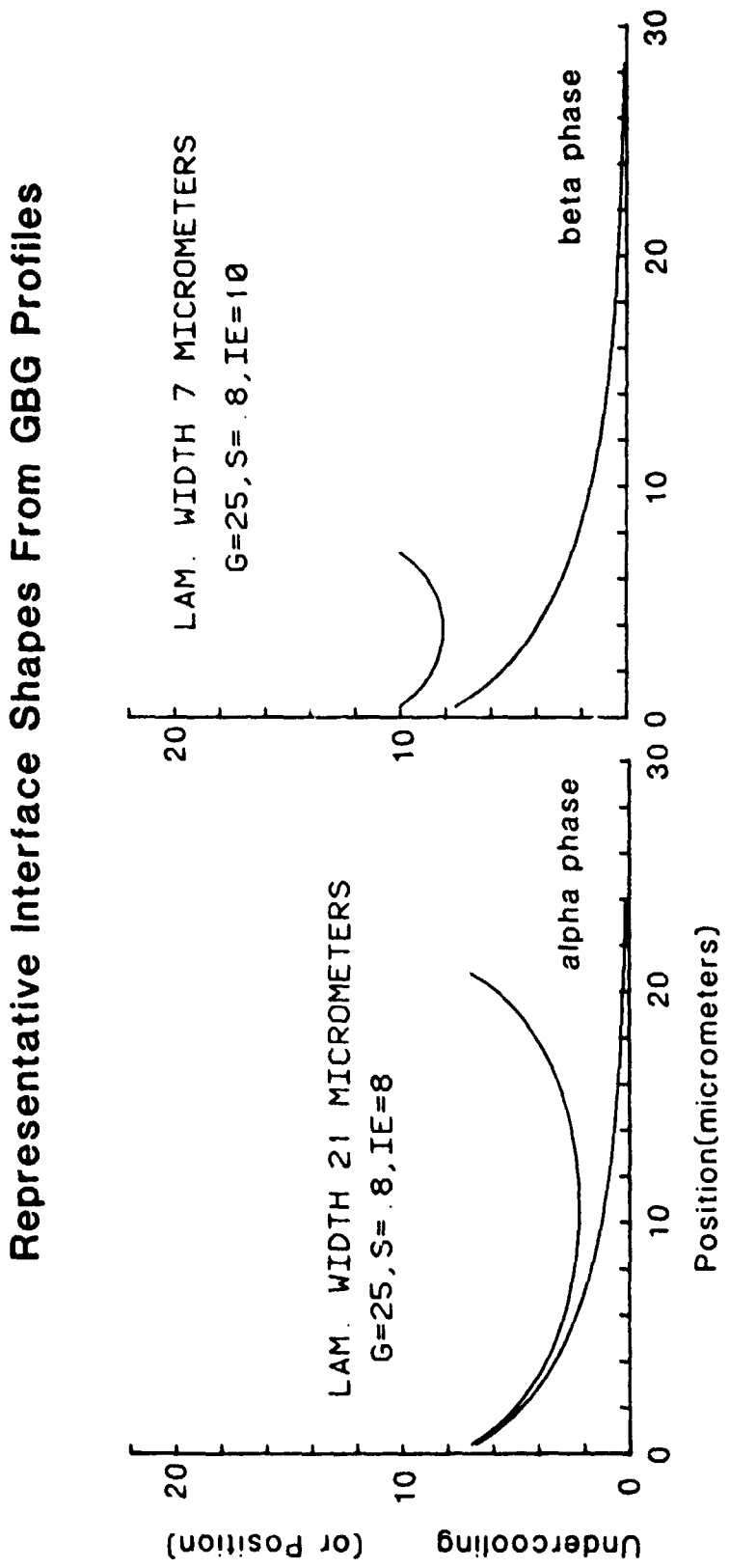
Representative Interface Shapes From GBG Profiles
LAM. WIDTH 21 MICROMETERS
G=25, S= .8, IE=8
alpha phase
LAM. WIDTH 7 MICROMETERS
G=25, S= .8, IE=10
beta phase
Undercooling (or Position)
Position(micrometers)
0
10
20
30

be arranged and the respective solid-liquid interfaces concatenated to form the hypothetical stationary eutectic interface. The formulation of a growing eutectic interface would require the additonal undercooling contribution from ΔT_D. This can be calculated from the Jackson and Hunt [8] solution to the diffusion equation for a eutectic, or alternatively, the similar solution by Donaghey and Tiller. [32] The local curvature of the stationary interface would be reduced according to the variations in the solute concentration, perhaps to the point where negative curvature developed. The magnitude of the ΔT_D contribution would depend upon the selected interface velocity and the phase diagram for the system.

Two details of forming an interface in this way have been omitted as no immediate resolution of the problems these details pose has been found. The author feels that further analysis of these details will render a satisfactory solution.

The angle relationships at the trijunction cannot be so simply treated as they were in the above discussion. False dihedral angles could be calculated for the hypothetical interface as any interfacial torques would have to be added to the calculation. As found for the organic system studied, significant interphase boundary torques were measured. Thus, the assumption that all three interfacial energies be isotropic may be a poor one. Another problem associated with the dihedral angles at the trijunction results from attempting to join two cusps, from neighbouring lamellae. It is conceivable that if

one phase is narrower than the other due to volume fraction considerations, the undercooling calculated by summing the two Bolling and Tiller curves may cause the free end of the cusp (where the tangent has the characteristic angle) to intersect the neighbouring curve (from the other phase) at a point other than at the free end for this second curve. To forcibly join either of the free ends under these circumstances would alter the interfacial tension balance.

One could resolve the problem by introducing a suitable torque in the interphase boundary to allow the angles to differ. This measure is unsatisfactory unless the value for the torque is known.

Another problem is encountered when a change in temperature gradient is made and when the two solid-liquid interfacial energies differ significantly or when the volume fraction is not close to one-half. A change in G would cause the two cusp shapes to change by differing amounts. The free end of each cusp would then attain a different degree of undercooling and a matching problem occurs again. This latter point can be illustrated in the following way: a comparison will be made between a large and small width of lamella, much like the types found in the slowly grown organic eutectic. Let the major phase solid-liquid interface consist of two Bolling and Tiller curves end to end like the one in Fig. 10.19 and let the minor phase solid-liquid interface resemble those in the same

figure. Let this hypothetical inferface exist in a certain temperature gradient at equilibrium. Next, steepen the temperature gradient. The larger interface profile will become compressed in the heat flow direction and the average radius of curvature will be reduced. The minor phase interface profile already has a uniform curvature and this curvature is limited by the lamellar width (assumed not to change). The position of this interface will move in the temperature gradient in such a way that the Gibbs - Thomson relation is satisfied. As a result, the new relative positions of the two profiles in the heat flow direction will not match up in the new temperature gradient unless some change in dihedral angle or torque occurs.

The difficulty in matching the two interface profiles is similarly complicated by considering changes in volume fractions or lamellar spacing. For example, reduce the volume fraction of the minor phase continually. The solid-liquid interface shape will be a segment of a circle, whose radius of curvature constantly will decrease as the lamellar width decreases. As this occurs, the interface position will have to move to higher undercoolings further from the isotherm for zero curvature. Clearly, only for a small range of undercoolings can this interface be mated to the other interface to form a cusp at the trijunction with the characteristic angles observed in the organic. Similar problems in matching the two interface profiles occurs

when the two interfacial energies differ significantly.

There seems to be some regulatory mechanism which will permit the interface to accommodate all these conditions in order that a planar, lamellar eutectic interface could grow in a wide range of temperature gradients and growth rates. The regulatory mechanism required here would have to do with the balance of the interfacial tensions. Such a mechanism may be related to the "minimum undercooling" criterion (see section 8.1) which accounts for the relationship between lamellar spacing and growth rate (one of the first empirically derived relations).

Observations of the impure eutectic interfaces indicated that the only form of morphological modification induced was that caused by constitutional undercooling. It was possible to grow planar eutectic interfaces with impurities if the growth rates were sufficiently low. Higher growth rates than those for planar growth caused irregular structures to form as the eutectic interface broke down.

The behaviour of eutectic grains containing "special" boundaries during conditions of constitutional undercooling was markedly unusual. A solid-liquid eutectic interface with intersecting "special" boundaries was found to grow with lower undercooling than an interface with higher energy phase boundaries. The interface with "special" boundaries would lead the interface

with higher energy phase boundaries when the eutectic was pure. This behaviour is duplicated for the impure interface as well. Under conditions of constitutional undercooling, the leading edge of the interface containing the eutectic grain with "special" boundaries rejects solute prior to the remainder of the interface. The solute then collects in higher concentrations than usual on the latter portion of the solid-liquid interface, while the interface with "special" boundaries continues to grow into liquid with less undercooling. Eventually, the solute buildup suppresses the growth of the "higher energy" solid-liquid interface and the "special" boundary interface grows further into the liquid. The process is self-perpetuating. This sequence of events describes a selection mechanism which favours the growth of eutectic grains with "special" boundaries. Examples of such grains are shown in Fig. 10.12. As the resulting microstructure of these grains differs from that from the growth of interfaces with the higher energy phase boundaries, the structure is cons dered modified. The difference in undercooling between the "special" solid-liquid interfaces and the "high energy" solid-liquid interfaces was found to be very small for a pure eutectic. It is possible that a small quantity of an impurity with a small distribution coefficient could, under constitutional undercooling conditions, accentuate the slight difference in undercooling between the two types of interfaces. These principles of eutectic modification should apply equally well to any other system (such as a metal based system).

12. CONCLUSIONS AND SUMMARY

The Carbon Tetrabromide - Hexachloroethane organic system was studied in this work. Particular attention was given to the application of the eutectic alloy as a model system for non-faceted, non-faceted, metallic eutectic growth. A Temperature Gradient Microscope was specially constructed to observe and photograph a unidirectionally growing solid-liquid interface in controlled conditions. A phase diagram was constructed and the variation of enthalpy of fusion, density, entropy of fusion and solid-liquid interfacial free energy with concentration of Hexachloroethane was measured and reported.

The solid-liquid interfacial free energies of a range of alloys were measured using a grain boundary groove technique. This technique, as well as another method based on the Gibbs - Thomson relation, were successfully used to measure the individual solid-liquid interfacial free energies of the two solid phases and the melt for a eutectic interface. The values measured checked with those obtained from the single phase grain boundary groove measurements and those based on empirical relations. The solid-liquid interfacial energies of both eutectic phases were found to be isotropic. From this knowledge, measurements of both the solid-solid interphase interfacial free energy and the associated torque of this boundary could be made from the dihedral angle formed between the interfaces at the trijunctions.

In addition "special" or low e rgy phase boundaries were observed, their interfacial energies measured and their influence on the interface shape studied. Calculations and measurements showed that the overall interface undercooling during growth was as small as 0.05 degrees Celsius.

Experimental conditions were developed which could allow the observation of an interface which had effectively no ΔT_D or, on the other hand, another interface with no ΔT_R. These are the main undercooling contributions in the Jackson and Hunt theory of eutectic growth.

It is concluded that for this system, the eutectic interface morphology is strongly dependent on the interfacial free energies found at the eutectic trijunctions and on the temperature gradient (ie. ΔT_R). The interface morphology was not found to be so strongly dependent on the rapid cross-diffusion between the lamellae of the components of the eutectic in the liquid ahead of the interface (ie. ΔT_D).

13. APPENDICES

Appendix A

Listing of Polynomial Coefficients

Phase Diagram (T°C vs. w/o)

Liquidus Hex-Rich

$$Y = 63.64555 + 2.4618683x - 0.0185x^2 + 6.197668E\text{-}5x^3$$

Solidus Hex-Rich

$$Y = 49.20405 + 2.4341x - 0.022967x^2 + 1.23461E\text{-}4x^3$$

Liquidus CBr_4-Rich

$$Y = 91.783639 - 0.5760037x - 0.053909x^2$$

Solidus CBr_4-Rich

$$Y = 91.82861842 - 1.819167x + 0.0198209x^2$$

Eutectic Tie Line

$$Y = 83$$

Density @ R.T. (gms/cm^3 vs. w/o)

$$Y = 3.27628 - 0.038526x + 4.1229E\text{-}4x^2 - 1.49427E\text{-}6x^3$$

Enthalpy per unit weight (calories per grams vs. w/o)

$$Y = 2.41598 - 8.2428E\text{-}4x - 2.3655E\text{-}4x^2 + 1.8555E\text{-}5x^3 - 9.8258E\text{-}8x^4$$

Entropy per unit volume ($J/m^3°K$ vs. w/o)

H = w/o Hex

$$S = 89767.765 - 949.41115H + 4.44487H^2 + 0.2473927H^3 - 0.00126H^4$$

V_f vs. R (fraction <1) (R μm/sec)

$V_f = 0.29731 - 0.07935\ R$ quality of fit(r) = -.57

ΔT vs. Curvature (°K) (1/micrometer)

ZVI data $\Delta T = 0.0579211\ \kappa - 0.003967$

growing interface $\Delta T = 0.0147\ \kappa - 0.00132$

Linear Speed vs. RPM

Vel. = 0.265 μm/sec per RPM

δ vs. θ^2 (Glicksman-Nash)

$$\theta^2 = -0.0041153 + 0.491258 - 10.8199\delta^2 + 121.264\delta^3 - 511.347\delta^4 + 802.1579\delta^5$$

γ_{SL} vs. w/o Hex.

α phase $\gamma_{SL} = 6.839 + 0.2269H + 0.0156H^2$

β phase $\gamma_{SL} = 29.2528 - 1.6903H + 0.02735H^2$

H = w/o Hexachloroethane in Carbon Tetrabromide

Appendix B

Consequences of the Glicksman-Nash Method

The simplicity of the measurement from a grain boundary groove is a strong advantage of the Glicksman-Nash method. The method depends upon interpolating a term from the graph Fig. 8.5. Application of the method on many grooves has raised some questions about how limited the method can be. The problems stem from the shape of the curve in Fig. 8.5. For example, a small spacing between the grooves (2λ) results in the ratio δ to become larger and the upper portion of curve is needed to obtain θ. It was found from experience, that for values of $\delta>0.2$, a small increase in δ (e.g. a small reduction in spacing of the grain boundary groove) would lead to a large increase in θ^2 and a correspondingly large increase in the calculated value for γ_{SL}. The upper right portion of the curve is almost horizontal. A small error in measurement would cause a large difference in the calculated γ_{SL} in this region of the graph. As explained before, grain boundary grooves do not generally remain in such close proximity to one another that δ would be >0.2. Thus, if one were to restrict the application of the method to well equilibrated grooves, this upper portion of the graph would not be encountered.

Note that grain boundary grooves can, for long periods of time, exist sufficiently nearby to one another that the

curvatures of the grooves mutually interact. Under these circumstances, the midportion of the plot in Fig. 8.5 would be of use when measuring γ_{SL}. The mutual influence of the groove curvatures on one another diminishes as the groove spacing increases. At some point, each groove will become perfectly isolated from its neighbour. Unfortunately, under these circumstances, $\delta \to 0$. For large grain boundary groove spacings then, δ is very small and one would have to interpolate θ^2 from the lower portion of the graph in Fig. 8.5. In this region, however, large variations in λ , or errors in measurement are insignificant since the value of θ^2changes little and so the calculation of γ_{SL} is equally imprecise. In this region of the graph, the curve is nearly vertical. Eventually, a practical limit would be reached in the spacing, λ, where no measurable change in groove shape results from the proximity of another groove. It was determined from experience that the value of δ for this condition occurred at $\tilde{}0.06$. Below this value, any spacing would be usable to calculate γ_{SL}.

A graphic explanation of the above is given in the graph, Fig. A-1. In this graph, for a given d, ΔS_f, and G the calculated γ_{SL} was plotted for a range of values of λ, and repeated for some representative values of d. The points on the curves which are to the left of the horizontal lines were obtained from the graph in Fig. 8.5. The lower knees on each curve occur when $\delta \simeq 0.06$. The upper knees occur when $\delta \simeq 0.22$.

Fig. A-1

Variation of Interfacial Energy With Groove Spacing

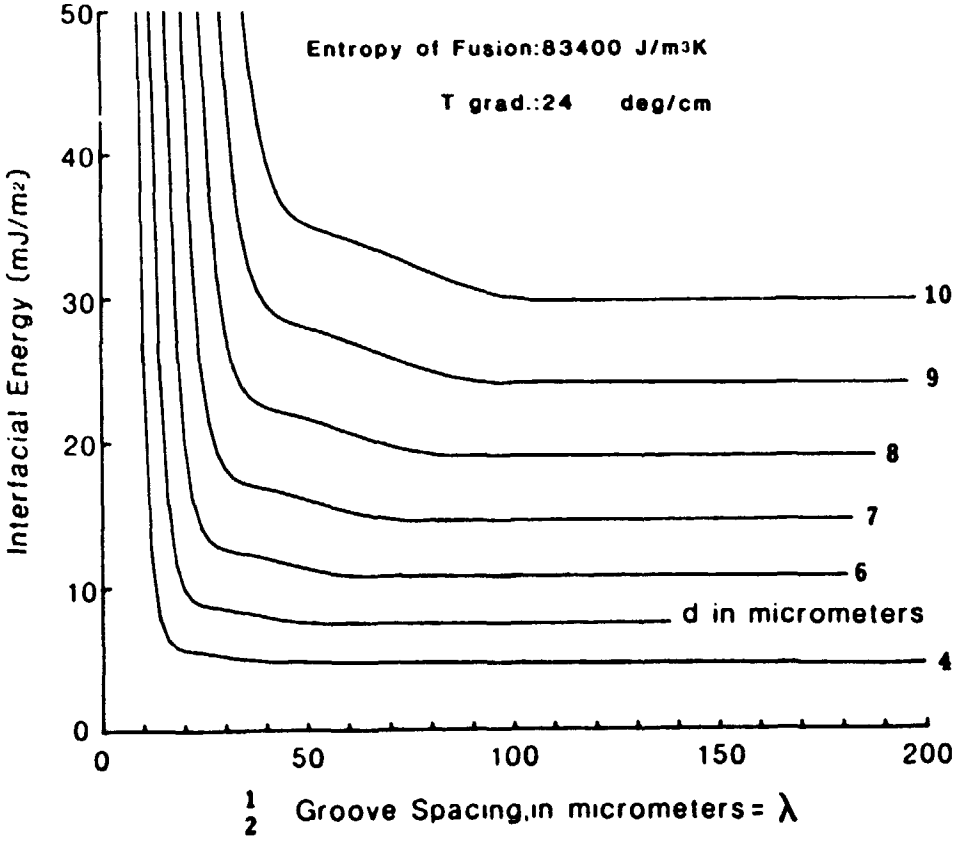

The actual form of the curve to the right of the lower is not known explicitly, but rather was deduced from examining the details of the analysis. Clearly, an isolated grain boundary groove should have only one representative interfacial free energy.

In the experiments performed here, the value of δ was frequently less than the value for the lower knee on the plot, Fig. A-1. The single value of δ=0.06 would then be equally representative for any case where $\delta \leq 0.06$. The typical values of d for the grooves generated in this work ranged from two to twelve micrometers. Equilibrated grooves were often 1~0 micrometers apart, resulting in values of λ in the area of 50-60 micrometers and values of $\delta \sim 0.05$ or less. Grooves such as these are isolated sufficiently that their shape matches the calculated groove profile from the Bolling-Tiller equation. Under these circumstances, one could use the Bolling-Tiller curve matching method to estimate γ_{SL} from these grooves. Such circumstances were obtained by setting δ=0.06 when measuring a curve drawn using the Bolling-Tiller equation with a selected γ_{SL} through the application of the Glicksman-Nash technique. The measured value of the interfacial energy reproduced the initially selected value. This test ensured that both methods would give a representative value of γ_{SL} from experimental grain boundary grooves.

An assumption made by Glicksman and Nash in the description of their method [12] was not found to be valid at

any time in this work. The assumption was that a random, high energy grain boundary would develop a grain boundary groove with a nearly zero dihedral angle at the base of the cusp. This was to be valid for the assumed case of solid-liquid interfacial energy isotropy. Of the hundred or more grain boundary grooves observed, none had, as visible to the eye, a dihedral angle lower than approximately forty degrees. When the groove angles were measured, the overall dihedral angle of the cusp was approximately eighty degrees. The deviation from the ideal conditions assumed by Glicksman and Nash would lead to an error in the measurement since the large dihedral angle in essence, reduces the effective value of d since the curvature of the groove is not as fully developed as it could be if it were, for example, a Bolling and Tiller groove with zero dihedral angle at the base of the cusp. As a consequence, it is believed that the Glicksman-Nash method underestimates the γ_{SL} for the system studied here by a few percent.

Appendix C

Specimen (Alloy) Data

System #	Composition	Source of Chemicals
1	Eutectic 8.6 w/o Hexachloroethane	Eastman Kodak (CBr_4) Matheson, Coleman & Bell (Hexachloroethane)
2	12 w/o Hexachloroethane	Eastman Kodak (CBr_4) Matheson, Coleman & Bell (Hexachloroethane)
3	20 w/o Hexachloroethane	Eastman Kodak (CBr_4) Matheson, Coleman & Bell (Hexachloroethane)
4	8.8 w/o Hexachloroethane	Matheson, Coleman & Bell (CBr_4) Matheson, Coleman & Bell (Hexachloroethane)
5	8.631 w/o Hexachloroethane Eutectic	Eastman Kodak (CBr_4) Eastman Kodak (Hexachloroethane)
6	8.59 Hexachloroethane 1.769 Azobenzene 89.643 Carbon Tetrabromide	Eastman Kodak (CBr_4) Eastman Kodak (Hexachloroethane)
7	(S5 + S6) 8.653 Hexachloroethane 0.058 Azobenzene 91.289 Carbon Tetrabromide	Eastman Kodak (CBr_4) Eastman Kodak (Hexachloroethane)
8	44.71 Carbon Tetra-bromide 55.29 Azobenzene	Eastman Kodak (CBr_4) Eastman Kodak (Hexachloroethane)
9	8.6568 w/o Hexachloroethane 91.2523 w/o Carbon Tetrabromide 0.0909 w/o Azobenzene	Eastman Kodak (CBr_4) Eastman Kodak (Hexachloroethane)
10	Carbon Tetrabromide	Eastman Kodak

System #	Composition	Source of Chemicals
11	0.099 w/o Azobenzene in Carbon Tetrabromide	Eastman Kodak
12	Eutectic 8.635 w/o Hexachloroethane	Eastman Kodak (CBr_4) Eastman Kodak (Hexachloroethane)
14	0.321 Azobenzene (remainder S12)	Eastman Kodak
15	0.1824 w/o Benzil (remainder S12)	Eastman Kodak
16	0.5168 w/o Azobenzene in Carbon Tetrabromide	Eastman Kodak
17	Eutectic 8.6135 w/o Hexachloroethane	Eastman Kodak (CBr_4) Eastman Kodak (Hexachloroethane)
18	0.3 w/o Succinonitrile in S17	
19	1.34 w/o Cyclohexanol in S17	
20	0.315 w/o Hexahchloro-ethane in Carbon Tetrabromide	Eastman Kodak (CBr_4) Eastman Kodak (Hexachloroethane)
21	Contin..ated	
22	0.334 w/o Succinonitrile in Carbon Tetrabromide	Eastman Kodak (CBr_4)
23	0.3613 w/o Cyclohexanol in Carbon Tetrabromide	Eastman Kodak (CBr_4)
24	0.2774 w/o Camphene in Carbon Tetrabromide	Kastman Kodak (CBr_4)
26	Pur..fied Carbon Tet..abromide	
27	8.5999 w/o Hexachloro-ethane in double refined Carbon Tetrabromide	

System #	Composition	Source of Chemicals
28	S27 + Hexachloroethane to give ~10 w/o Hexachloroethane	
29	S28 + Carbon Tetrabromide to give ~7.5 w/o Hexachloroethane	
30	S29 + Hexachloroethane to give ~8.0 w/o Hexachloroethane	Eastman Kodak (CBr_4) Eastman Kodak (Hexachloroethane)
31	11.3 w/o Hexachloroethane	
32	~9 w/o Hexachloroethane for convection cells	
33	8.708 Hexachloroethane unrefined Eutectic	Eastman Kodak (CBr_4)
34	8.65 Hexachloroethane Eutectic	Eastman Kodak (CBr_4)
35	19.839 Hexachloroethane	Eastman Kodak CBr_4)
36	Purified Carbon Tetrabromide	
37	0.2134 w/o Hexachloroethane in Carbon Tetrabromide (refined)	
38	0.4216 w/o Hexachloroethane in Carbon Tetrabromide (refined)	
39	1.0582 w/o Hexachloroethane in Carbon Tetrabromide (refined)	
40	2.45 w/o Hexachloroethane in Carbon Tetrabromide (refined)	
41	contaminated	

System #	Composition	Source of Chemicals
42	3.565 w/o Hexachloroethane in Carbon Tetrabromide	
43		
44		
45		
PD 1	15.52 w/o Hexachloroethane	Eastman Kodak (CBr_4) Eastman Kodak (Hexachloroethane)
PD 2	24.98 w/o Hexachloroethane	Eastman Kodak (CBr_4) Eastman Kodak (Hexachloroethane)
PD 3	47.49 w/o Hexachloroethane	Eastman Kodak (CBr_4) Eastman Kodak (Hexachloroethane)
PD 4	76.5 w/o Hexachloroethane	Eastman Kodak (CBr_4) Eastman Kodak (Hexachloroethane)
PD 5	7.52 w/o Hexachloroethane	Eastman Kodak (CBr_4) Eastman Kodak (Hexachloroethane)
PD 6	5.15 w/o Hexachloroethane	Eastman Kodak (CBr_4) Eastman Kodak (Hexachloroethane)
PD 7	85.92 w/o Hexachloroethane	Eastman Kodak (CBr_4) Eastman Kodak (Hexachloroethane)
PD 8	1.993 w/o Hexachloroethane	Eastman Kodak (CBr_4) Eastman Kodak (Hexachloroethane)

System #	Composition	Source of Chemicals
PD 9	11.777 w/o Hexachloro-ethane	Eastman Kodak (CBr_4) Eastman Kodak (Hexachloroethane)

Designations: S# - sample number

PD# - alloy used in determination of Phase Diagram

Appendix D

Properties of Organic Compounds Used for "Impurity" Additions

Azobenzene

Other names: Azobenzol, Benzeneazobenzene

$C_{12} - H_{10}N_2$
mol. wt. 182.22
d 1.2
mp 68°C
bp 293°C
insoluble in water
orange-red leaflets, crystale

[52]

Benzil

Other names: Bibenzoyl, Dibenzoyl, Diphenylglyoxal

1, 2 - Diphenlylenethanedione
$C_6H_5COCO - C_6H_5$
mol. wt. 210.22
d_4^{15} 1.23
mp 93°C
bp 346 - 348°C
insoluble in water
yellow crystals

[52]

Camphene

Other names: 2,2 - Dimethyl - 3 - methylenenorborane

$C_{10}H_{16}$
mol. wt. 136.23
mp 51 - 52°C
bp 158.5 - 159.5°
d_4^{54} 0.8422
practically insoluble in water [52]
γ_{SL} = 5.3±0.9 ergs/cm^2 (B-T)
γ_{SL} = 6±1 (G-N)
negligible anisotropy of γ_{SL} [11]
bcc structure at mp [1]

Cyclohexane

Other names: Hexahydrobenzene, Hexamethylene

C_6H_{12}
mol. wt. 84.16
insoluble in water
mp +6.47°C
bp 80.7°C
d_4^{20} 0.7781 [52]
f.c.c. structure at mp. [1]
surface tension γ_{LV} @ 20°C 25.5 dyne/cm [64]

Succinonitrile

Other names: Ethylenedicyanide, Butanedinitrile

NCC H_2 CH_2CN
mol. wt. 80.09
d_4^{45} 1.023
mp 57.15
d_4^{60} 0.9860
bp 265 - 267
slightly soluble in water [52]
b.c.c. structure @ mp. [1]
γ_{SL} 28±5 mJ/m^2 [11]
thermal diffusivity 1.16 = 10^{-3} cm^2/sec (α)(58°)
density liquid 0.970 g/cm^3 (58°)
viscosity μ = 0.0165 (g/cm-sec)(58°)
Prandl no. Pr = $\mu/\rho\alpha$ = 14.7
mp = 58.083±0.002 °C
volumetric expansivity β ($°K^{-1}$) = 5 x 10^{-4} [59]

APPENDIX E

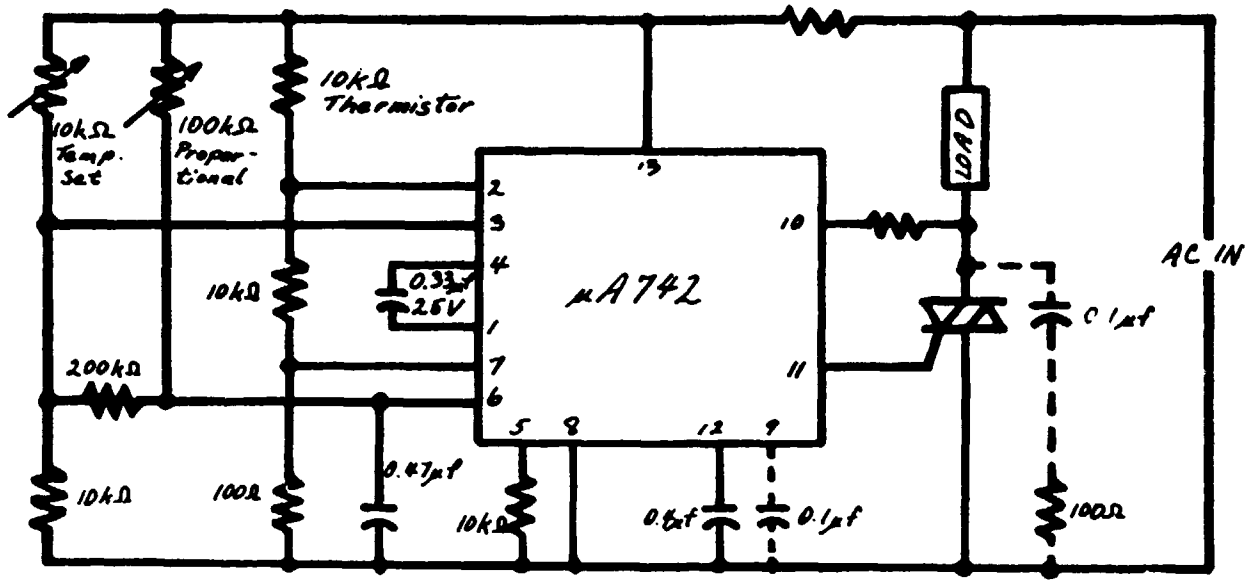

TEMPERATURE CONTROLER CIRCUIT

APPENDIX F

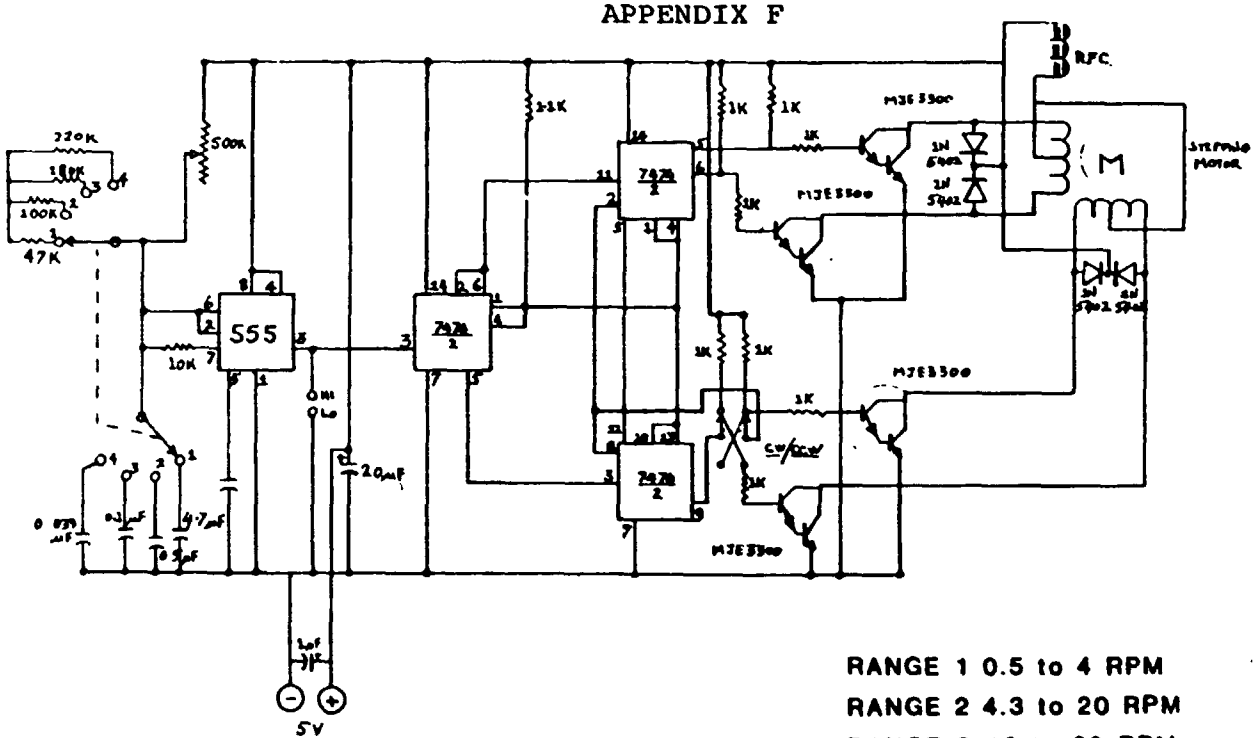

STEPING MOTOR DRIVE CIRCUITRY

RANGE 1 0.5 to 4 RPM
RANGE 2 4.3 to 20 RPM
RANGE 3 18 to 60 RPM
RANGE 4 52 to 150 RPM

Binary Gibbs-Thomson Effect Applicable to Grain Boundary Grooving

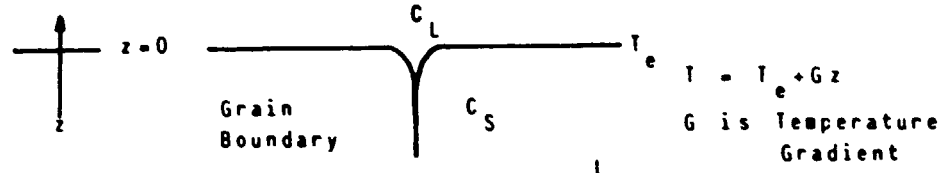

Assume Soret Effect in Liquid : $C_L = C_e^L + kz$
k^L contains Soret coefficient

Assume solid-liquid interface isotropic and ignore surface stresses.

At $z=0$, $\mu_1^S (C_e^S, T_e) = \mu_1^L (C_e^L, T_e) = \mu_1^e$

$\mu_2^S (C_e^S, T_e) = \mu_2^L (C_e^L, T_e) = \mu_2^e$

can solve for C_e^S and C_e^L.

At any z; where κ_1, κ_2 is curvature;

$$\mu_1^S (C^S, T_e + Gz) = \mu_1^e + (C^S - C_e^S) \frac{\partial \mu_1^S}{\partial C^S} + \frac{\partial \mu_1^S}{\partial T} Gz + \bar{V}_1^S \gamma (\kappa_1 + \kappa_2)$$

(and using Cahn's notation) $= \mu_1^e + \Delta C^S \mu_{1C}^S - \bar{S}_1^S Gz + \bar{V}_1^S \gamma (\kappa_1 + \kappa_2)$

$$\mu_1^L (C_e^L + kz, T_e + Gz) = \mu_1^e + kz\mu_{1C}^L - \bar{S}_1^L Gz$$

Combining:

$$\Delta C^S \mu_{1C}^S + \bar{V}_1^S \gamma (\kappa_1 + \kappa_2) = (G\Delta\bar{S}_1 + k\mu_{1C}^L) z$$

Similarly:

$$\Delta C^S \mu_{2C}^S + \bar{V}_2^S \gamma (\kappa_1 + \kappa_2) = (G\Delta\bar{S}_2 + k\mu_{2C}^L) z$$

Eliminating ΔC^S:

$$(\bar{V}_1^S \mu_{2C}^S - \bar{V}_2^S \mu_{1C}^S) \gamma (\kappa_1 + \kappa_2) = z (G[\Delta\bar{S}_1 \mu_{2C}^S - \Delta\bar{S}_2 \mu_{1C}^S] + k[\mu_{1C}^L \mu_{2C}^S - \mu_{2C}^L \mu_{1C}^S])$$

$$\kappa_1 + \kappa_2 = z \frac{G}{\gamma} \frac{|\Delta\bar{S}_i, \mu_{iC}^S|}{|\bar{V}_i^S, \mu_{iC}^S|} + z \frac{k}{\gamma} \frac{|\mu_{iC}^L, \mu_{iC}^S|}{|\bar{V}_i^S, \mu_{iC}^S|}$$

Binary Gibbs-Thomson; continued:

As a check for dilute solutions:

$$\mu_{2C} = RT/C \quad \text{and} \quad \mu_{1C} = RT \ll \mu_{2C}$$

$$(\kappa_1+\kappa_2) = \frac{zG}{\gamma} \frac{\Delta\bar{S}_1 \cdot RT/C^S}{\bar{V}_1^S \cdot RT/C^S} + \left[\frac{zk}{\gamma V_1^S} \frac{(1-R)}{1} \right]$$

Note: $\Delta\mu_i = 0$, $\Delta\bar{S}_i = \frac{\Delta\bar{H}_i}{T}$, Thermal Gradient $= G^t$

Gibbs Free Energy $= G$

$$\left.\begin{aligned} &(1-C)\,\mu_{1C}^L + C\mu_{2C}^L = 0 \\ &\frac{\partial G}{\partial C} = \mu_2 - \mu_1 \\ &\mu_{1C} - \mu_{2C} = \frac{\partial^2 G}{\partial C^2} \end{aligned}\right\} \quad \begin{aligned} \mu_{1C} &= C \frac{\partial^2 G}{\partial C^2} \\ \mu_{2C} &= -(1-C) \frac{\partial^2 G}{\partial C^2} \end{aligned}$$

$$(-\bar{V}_1^S C_1^S - \bar{V}_2^S C_2^S) \frac{\partial^2 G^S}{\partial C_S^2} \gamma (\kappa_1+\kappa_2) = z\left(G^t \frac{\partial^2 G}{\partial C^2} [-\Delta\bar{S}_1 C_1^S - \Delta\bar{S}_2 C_2^S] + [k \text{ term}]\right)$$

$$V^S \gamma (\kappa_1+\kappa_2) = \frac{zG^t}{T} \Delta H_{fp} \quad \text{+ final solution}$$

Note: Gibbs-Konovalov Rule $\quad \frac{\partial T}{\partial X} = \frac{T(C_L - C_S)}{\Delta H_{fp}} \frac{\partial^2 G}{\partial C^2}$

Rearranging terms of Binary G-T to appear like Single Component Gibbs-Thomson:

$$\frac{\gamma (\kappa_1+\kappa_2) TV^S}{\Delta H_{fp}} = zG^t \quad \text{cf.} \quad \Delta T = \frac{\gamma T_e}{\rho \Delta Hr}$$

$$\Delta H_{fp}^{\beta} = H^{\beta} - (X_A^{\beta}\bar{H}_A^{\alpha} + X_B^{\beta}\bar{H}_B^{\alpha}) \quad \text{for } \beta \text{ phase example.}$$

X_A is mole fraction of A in phase, $\bar{H}_A$ is partial molal enthalpy of component A in phase. H is molar enthalpy of phase.

14. REFERENCES

Solidification Theory and Interfaces

1. K.A. Jackson, J.D. Hunt; "Transparent Compounds That Freeze Like Metals", Acta Met., 13, p. 1212, 1965.

2. J.D. Hunt, K.A. Jackson; "Binary Eutectic Solidification", Trans. Met. Soc. AIME, 236, p. 843, 1966.

3. K.A. Jackson; "Crystal Growth", Suppl. Phys. Chem. Solids, 17, 1968.

4. K.A. Jackson; "Defect Formation, Microsegregation and Crystal Growth Morphology", Chapter 5, Solidification, ASM, 1971.

5. M.E. Glicksman; "Direct Observation of Solidification", Chapter 6, Solidification, ASM, 1971.

6. R.W. Kraft; "Laboratory-Scale Applications of Controlled Solidification", Chapter 8, Solidification, ASM, 1971.

7. M.C. Flemings; "Solidification Processing", McGraw-Hill, 1974.

8. K.A. Jackson and J.D. Hunt; "Lamellar and Rod Eutectic Growth", Trans. Met. Soc. AIME, 236, p. 1129, Aug. 1966.

9. D.R.H. Jones and G.A. Chadwick; "The Experimental Determination of the Kinetics of Solid-Liquid Interfaces in Transparent Materials using Temperature-gradient Zone Migration", Phil. Mag., 24, p. 1327, 1971.

10. D.R.H. Jones and G.A. Chadwick; "Experimental Measurement of the Solid-Liquid Interfacial Energies of Transparent Materials", Phil. Mag. 22, p. 291, 1970.

11. D.R.H. Jones; "The Measurement of Solid-Liquid Interfacial Energies from the Shapes of Grain Boundary Grooves", Phil. Mag. 27, p. 569, 1973.

12. G.E. Nash and M.E. Glicksman; "A General Method for Determining Solid-Liquid Interfacial Free Energies", Phil. Mag. 24, p. 577, 1971.

13. D.R.H. Jones and G.A. Chadwick; "Experimental Measurement of Solid-Liquid Interfacial Energies: The Ice-Water-Sodium Chloride System", J. Crystal Growth, 11, p. 260, 1971.

14. G.F. Bolling and W.A. Tiller; "Growth from the Melt, I", Journal of Applied Physics, 31, n. 8, p. 1345, 1960.

15. G.F. Bolling and W.A. Tiller; "Growth from the Melt, II", Journal of Applied Physics, 31, n. 11, p. 2040, 1960.

16. R.J. Schaefer, M.E. Glicksman, J.D. Ayers; "High Confidence Measurement of Solid/Liquid Surface Energy in a Pure Material", Phil. Mag., 32, p. 725, 1975.

17. L.M. Hogan, R.W. Kraft, F.D. Lemkey; "Eutectic Grains", Advances in Materials Research, 5, p. 83, 1971.

18. W.M. Rumball, V. Kondic; "Binary Eutectic Classification", Trans. Met. Soc. AIME, 239, p. 586, 1967.

19. M. Hillert; "Eutectic and Peritectic Solidification", Proc. Sheffield Conference on Solidification, Solidification and Casting of Metals, The Metals Society, 1979.

20. G.E. Nash, M.E. Glicksman; "A Self-Consistent Theory of Steady-State Lamellar Solidification in Binary Eutectic Systems", N.R.L. Report, n. 2940, Nov. 1974.

21. W.A. Tiller; "Polyphase Solidification", Liquid Metals and Solidification, A.S.M., 1958.

22. C. Zener;
Trans. AIME, 167, p. 550, 1946.

23. G.A. Chadwick;
Progress in Materials Sci., 12, p. 97, 1963.

24. S.M.D. Borland, R. Elliott; "Growth Temperatures in Al-$CuAl_2$ and Sn-Cd Eutectic Alloys", Met Trans. A, 9A, p. 1063, 1978.

25. A. Moore, R. Elliott;
Proc. Conf. Solidification of Metals, Brighton, p. 167, Iron and Steel Inst., London, 1967.

26. H.E. Cline; "Stability of Lamellar Eutectics", J. Appl. Phys., 50(7), p. 478, July 1979.

27. G.E. Nash; "A Self-Consistent Theory of Steady-State Lamellar Solidification in Binary Eutectic Systems", N.R.L. Report n. 7956, Washington D.C., 1976.

28. G.A. Chadwick; "Interlamellar-Spacing Measurements in Certain Binary Eutectic Systems", J. Inst. of Metals, 92, p. 18, 1963-1964

29. E.P. Whelan, C.W. Haworth; "The Calculation of Interphase Boundary Energies in Binary Lamellar Eutectic Alloys", J. Inst. of Metals, 93, p. 402, 1965.

30. R.S. Fidler, M.N. Croker, R.W. Smith; "The Thermodynamics and Morphologies of Eutectics Containing Compound Phases", J. of Crystal Growth, 13/14, p. 739, 1972.

31. M.N. Croker, M. McParlan, D. Baragar, R.W. Smith; "Anomalous Eutectic Growth I, II", Journal of Crystal Growth, 29, p. 85, 1975, and 30, p. 198, 1975.

32. L.F. Donaghey, W.A. Tiller; "On the Diffusion of Solute During the Eutectoid and Eutectic Transformations, Part I", Mat. Sci. and Eng., 3, p. 231, 1968-1969.

33. M. Colin, G. Lesoult, M. Turpin and J. Zeyons: J. Cryst. Growth, 28, p. 103, 1975.

34. R.W. Series, K.A. Jackson, J.D. Hunt; "The Use of an Electric Analogue to Solve the Lamellar Eutectic Diffusion Problem", J. Cryst. Growth, 40, p. 221, 1977.

35. R. Elliott; "Review, Eutectic Solidification", Int. Metals Reviews, p. 161, Sept. 1977.

36. G.A. Chadwick; "Metallography of Phase Transformations", Crane, Russak and Co. Inc., 1972.

37. E. Arbel, J.W. Cahn; "A Method for the Absolute Measurement of Anisotropic Surface Free Energies", Surf. Sci., 66, p. 14, 1977.

38. K.A. Jackson, "A Review of the Fundamental Aspects of Crystal Growth", Part A2, p. 17, Proc. ICCG, Boston, 1966, Crystal Growth, ed. H. Steffen Peiser, Pergamon, 1967.

39. D.R. Uhlmann, T.P. Seward III, B. Chalmers; Trans. Met. Soc. AIME, 236, p. 527, 1966.

University of Toronto Theses

40. W.F. Kaukler, MASc. Thesis, 1977.

41. M. Ruggiero, MASc. Thesis, 1979.

42. L.R. Morris, PhD. Thesis, 1969.

43. G. Haour, PhD. Thesis, 1975.

44. W.F. Kaukler, BASc. Thesis, 1975.

45. R.S. Good, L.A. Girafalco, "A Theory for the Estimation of Surface and Interfacial Energies I", J. Phys. Chem., 61, p. 904, July 1957.

46. L.A.K. Staveley; "Thermodynamic Studies of Molecular Rotation in Solids", J. Phys. Chem. of Solids, 18, p. 46, 1961.

47. P.F. Aurbourg; "Interaction of Second Phase Particles with a Crystal Growing from the Melt," June 1978, PhD. Thesis, M.I.T.

48. R.S. Bradley, T. Drury; "The Vapour Pressure and Lattice Energy of Carbon Tetrabromide", Trans. Faraday Soc., 55, p. 1844, 1959.

49. O. Kubachewski, E.L. Evans, C.B. Alcock; "Metallurgical Thermochemistry", 4th Ed., Pergamon, 1974.

50. J. Timmermans, "Plastic Crystals", J. Phys. Chem. Solids, 18, p.1, 1961.

51. W.J. Dunning; "Crystallographic Studies of Plastic Crystals", J. Phys. Chem. Solids, 18, p. 21, 1961.

52. "The Merck Index"; 8th Ed., Merck & Co. Inc., 1968.

53. J. Timmermans; "Timmermans Physico-Chemical Constants of Pure Organic Compounds", Vol. 1, p. 248, p. 228.

54. "Encyclopedia of Chemical Technology", Kirk & Othmer Ed., Second Edition, Vol. 5, 1963. Interscience Publishers.

55. "Practicing Scientist's Handbook", Table 200, 201, Van Nostrand Rienhold Co.

56. "Crystal Data, Organic Compounds"; Vol. 1, 3rd Ed., U.S. Dept. of Commerce, Nat'l Bureau of Standards, 1972.

57. C.J. Smithells; "Metals Reference Book", 5th Ed., Butterworths, 1978.

58. "Dictionary of Organic Compounds", V3, p. 1587. Eyreand Spottiswoode Pub. 1968, 4th Ed., London.

59. M.E. Glicksman; paper 78-220, AIAA 16th Aerospace Science Meeting, Huntsville, Alabama, January 1978.

Mixed Category

60. M. Macecek, J.W. Rutter, G.A. Turner; "Solidification-A Close Circuit TV Teaching Aid", Metals and Materials Educational Series, p. 69, Jan. 1974.

61. J.D. Hunt, K.A. Jackson, H. Brown; "Temperature Gradient Microscope Stage Suitable for Freezing Materials with Melting Points Between -100 and 200°C", Rev. Sci. Instr., 37 n. 6, p. 805, 1966.

62. Manual for Operation of Perkin-Elmer Differential Scanning Calorimeter, DSC-2.

63. L.E. Murr, "Interfacial Phenomena in Metals and Alloys", Addison-Wesley Pub., 1975.

64. Chemical Rubber Co.; "Handbook of Chemistry and Physics", ed. Weast, 56th Ed. 1975.

65. S.D. Conte, C. de Boor; "Elementary Numerical Analysis", McGraw-Hill, 2nd Ed., 1972.

66. C. Herring, "Surface Tension as a Motivation for Sintering", Chapter 8, The Physics of Powder Metallurgy. W.E. Kingston ed. McGraw-Hill Book Co. N.Y., p. 143, 1951.

67. D.W. Hoffman, J.W. Cahn; "A Vector Thermodynamics for Anisotropic Surfaces I", Surf. Sci., 31, p. 368, 1972.

68. J.W. Cahn, D.W. Hoffman; "A Vector Thermodynamics for Anisotropic Surfaces, II", Acta Met., 22, p. 1205, 1974.

69. R.A. Swalin; "Thermodynamics of Solids", Second Edition, p. 232, John Wiley & Sons, New York, 1972.

Interfaces, Miscellaneous

70. D.C. Jenkinson, L.M. Hogan; "The Modification of Aluminium-Silicon Alloys with Strontium", J. Cryst. Growth, 28, p. 171, 1975.

71. M. Hirai, T. Sato, G. Ohira; "Interfacial Stability of α-Liquid Interface of Unidirectionally Solidified Al-$FeAl_3$ Alloy", J. Crystal Growth, 38, p. 340, 1977.

72. J.E. Gruzleski, W.C. Winegard; "The Cellular Structure in the Sn-Cd Eutectic", Trans. Met. Soc. AIME, 242, p. 1785, 1968.

73. W.M. Rumball; "Cellular Growth in Eutectic Systems", Metallurgia, p. 141, Oct. 1968.

74. D.J.S. Cooksey, M.G. Day, A. Hellawell; "The Control of Eutectic Microstructures", B22, p. 151, Proc. ICCG, 1966, Crystal Growth, ed. H.S. Peiser, Pergamon, 1967.

75. R.J. Brigham, G.R. Purdy, J.S. Kirkaldy; "Unidirectional Solidification of Fe-C, Ni-C and Fe-C-Si Eutectics", B23, p. 161, Proc. ICCG, Boston, 1966.

76. H. Kerr, W.C. Winegard; "Eutectic Solidification", B25, p. 179, Crystal Growth, ed. H.S. Peiser, Oxford, Pergamon, 1967., Proc. ICCG, Boston, 1966.

77. H.E. Cline, J.C. Walter, E.F. Koch, L.M. Osika, "The Variation of Interface Dislocation Networks with Lattice Mismatch in Eutectic Alloys", Acta Met., 19, p. 405, May, 1971.

78. J.C. Baker, J.W. Cahn; "Thermodynamics of Solidification", chapter 2, Solidification, ASM, 1971.

79. D.R.H. Jones; "Review, The Free Energies of Solid-Liquid Interfaces", J. Mat. Sci, 9, p. 1, 1974.

80. M.E. Glicksman, C.L. Vold; "Determination of Absolute Solid-Liquid Interfacial Free Energies in Metals", Acta Met., 17, p. 1, 1969.

81. W.A. Miller, G.A. Chadwick; "On the Magnitude of the Solid/Liquid Interfacial Energy of Pure Metals and its Relation to Grain Boundary Melting", Acta Met., 15, p. 607, April 1967.

82. G. Grange, R. Landers, B. Mutaftschiev; "Conact Angle and Surface Morphology of KCl Crystal-Melt. Interface Studied by the "Bubble Method", Surface Science, 54, p. 445, 1976.

83. A.W. Neumann; "Contact Angles and Their Temperature Dependence ", Adv. Coll. Sci., 4, p. 105, 1974.

84. M.E. Glicksman, G.E. Nash; "A Self Consistent Theory of Steady-State Lamellar Solidification in Binary Eutectic Systems", Proc. Conference as In-Situ Composites II, Xerox, 1976.

85. S.N. Omengi, R.P. Smith, A.W. Neumann; "Determination of Solid-Melt Interfacial Tensions and of Contact Angles of Small Particles from the Critical Velocity of Engulfing", J. of Colloid and Interface Sci., 75, n. 1, May 1980.

86. D. Turnbull, R.E. Cech; "Microscopic Observation of the Solidification of Small Metal Droplets", J. Appl. Phys., 21, p. 894, 1950.

87. W.C. Johnson, J.M. Blakely, ed., "Interfacial Segregation", American Society for Metals, 1979. (seminar proceedings, Oct. 1977).

88. H. Mykura; "Twin Boundary Free Energies and the Variation of Surface Free Energies with Crystallographic Orientation", Acta Metallurgica, 5, p. 346, 1957.

89. W.A. Miller, W.M. Williams; "Anisotropy of Grain Boundary Energy and its Influence on Boundary Morphology in Sheet", Acta Metallurgica, 15, p. 1077, 1967.

90. M.S. Masteller, C.L. Baner; "Estimation of Grain Boundary Torques in Bicrystalline Specimens", Scripta Metallurgica, 10, p. 1033, 1976.

91. J. Basterfield, W.A. Miller, G.C. Weatherly; "Anisotropy of Interfacial Free Energy in Solid-Fluid and Solid-Solid Systems", Canadian Metallurgical Quarterly, 8, no. 2, p. 131, 1970.

92. J.W. Cahn; National Bureau of Standards, Washington, D.C., Private communication, Jan. 1981.

APPROVAL

A QUANTITATIVE STUDY OF FACTORS INFLUENCING LAMELLAR EUTECTIC MORPHOLOGY DURING SOLIDIFICATION

By W. F. S. Kaukler

The information in this report has been reviewed for technical content. Review of any information concerning Department of Defense or nuclear energy activities or programs has been made by the MSFC Security Classification Officer. This report, in its entirety, has been determined to be unclassified.

ROBERT J. NAUMANN
Chief, Space Processing Division

for J. E. KINGSBURY
Acting Director, Space Sciences Laboratory